Alterations in Colorectal Cancer Cell-extracellular Matrix Interactions Upon Acquisition of Chemotherapy Resistance.

by

Spencer Iner Thomas Berg

A thesis

presented to the University of Waterloo

in fulfillment of the

thesis requirements for the degree of

Master of Science

in

Pharmacy

Waterloo, Ontario, Canada, 2015

Author's Declaration

I hereby declare that I am the sole author of this thesis. This is a true copy of my thesis, including any required final revisions, as accepted by my examiners.

I understand that my thesis may be made electronically available to the public.

Abstract

Adjuvant chemotherapy is an essential component in the treatment of advanced colorectal cancer (CRC). Unfortunately, many patients experience recurrence with aggressive, chemotherapy-resistant disease for which the prognosis is poor and treatment options are limited. Understanding the changes that cancer cells undergo during the acquisition of a drug-resistant phenotype is therefore of critical importance in improving CRC patient outcomes. We chose to study resistance to the CRC chemotherapy agent, irinotecan, by first creating a CRC cell line that is highly resistant to its active metabolite (SN-38). In particular, we were interested in how SN-38 resistant CRC cells (HT-29S) were altered from parental, drug-sensitive CRC cells (HT-29) in their relationship with a feature of their microenvironment, the extracellular matrix (ECM). We found that HT-29S cells form a matrix composed of the ECM glycoprotein fibronectin when cultured as 3-dimensional spheroids, whereas HT-29 cells do not. The increase in fibronectin matrix deposition coincided with an increased fibronectin adhesive capacity of the SN-38-resistant cells, likely due to an increased expression of the integrin α5 subunit, which together with integrin β1 forms the primary fibronectin receptor. Furthermore, we demonstrated an activation of a phosphoinositide-3-kinase (PI3K)/protein kinase B (Akt) pro-survival signalling pathway downstream of integrin α5β1 ligation to fibronectin. Inhibition of this signalling pathway with the PI3K inhibitor LY294002 sensitized HT-29S cells to SN-38, but did not alter the response of the parental cell line to the chemotherapy agent. Finally, we have determined that HT-29S cells appear to undergo an epithelial to mesenchymal transition during the acquisition of chemotherapy resistance, and that this transition may be responsible for the upregulation of integrin α5 in the resistant population.

Acknowledgements

First and foremost, I must thank my supervisor Dr. Jonathan Blay for his invaluable guidance and support throughout this project. I have benefited immensely from his expertise and enjoyed greatly his sense of humour. I would also like to express my gratitude to my advisory committee, Dr. Michael Beazely and Dr. Mungo Marsden for their excellent advice and input. A very special thank you goes out to Dr. Murray Cutler, for his mentorship in and outside of the lab. I am grateful to my fellow graduate students at the school of pharmacy, who have welcomed me and have provided advice, a listening ear, and a distraction, as needed. Thank you to Rowena Rodrigo for your companionship and for being my biggest supporter. Finally but certainly not least of all, a sincere thank you to my family and friends outside of school for your continual support, and for not taking my absence personally when I couldn't get away from the lab.

Table of Contents

Abbreviations

Acronym	Name
AFU	Arbitrary Fluorescence Units
AML	Acute Myeloid Leukemia
APC	7-ethyl-10-[4-N-(5-aminopentanoic acid)-1-piperidino]-carbonyloxycamptothecin
ATCC	American Type Culture Collection
BCL2	B-Cell Lymphoma 2 (gene)
Bcl-2	B-Cell Lymphoma 2 (protein)
BCRP	Breast Cancer Resistance Protein
bFGF	Basic Fibroblast Growth Factor
BSA	Bovine serum albumin
CAM-DR	Cell Adhesion-Mediated Drug Resistance
CaMK	Ca^{2+}/Calmodulin-Dependent Protein Kinase
CDH17	Cadherin 17
cDNA	Complimentary DNA
CE	Carboxylesterase
CHO	Chinese Hamster Ovary
CRC	Colorectal cancer
CREB	cAMP Response Element Binding Protein
DAPI	2-(4-amidinophenyl)-1H-indole-6-carboxamidine
DEPC	Diethylpyrocarbonate
DMEM	Dulbecco's Modified Eagle Medium
DMSO	Dimethyl sulfoxide
dNTP	Deoxynucleotide triphosphate
DTT	Dithiothreitol
ECM	Extracellular Matrix
EMT	Epithelial to Mesenchymal Transition
ER	Endoplasmic Reticulum
EtBr	Ethidium bromide
FAK	Focal Adhesion Kinase

FBS	Fetal bovine serum
FFPE	Formalin-Fixed, Paraffin-Embedded
FHRK	Forkhead Box Protein
GAPDH	Glyeraldehyde-3-phosphate dehydrogenase
gDNA	Genomic DNA
GSK3β	Glycogen Synthase Kinase 3 Beta
H&E	Hematoxylin and Eosin Y
HER2	Human Epidermal Growth Factor Receptor 2
HIF-1α	Hypoxia-Inducible Factor 1 α
HRP	Horseradish peroxidase
HUVEC	Human Umbilical Vein Endothelial Cells
ITGA5	Integrin α5 (gene)
IV	Intravenous
JUP	Junction Plakoglobin (gene)
LDV	Leucine-Aspartic Acid-Valine
mAb	Monoclonal Antibody
MAPK	Mitogen-Activated Protein Kinase
MeOH	Methanol
M-MLV	Moloney Murine Leukemia Virus
MMP	Matrix Metalloproteinase
MRD	Minimal Residual Disease
MTT	3-(4,5-dimethylthiazol-2-yl)-2,5-diphenyltetrazolium bromide
MTX	Methotrexate
NF-κB	Nuclear Factor Kappa-Light-Chain-Enhancer of Activated B-cell
NPC	7-ethyl-10-[4-(1-piperidino)-1-amino]-carbonyloxycamptothecin
NTC	No Template Control
PAGE	Polyacrylamide Gel Electrophoresis
PBS	Phosphate-buffered saline
PCR	Polymerase chain reaction
PFA	Paraformaldehyde
P-gp	P-Glycoprotein

PK	Pharmacokinetic
PLL	Poly-L-lysine
PVDF	Polyvinylfluoridine
qRT-PCR	Quantitative Reverse Transcription Polymerase Chain Reaction
RGD	Arginine-Glycine-Aspartic Acid
RIE1	Rat Small Intestinal Epithelial Cell Line
RIPA	Radioimmunoprecipitation Assay
RPL27	Ribosomal Protein L27 (gene)
RPM	Revolutions per minute
RTK	Receptor Tyrosine Kinase
SCLC	Small Cell Lung Cancer
SDS	Sodium Dodecylsulfate
SEM	Standard Error of the Mean
Shc	Src Homology 2 Domain Containing Transforming Protein 1
SN-38	7-Ethyl-10-hydroxy-camptothecin
SNAI1	Snail Family Zinc Finger 1 (gene)
SNAI2	Snail Family Zinc Finger 2 (gene)
SRC-1	Steroid Receptor Coactivator 1
TBS-T	Tris-buffered saline, 0.1% tween-20
TJP1	Tight Junction Protein 1 (gene)
TNFα	Tumour Necrosis Factor Alpha
TopoI	Topoisomerase I
TWIST1	Twist-Related Protein 1 (gene)
uPA	Urokinase-type Plasminogen Activator
VIM	Vimentin (gene)
Wnt	Wingless Type
ZEB1	Zinc Finger E-Box Binding Homobox 1 (gene)
ZEB2	Zinc Finger E-Box Binding Homobox 2 (gene)
Zeb-2	Zinc Finger E-Box Binding Homobox 2 (protein)

Tables and figures

Chapter 1: Introduction

1.1 Colorectal Cancer

1.1.1 Background

Malignancies that originate in the epithelial cell layer of the colon or rectum are collectively known as colorectal cancers (CRCs). These cancers represent a significant disease burden as the most recent available data indicates that CRC is second only to lung cancers as a cause of cancer-related deaths among Canadians[1]. This is partially due to the high prevalence of the disease, as CRC is the second and third most commonly diagnosed form of cancer in male and female Canadians respectively[1]. A decline in the incidence and increase in relative survival has been observed for CRC in recent years, however these observations are generally attributed to improved screening for early-stage tumours rather than improved therapies[1]. There is therefore a significant need for improvement at the treatment stage of CRC management.

1.1.2. Colorectal Cancer Therapy

The recommended treatment(s) for CRC is largely dependent upon the stage at which the disease is detected and diagnosed. Pre-cancerous polyps and very early stage tumours are often curable with surgical resection of the neoplasm, without any requirement for adjuvant (post-surgery) chemotherapy. However as the cancer progresses into a later stage, the addition of chemotherapy offers a potentially significant survival benefit, as has been demonstrated in a number of large-scale clinical trials at various stages and using different chemotherapy regimens[2–6]. The backbone of most CRC chemotherapy regimens is 5-fluorouracil (5-FU)[7]; a uracil analogue which has numerous activities, including inhibition of thymidylate synthase (TS) and incorporation into RNA (reviewed in [8]). 5-FU is usually administered in combination with

leucovorin, which enhances the activity of 5-FU by increasing the available 5'-formyltetrahydrofolate within the cell[8]. Clinical trials have demonstrated a survival benefit in CRC patients treated with 5-FU, with or without leucovorin[2,4,5]. Very advanced CRC patients are often treated with another chemotherapy agent, in addition to 5-FU and leucovorin, oxaliplatin[7]. Oxaliplatin is a platinum-based drug which is thought to form adducts with cellular DNA, causing lethal damage to the cell[9]. The addition of oxaliplatin to a CRC treatment regimen has been validated in several very large clinical trials to significantly improve patient survival[10,11]. The third main chemotherapy agent used in treating CRC is irinotecan, a topoisomerase I (TopoI) inhibitor that has demonstrated efficacy in treating very advanced and metastatic CRC, including in patients for whom 5-FU has failed[12–14]. Chemotherapy may also provide a palliative benefit in patients with very advanced, disseminated disease where a curative approach is not feasible[7,14–16]. Chemotherapy agents are therefore essential to adequately treat advanced, aggressive CRCs.

1.2 Irinotecan and Topoisomerase Inhibitors

1.2.1 Camptothecin Family

Irinotecan is a derivative of the natural product alkaloid camptothecin, which was originally isolated from the bark of the *Camptotheca acuminata* tree[17]. Camptothecin and its derivatives exert their anti-cancer effects

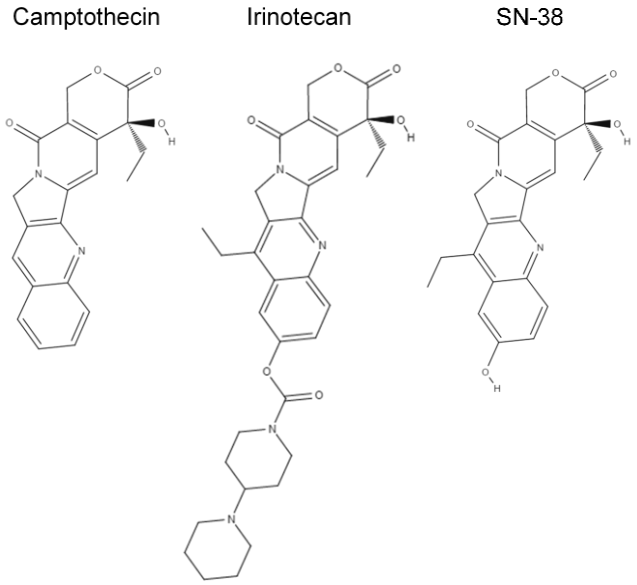

Figure 1.1: Camptothecin family of TopoI inhibitors.

The chemical structures of camptothecin, irinotecan, and SN-38 are shown above. Images were constructed using the open source web-based program MolView.

through inhibition of TopoI[18]. DNA transcription and replication require the separation of the two DNA strands, which introduces supercoiling into the molecule. TopoI enzymes are able to introduce single strand breaks into DNA, which allow unwinding to occur and relieve the supercoiling-induced strain. TopoI is then able to repair the DNA break it previously introduced[19].

Camptothecin family members poison TopoI activity by stabilizing the TopoI-DNA interaction, forming a "cleavable complex" and preventing repair of TopoI-introduced single strand breaks[18]. During DNA synthesis, advancing replication forks collide with these trapped cleavable complexes and convert them into double strand DNA breaks, which is lethal to the cell[20–22]. TopoI's mechanism of action and inhibition by camptothecins is outlined in figure 1.2.

The dependence on DNA synthesis to generate DNA damage with camptothecin treatment is supported by observations that camptothecin treatment mostly targets cells in the S-phase of the cell cycle, and that the effects of camptothecins can be blocked by simultaneous treatment with inhibitors of DNA synthesis[23,24]. More recent studies however have demonstrated that camptothecins are also capable of inducing apoptosis in quiescent, non-dividing cells such as neurons[25]. This non-S-phase cytotoxicity likely involves camptothecin-mediated inhibition of transcription elongation, which has been previously observed[26] and is probably a result of a collision between trapped TopoI and RNA polymerase II on the template strand[27].

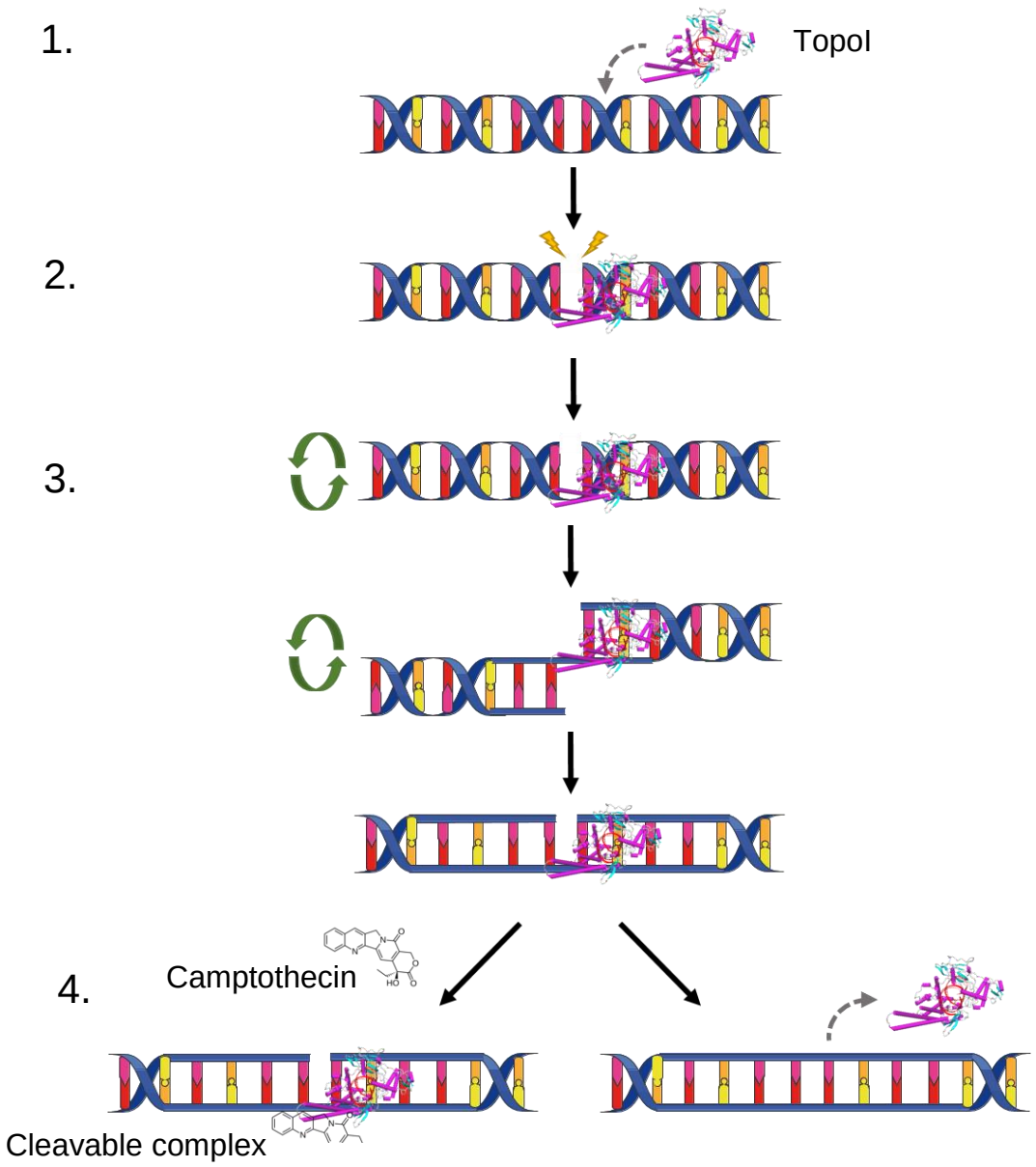

Figure 1.2: TopoI-mediated removal of torsional strain in DNA.

1. TopoI binds to DNA experiencing torsional strain during replication or transcription.
2. The TopoI enzyme introduces a single strand break in the DNA.
3. DNA rotates around the single strand break to unwind and relieve the torsional strain.
4. TopoI repairs the single strand break and separates from the DNA. Camptothecin blocks the repair and traps TopoI on the DNA.

These images are adapted from Servier Medical Art by Servier, licensed under CC BY 3.0. TopoI ribbon structure generated by the open source software MolView.

1.2.2. Use of Irinotecan in Colorectal Cancer Therapy

Camptothecin's development into an anti-cancer agent was unfortunately limited by its poor solubility and excessive toxicity (reviewed in [28]) and so derivatives of camptothecin were developed instead. One such derivative that retained camptothecin's powerful anti-cancer properties while being better tolerated and more soluble was the aforementioned CRC chemotherapy agent, irinotecan[29]. Despite impressive activity against murine tumours, it was demonstrated that irinotecan had little direct anti-cancer activity; the *in vitro* half-maximal concentration (EC50) (i.e. the concentration of the compound that elicited a response halfway between the baseline and maximum possible response) of irinotecan was found to be >1000-fold that of camptothecin[30]. However, incubating irinotecan in mouse serum or tissue homogenate resulted in the conversion of the drug to a metabolite, 7-ethyl-10-hydroxycamptothecin (SN-38) which showed anti-cancer effects of similar potency to camptothecin itself[30]. Further studies confirmed the metabolism of irinotecan to SN-38 in human serum[31], as well as identified its conversion within the liver[32], small intestine (and to a lesser degree, the colon)[33], and even by select cancer cell lines[34] by carboxylesterase (CE) eznymes[35].

Irinotecan metabolism *in vivo* is complex. SN-38 is further metabolised within the liver by conjugation to a glucuronic acid moiety to form SN-38 glucuronide (SN-38G)[36–38], a step which is believed to aid in detoxification and excretion of the drug[39]. SN-38G may however be converted back to active SN-38 to a significant degree within the lumen of the ileum and colon by β-glucuronidases produced by the resident microflora[40]. This reclaimed SN-38 appears to contribute to the toxic side effects of the drug, which centre around gastrointestinal distress involving diarrhea[40]. Irinotecan may also be converted to two additional inactive derivatives by cytochrome P450 (CYP) enzymes in the liver, mostly CYP3A4. These derivatives are called 7-

ethyl-10-[4-N-(5-aminopentanoic acid)-1-piperidino] - carbonyloxycamptothecin (APC) and 7-ethyl-10-[4-(1-piperidino)-1-amino]-carbonyloxycamptothecin (NPC). SN-38, SN-38G, and irinotecan may all be excreted through the biliary system into the intestines by p-glycoprotein (P-Gp) and canilicular multispecific organic anion transporter (cMOAT) enzymes[35]. Excretion of irinotecan and its metabolites mainly occurs in the feces, followed by the urine[41]. The *in vivo* metabolism of irinotecan as well as its major clearance routes are outlined in figure 1.3.

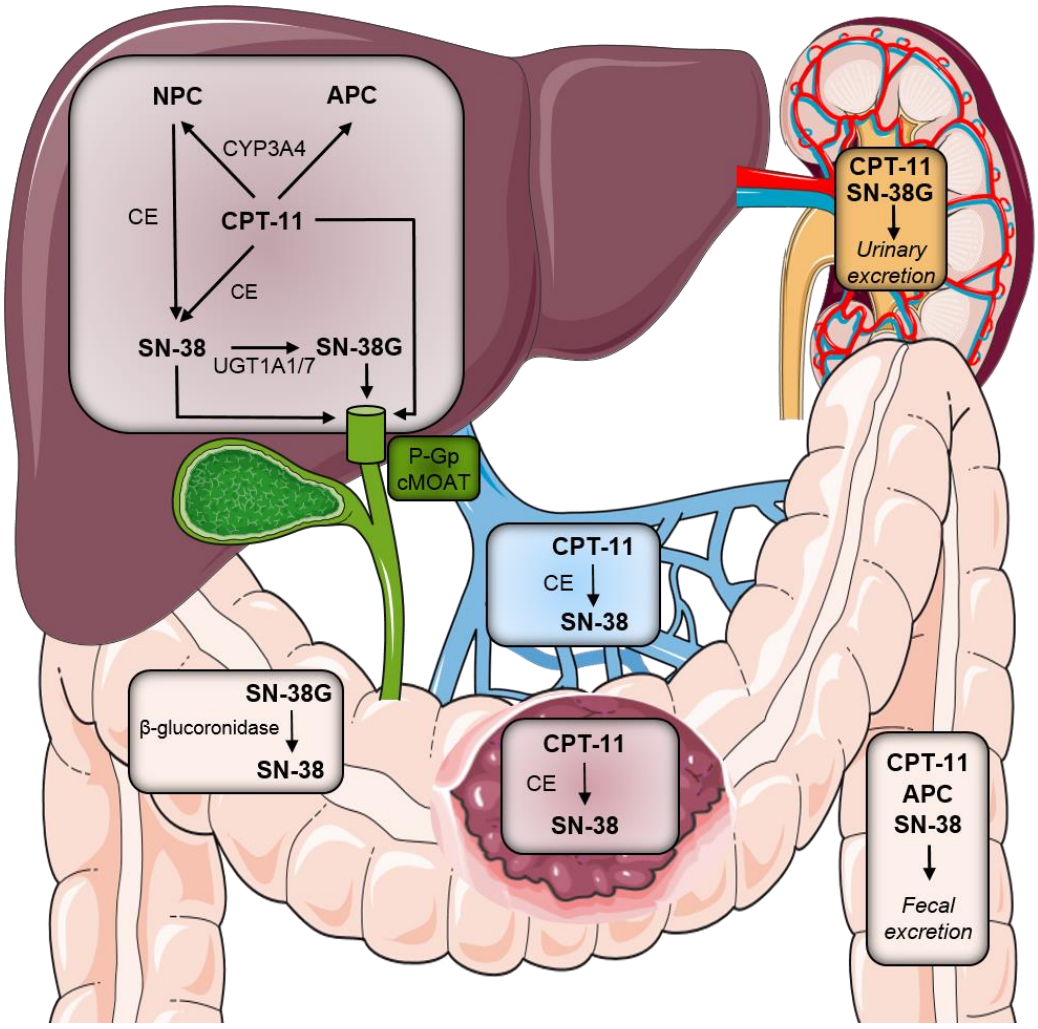

Figure 1.3: Irinotecan metabolism and excretion.

Pharmacokinetics of irinotecan (CPT-11) *in vivo* after intravenous administration. CPT-11 and its metabolites are shown in bold, clearance routes in italics, and proteins in normal font.

These images are adapted from Servier Medical Art by Servier, licensed under CC BY 3.0.

1.3 Chemotherapy Resistance

1.3.1 Common resistance mechanisms

Although chemotherapy has well-demonstrated benefits in the management of advanced CRC, these benefits typically only translate to a moderate improvement in survival. For example, the IMPACT study on 5-FU and leucovorin adjuvant chemotherapy in Dukes stage B and C CRC patients found that the chemotherapy-treated patients had a one-year survival of 83% versus 78% in the untreated group[2]. A similar pattern can be observed for all available chemotherapy agents or regimens; survival may be improved but a substantial number of patients will still relapse or fail to respond to therapy. Even patients who experience a complete response as diagnosed by X-ray computed tomography (CT) or other imaging techniques often retain viable cancer cells at disease sites, called minimal residual disease[42]. These cells may remain dormant during chemotherapy and for a period time afterwards, but eventually (up to months or years later) awaken and proliferate, causing recurrent tumours that are often more resistant to chemotherapy[43]. Furthermore, although chemotherapy improves survival of CRC patients, those who experience recurrence after chemotherapy face a worse prognosis than patients who were originally treated with surgery alone[44]. The development of new treatment options to specifically target these resistant populations would substantially improve patient outcomes, and so there is a pressing need to understand the changes that occur within cancer cells upon achieving chemotherapy resistance.

One common mechanism for drug resistance in cancer cells is the upregulation of efflux pump proteins, such as P-gp encoded by the *MDR1* gene[45]. P-gp and other efflux pumps are able to transport a wide variety of compounds from the cytosol to the extracellular space or into lysosomes, including some chemotherapy drugs[45,46]. By removing a drug from the cell, efflux

pumps can block their activity and thus promote drug resistance. Evidence exists that efflux pump-mediated resistance is clinically relevant; an analysis of acute myeloid leukemia (AML) patients at the time of diagnosis and disease relapse found a gene-level upregulation of the breast cancer resistance protein (BCRP) efflux, occurred with disease progression[47].

Specific inhibitors of the various drug-efflux pumps have been developed in an attempt to improve patient response to chemotherapy, especially against refractory cancer. Despite promising pre-clinical data however, three successive generations of these inhibitors have failed to demonstrate a survival benefit for patients (reviewed in [48]). Among the possible explanations for the disappointing clinical performance of these inhibitors is that alternative drug-resistance programs are alternatively or concurrently active in these advanced, chemo-refractory cancers. The strong influence of the local microenvironment on a cancer cell's behaviour suggests that the microenvironment may be one of these alternative contributing factors to chemotherapy resistance, and so we examined the effects of the microenvironment on the behaviour of our SN-38-resistant CRC derivatives. We were particularly interested in one component of the tumour microenvironment: the extracellular matrix (ECM).

1.4 The Extracellular Matrix

1.4.1 Extracellular Matrix Background

ECMs are complex interwoven networks formed from a large and diverse family of proteins and proteoglycans (reviewed in [49]).~~THey~~ They contribute to many important connective tissues, including bone, basement membranes, cartilage, and interstitial tissues[49]. There is a great deal of variety between the types of ECM proteins produced across metazoa, however every animal appears to produce at least a few ECM molecules. *Drosophila melanogaster* and *Caenorhabditis elegans*, for example, express the "core" basement membrane proteins type IV

collagen, laminin, entactin, and perlecan-type proteoglycans, but do not express the ECM glycoprotein fibronectin, which is found in humans and other vertebrates[50]. Even sponges express some collagens and other ECM-associated proteins[51], although these are apparently much simpler than the ECMs found in higher animals.

The traditional earlier view of the basement membrane and other ECMs in relation to cancer was that of a barrier against invasion and metastasis. While this is certainly one of the functions of the ECM that is relevant to the progression of the disease, it is becoming increasingly apparent that ECM proteins may have additional pro-cancer functions as well. The ECM glycoprotein fibronectin is an excellent example of this, as fibronectin upregulation in breast and colon cancers has been associated with disease progression, relapse, and poor overall survival[52–54].

1.4.2 Fibronectin

Fibronectin was discovered as a fibroblast-derived protein in a pair of publications released in 1973, by Erkki Ruoslahti and Richard Hynes. The former demonstrated that chicken fibroblasts produced a surface antigen that was also remarkably abundant in the animal's serum[55], while the latter published a set of radiolabelling experiments identifying a large extracellular protein in hamster and human fibroblast cell lines[56]. Fibronectin was at this point known by a variety of names, includes "large, extracellular, transformation-sensitive" (LETS) and "soluble fibroblast surface antigen" (SFA) but the precise nature of the protein was not well understood[57,58].

Electron microscopy and immunofluorescence experiments on the newly-discovered ECM protein revealed its fibrous nature[59], and a co-localization of these extracellular fibres with

actin microfilaments within the cytosol[60–62], suggesting a functional link between the two. This link was proposed to be an integral membrane protein connecting fibronectin fibrils and the actin cytoskeleton[58]. It is now known that the integrin family of cell surface receptors establishes this link between fibronectin (along with other ECM proteins) and the cytoskeleton.

1.5 Integrin Family of Cell-Surface Receptors

1.5.1 Discovery of the Integrin Family

Several years after the discovery of fibronectin, it was demonstrated that a certain antibody against the "cell substrate attachment" (CSAT) antigen was capable of blocking the adhesion of cells to fibronectin and other ECM proteins[63]. The CSAT antibody, when coated onto the wells of a tissue culture plate, was also capable of promoting adhesion of cells to the plate[63]. This suggested that the CSAT antigen was not on the ECM proteins themselves but was instead a receptor expressed on the cell surface. This hypothesis was confirmed when the CSAT antigen was successfully cloned and demonstrated to be a transmembrane protein[64]. The new protein was named "integrin" (now known as integrin β1) to reflect its status as an integral membrane protein. Homologues of integrin had already been suggested and were very soon also cloned, starting with integrin β2 from leukocytes and splenic tissue[65,66]. Thus, the integrin superfamily of transmembrane ECM receptors was born.

1.5.2 Function of the Integrins

As integrins are the primary receptors for the various constituents of the ECM, it is not surprising to learn that they are also highly conserved across the metazoa. Genetic studies have demonstrated the existence of integrin homologues in drosophila, nematodes, coral, and sponges[50,67]. Much like the limited repertoire of ECM components in these lower animals however, there are far fewer integrin family members in these organisms than are found in

mammals and other vertebrates; humans have 18 known integrin α subunits, compared to five in drosophila and only two in nematodes[50]. Possible homologues to animal integrins have been detected in a protist species believed to be ancestral to animals and fungi, suggesting that integrins first developed in these species and were subsequently lost in fungi and other non-animal descendants[68].

It is now known that integrins function as are heterodimers formed from an α and β subunit; different combinations of subunits create distinct receptors with particular sets of ligands, tissue tropisms, and downstream functions[69,70]. Integrin heterodimers not only anchor cells to particular ECM substrates, but also transduce information about the extracellular environment across the membrane to the interior of the cell, initiating intracellular signalling pathways and altering cellular behaviour.

1.5.3 Inside-out versus Outside-in Signalling

In contrast to the classical "outside-in" pathway, it is also possible for integrins to transmit information about a cell's current state to the extracellular environment in a reversed, "inside-out" fashion. Intracellular events can "activate" an integrin dimer by introducing conformational changes that alter the affinity of the receptor for its ligands[71]. In the low affinity, inactive state, the β-subunit is tilted towards the α-subunit in a stable conformation maintained by intramembrane bonds between the two[71]. Activation of the integrin involves shifting of the β-subunit away from the α-subunit to form the high-affinity "active" receptor[71]. Certain adapter proteins that interact with the cytoplasmic tail of the β-integrins, such as talin or the various kindlin kinases, appear to be involved in the activation process as overexpression of these proteins can result in spontaneous integrin activation[72–74]. Inside-out signaling is important for many cellular events, such as leukocyte diapedesis in response to inflammation[75] (reviewed in [76])

or response to DNA-damage induced by ionizing radiation or bacterial genotoxins[77]. It is therefore important to remember that integrin activity may be as much of an expression as it is a determinant of a cell's behaviour.

1.5.4 Influence of Integrins on Cell Behaviour

As a highly conserved family of proteins with many different members, it is not surprising that integrins have important and far-reaching effects on cellular behaviour. These effects range from anchoring epithelial sheets to basement membranes, promoting the normal development of tissues, directing wound-healing in damaged tissues, and even controlling the migration of normally non-adherent cells such as leukocytes. Part of the reason for the wide variety of integrin functions is the large size of the family; mammals have 18 α and 8 β subunits forming 24 known heterodimers. Furthermore, any one of these heterodimers can have multiple ligands and effects on cell behaviour. As an example, integrin α9β1 has been demonstrated to promote the differentiation of hematopoietic stem cells in response to cytokines[78], to coordinate embryonic lymphatic leaflet development in concert with a splice variant of fibronectin[79], to promote nitrous oxide formation that enhances cellular migration[80], and to support lymphocyte egress from lymph nodes under inflammation, without being expressed on the lymphocytes themselves[81].

1.5.5 The Role of Integrins in Cancer

Many of the conventional functions of integrins, such as promoting cell migration or survival, are also functions that are frequently co-opted by a tumour to promote its own growth or to enable aid in metastasis. For example, both of the integrin receptors α2β1 and α5β1 can promote CRC metastasis to the liver through interactions with their ECM ligands, type IV collagen and fibronectin respectively[82–84], and the αVβ3 receptor for vitronectin has been

demonstrated to promote breast cancer invasion and metastasis *in vitro* and *in vivo*[85]. However, integrin αVβ3 also serves of an example of the anti-cancer roles this family can fulfill. Despite promoting metastasis, αVβ3 can supress cancer cell proliferation and tumour size, and its expression is repressed by the well-established pro-cancer MYC protein[85]. Some integrins may act in opposition to each other, and in certain cases this is relevant for tumour progression. For example, integrin α5β1has been demonstrated to promote cancer cell invasion through secretion of various MMPs, including MMP1 and 9[86,87]. This can be prevented however by the activity of another integrin receptor, α4β1 which also binds fibronectin but at a separate site from α5β1[86,87]. Of the many pro and anti-cancer effects that may be mediated through integrins, the effect of integrin-ECM interactions on cell survival is of particular interest in cancer.

1.5.6 Cell Adhesion-mediated drug resistance

Integrin-ECM interactions may supress a specialized form of apoptosis called anoikis, which occurs in epithelial cells that lose their normal attachments to the underlying basement membrane ECM[88]. This function serves as a safeguard against cancer development; epithelial cells that detach from the basement membrane will normally undergo anoikis instead of settling and potentially expanding in a foreign tissue site. It is becoming increasingly clear however that the survival signals provided by an integrin-ECM interaction may be co-opted by cancerous cells to protect against other stressors, and many types of cancer have now been shown to resist cytotoxic chemotherapy when provided with the opportunity to form adhesions to ECM proteins. This co-opting of ECM-derived survival signals is known as cell adhesion-mediated drug resistance (CAM-DR). For example, small cell lung cancer (SCLC) cells provided with an exogenous source of the ECM proteins fibronectin or laminin show an increased resistance to a number of chemotherapy agents, including etoposide, cis-platinum, and doxorubicin, as well as

to ionizing radiation[89,90]. This effect occurred through prevention of apoptosis induction by activation of a phosphoinositide-3-kinase (PI3K)/glycogen synthase kinase 3 beta (GSK3β) pathway and was not achieved with poly-L-lysine, a non-ECM-derived adhesive substrate[90]. Similarly, AML cells provided with exogenous fibronectin were more resistant to the chemotherapy drug daunorubicin through a PI3K/GSK3β but not focal adhesion kinase (FAK) dependent pathway, an effect which was attributed to the α5β1 and α4β1 integrins[91]. Integrin α4β1 may also contribute to cytosine arabinoside (AraC) resistance and minimal residual disease following therapy in AML patients by supporting survival of leukemic cells in the bone marrow stroma[92]. Stratifying AML patients by their α4β1 status revealed that α4β1-negative patients had a significantly better overall and disease-free survival than α4β1 positive patients[92]. Adhesion of multiple myeloma cells to fibronectin promoted resistance to doxorubicin, and serial passage of myeloma cells in the presence of doxorubicin or the alkylating agent melphalan generated resistant derivatives to these drugs that had an enhanced expression of the integrin α4, β1, and β7 subunits[93]. Notably, the resistance programs in these cells did not appear to involve the drug pumps described in section 1.3.1, as there was no observed change in intracellular drug accumulation or efflux[93]. Ovarian and breast cancer cells challenged with docetaxel were also able to partially resist the cytotoxic effects of the drug when allowed to adhere to fibronectin through activation of Akt and upregulation of the anti-apoptotic protein, survivin[94]. However, the cellular receptor involved in mediating this effect was not identified by the study[94]. Another series of experiments in ovarian cancer cells showed that knockdown of the β1 integrin could enhance the anticancer effects of bevacizumab by supressing a FAK/signal transducer and activator of transcription 1 (STAT1) signalling pathway[95]. In this case however, the authors did not identify the α integrin subunit(s) or ECM components involved[95]. Thus, while there is data

supporting CAM-DR as a powerful mode of chemotherapy resistance in several types of cancer, many studies have failed to fully identify the integrin subunits and ECM proteins involved. Furthermore, CAM-DR has often been studied in the context of transient, spontaneous resistance upon provision of exogenous ECMs, rather than as an acquired trait. The role of CAM-DR has also not been adequately studied for all types of cancer or chemotherapy agents, including CRC and irinotecan.

1.6 Integrin α5

1.6.1 Background

One integrin subunit that has recently garnered significant attention in cancer is α5, which forms a single known heterodimer in humans with the β1 integrin subunit. The α5β1 heterodimer is also known as the primary fibronectin receptor, and it interacts with fibronectin at an arginine-glycine-aspartic acid (RGD) motif present in the tenth type III repeat with relatively low affinity [96,97]. Several other integrins are also able to bind this motif in fibronectin and other ECM proteins in a similar RGD-dependent manner, including αV, α8, and αIIb-containing heterodimers, although some other integrins known to bind fibronectin *in vivo* do so at a separate, non-RGD site within the glycoprotein(reviewed in [98]). An example of this is α4β1, which binds fibronectin at the C-terminal connecting segment 1 (CS-1) site to leucine-aspartic acid-valine (LDV) motif[86,87,98]. Although α5β1 is not unique in its ability to bind fibronectin, or even the domain which it binds to, its interaction with fibronectin is substantially different from most integrins. The α5β1 receptor is (unlike other fibronectin-binding receptors such as αvβ1 or αβ3) able to construct a fibronectin matrix from soluble, folded-up fibronectin dimers[99–102]. The conversion of fibronectin into a fibrous matrix by integrin α5β1 requires the application of tension to unfold the soluble fibronectin dimers, and may be supported αVβ3 “anchoring” the

cell via an interaction with another ECM protein, vitronectin[103]. It has also been shown that the G-protein coupled receptors (GPCR) may be able to promote fibronectin matrix assembly via inside-out activation of integrin α5β1[104]. Normal colonic epithelial cells express abundant integrin α5, but the expression of this and other integrin subunits appear to be progressively lost along malignant transformation[105].

1.6.2 Anti-Cancer Effects of Integrin α5β1

Like many of the integrins, the role of α5β1 in cancer has been somewhat controversial or unclear. Ectopic expression of integrin α5 in the Chinese hamster ovary (CHO) cell line resulted in an increased accumulation of pericellular fibronectin as well as increased adhesive capacity for fibronectin, but seemingly at the cost of many pro-cancer characteristics[106]. The transfected CHO cells proliferated at a lower rate, became growth arrested at lower cell densities, and were less capable of forming tumours when introduced into nude mice[106]. Other studies have confirmed that the overexpression of integrin α5 in cancer cell lines can repress the malignant behaviours of these cells. Integrin α5 was found to be highly expressed in the non-metastatic 67NR breast cancer cell line, and poorly expressed by highly metastatic 4T1 breast cancer cells[107]. Overexpression of integrin α5 in 4T1 reduces the migration, invasion, and pulmonary metastasis of these cells, and transfection of α5 into these cells results in G1/S checkpoint arrest[107]. A similar suppression of cellular proliferation was observed by overexpression of integrin α5 in the CRC cell line HT-29, which does not usually express this subunit[108,109]. Aggressiveness of the cancer seemed to also be attenuated with forced integrin α5 expression; a significantly higher inoculum of α5-expressing HT-29 cells than parental cells were required to form tumours upon subcutaneous injection into nude mice, and the tumours that did form from α5-expressing cells were much more well-differentiated[108]. Interestingly, both of these studies

observed that many of the cancer-suppressing features associated forced integrin α5 expression could be reversed by allowing the cells to adhere to fibronectin[108,109]. More recently and in line with these results, a mass spectrometry-based proteomic study of formalin-fixed, paraffin-embedded (FFPE) samples from 30 CRC patients at different stages demonstrated a decrease in integrin α5 expression during CRC progression[110]. Overall, there is a strong case for the anti-cancer effect of integrin α5.

1.6.3 Pro-Cancer Effects of Integrin α5β1

In direct contrast to the preceding results, significant evidence has also accumulated in support of a pro-cancer role for the primary fibronectin receptor. Although reduction in integrin α5 expression has been observed by some studies during CRC progression, CRC cell lines stratified into groups by their aggressiveness show a substantial difference in integrin α5 expression with the highly-aggressive CRC cell lines expressing abundant integrin α5[111]. It was also shown ectopic expression of integrin α5 in one of the less aggressive cell lines, GEO, caused it to become significantly more aggressive upon xenografting into nude mice[111]. Importantly, the cell line HT-29, for which integrin α5-mediated inhibition of proliferation and aggression was observed, was not included in this study. Recently, the pro-invasive effects of the transmembrane protease, serine 4 (TMPRSS4) in SW480 CRC cells has been demonstrated to be mediated through an upregulation of integrin α5 and increased signalling from the α5β1 receptor[112]. It was further demonstrated by immunohistochemistry studies of samples from 63 CRC patients that the expression of both integrin α5 and TMPRSS4 increased with CRC stage[112]. Integrin α5β1 has also been implicated to promote cancer by supporting the generation of new blood vessels within tumours in response to various pro-angiogenic factors including basic fibroblast growth factor (bFGF) or tumour necrosis factor alpha (TNFα)[113]. Another study using human placental

multipotent mesenchymal stromal cells (hPMSCs) differentiated into endothelial-like cells has demonstrated a role for integrin α5β1 in angiogenesis through an interaction between the integrin heterodimer and fibronectin, promoting migration and capillary-like structure formation by these cells[114]. This is significant not only because angiogenesis is an essential process to tumour progression that is being targeted clinically, but also because it adds another consideration to the debate over α5β1's contribution to cancer progression. Many studies have focused on the effects of α5β1 expression on the cancer cells themselves, neglecting the possibility that α5β1 on endothelial cells of the tumour neovasculature contributes to cancer progression.

1.6.4 Integrin α5 as an Angiogenesis Target for Chemotherapy

While there is still some confusion over the precise role of integrin α5β1 in cancer progression - whether it serves a pro- or anti-cancer function when expressed in the malignant cell itself - sufficient evidence exists of the fibronectin receptor's contribution to tumour angiogenesis to have warranted development of inhibitors targeting this receptor. A challenge in developing these inhibitors is that many integrin heterodimers recognize the same RGD motif in fibronectin and other ECM proteins as integrin α5β1. However, a phage display strategy has been used to develop a cyclic peptide which binds integrin α5 with far greater affinity than other RGD-dependent integrins[115]. This peptide has been used to successfully inhibit tumour angiogenesis in the chick chorioallantoic membrane (CAM) *in vivo* model through inhibition of a fibronectin-integrin α5β1interaction[116]. Another non-RGD based peptide inhibitor of integrin α5β1called ATN-161 (Ac-PHSCN-NH_2), used in conjunction with 5-FU has been shown to reduce the expansion of liver metastases and improve survival in mice injected intrasplenically with CRC cells, apparently through an anti-angiogenic effect[117]. ATN-161 was also capable of inhibiting the proliferation of breast cancer cells introduced subcutaneously into mice, as well as

reducing the incidence and size of metastases[118]. These effects appeared to be due to the anti-angiogenic effect of the drug, as treatment with ATN-161 reduced the microvessel density within *in vivo* tumours but had no effect on the proliferation of the cancer cells *in vitro*[118]. Not all fibronectin receptor inhibitors are peptide-based; recently several monoclonal antibodies targeting this receptor have also been developed. One such agent is volociximab, a chimeric antibody based on the IIA1 mouse monoclonal antibody (mAb) targeting the intact α5β1 heterodimer (but not either subunit alone)[119]. Volociximab or its Fab region alone are capable of blocking endothelial tube formation and inducing apoptosis in dividing but not senescent human umbilical vein endothelial cells (HUVEC) *in vitro*, and in preventing *in vivo* neovascularization in a cynomolgus model[119]. Phase I clinical trials of volociximab in several advanced, aggressive solid cancers have indicated the antibody is well-tolerated at doses up to30 mg/kg, with pharmacokinetic (PK) data indicating that the trough drug concentration consistently remained above the target of 150 μg/mL in patients treated with three week cycles of 20 or 30 mg/kg volociximab[120,121]. Unfortunately, a phase II study of volociximab in highly aggressive, oxaliplatin-resistant ovarian or peritoneal cancers was terminated early due to a lack of response in the first 14 patients treated[122]. The drug was still well-tolerated however, and the authors suggest that studies of volociximab therapy in earlier stage disease or as part of a combination therapy is still warranted[122]. Another mAb targeting integrin α5β1 has been developed by Pfizer, PF-04605412, however a recent phase I study of this antibody in solid cancers was terminated early due to adverse effects and insufficient drug exposure at the maximum tolerated dose[123].

1.6.5 Integrin α5 and Cell Stress

Most efforts towards integrin α5β1 inhibitors for cancer therapy have focused on the angiogenic function of the heterodimer, however extensive evidence has suggested that integrin

α5β1 can also suppress apoptosis in response to a diverse range of stressful situations a cell may face. For example, many cell lines are dependent *in vitro* on the inclusion of serum in their culture media; extended deprivation of these cell lines from serum results in cell death. It was discovered that ectopic expression of integrin α5 in HT-29, CHO, or a normal rat small intestinal cell line (RIE1) protects these cells from apoptosis induced by serum withdrawal[124–126]. This effect was promoted by an adhesion to fibronectin and appeared to be mediated by the anti-apoptotic B-cell lymphoma 2 (Bcl-2) protein[125,126]. Importantly, this effect appeared to require the full cytoplasmic domain of integrin α5, and could not be achieved with a different fibronectin-binding integrin, αVβ1[125,126]. The protective effect of integrin α5β1 expression was not specific to serum deprivation but could also defend the cell against treatment with various cytotoxic drugs, including staurosporine (a protein kinase inhibitor) and etoposide (a type II topoisomerase inhibitor)[126]. A similar effect has been observed in breast cancer cells that upregulate integrin α5 expression dependent on the human epidermal growth factor receptor 2 (HER2) and hypoxia inducible factor 1 α (HIF-1α)[127]. The HER2 dependent upregulation of integrin α5 caused the cells to become more adhesive towards fibronectin and more resistant to a variety of insults, including serum withdrawal, hypoxia, and chemotherapy[127]. It seems likely that the protective effect of integrin α5β1, at least against chemotherapy, is mainly mediated by the upregulation of Bcl-2. This protein has been implicated in abrogating the cytotoxic effects of chemotherapy drugs like etoposide, methotrexate (MTX), or Ara-C in a wide range of cell types, including leukemia cells[128], B-cells[129], and the cervical cancer cell line HeLa[130]. Because of its ability to promote cell survival during toxic insults, it may be possible for integrin α5β1 to mediate an acquired CAM-DR program in CRC cells.

1.6.6 Integrin α5 Survival Signalling Pathways

Integrins are not receptor tyrosine kinases (RTKs) and do not possess intrinsic kinase activity themselves, but are still able to activate intracellular signalling pathways through the coupling of adapter proteins recruited to their cytoplasmic domains. The upregulation of Bcl-2 by α5β1 ligation to fibronectin requires activation of the PI3K/Akt pathway[126,131,132]. Activation of the adaptor protein Src homology 2 domain containing transforming protein 1 (Shc) and a Ras GTPase have also been demonstrated as essential for Bcl-2 expression downstream of integrin α5β1 engagement and it has been suggested that these proteins are responsible for activating PI3K[131,132]. Akt activated by PI3K in turn phosphorylates the transcription factors nuclear factor kappa-light-chain-enhancer of activated B-cells (NF-κB), cAMP response element binding protein (CREB), and a forkhead box protein (FKHR)[131]. NF-κB and CREB are activated by Akt and promote transcription from the *BCL2* gene, whereas phosphorylated FKHRs are inactive and unable to inhibit *BCL2* transcription[131]. The interaction between fibronectin and integrin α5β1 further results in the activation of FAK, which is also required for Bcl-2 expression[125,131,132]. FAK activation appears to act in parallel to the PI3K/Akt pathway, and integrin α5β1 receptors with a truncated α5 cytoplasmic domain cannot activate FAK but retain phosphorylated Akt[125,131]. Cell spreading upon adhesion to fibronectin has also been attributed to FAK[125] and may contribute to the activation of a third pathway downstream of the fibronectin-integrin α5β1 interaction that promotes Bcl-2 expression; activation of the Ca^{2+}/calmodulin-dependent protein kinase (CaMK) IV[131]. Activation of CaMK IV has previously been attributed to Ca^{2+} release

from the nucleus upon cell spreading[133] and in his system appears to activate NF-κB and CREB alongside Akt[131]. These signalling pathways are outlined in figure 1.4 below.

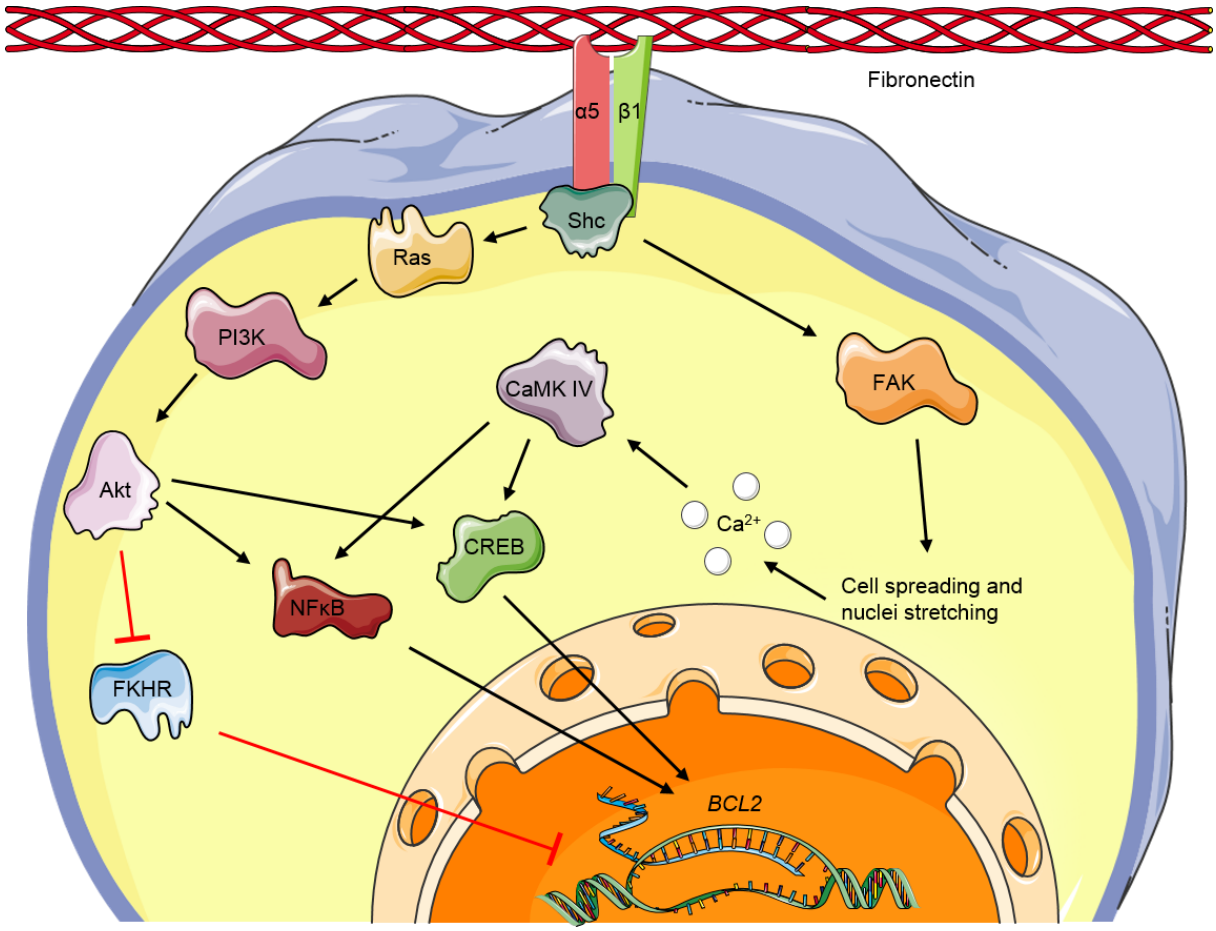

Figure 1.4: Fibronectin-integrin α5β1 pro-survival signalling.

The pro-survival pathway activated by engagement of the integrin α5β1 heterodimer with its ligand fibronectin, and terminating with expression of the *BCL2* gene. Black arrows represent activating signals while red lines represent inhibitory signals.

These images are adapted from Servier Medical Art by Servier, licensed under CC BY 3.0.

1.7 Rationale of the Project

Cancer recurrence after chemotherapy represents a major issue in CRC management as it often coincides with a reduced response to chemotherapy and more aggressive disease. Understanding the mechanisms by which resistance occurs and the changes cancer cells experience during the acquisition of resistance is therefore a high priority in developing better treatment strategies and agents. As the extracellular environment and in particular the ECM are strong determinants of cancer cell behaviour and survival, we chose to study the consequences of altered cancer cell-ECM interactions in a CRC cell line (HT-29) upon attaining a high level of resistance to the chemotherapy active metabolite SN-38. We have generated an SN-38-resistant derivative of HT-29 for this purpose (HT-29S).

Chapter 2: Objectives and hypothesis

2.1 Hypothesis

HT-29S resistance to SN-38 is mediated by upregulation of integrin α5 and the subsequent activation of a fibronectin-integrin α5β1-PI3K pro-survival pathway that promotes the expression of *BCL2*.

2.2 Objectives

1. Identify alterations in HT-29 cell interactions with the ECM upon acquisition of SN-38 resistance.
2. Identify cellular receptors involved in altered ECM interactions.
3. Determine if alterations in ECM interactions contributes to the resistant status of these cells, and by which mechanism.

Chapter 3: Methods

3.1 Cell culture

3.1.1 Generation of an SN-38-Resistant Cell Line

We have previously generated a derivative of the HT-29 CRC cell line that is highly resistant to SN-38 through sequentially increasing exposure to the drug in culture media, as outlined in figure 3.1. We have named this resistant lineage "HT-29S". Resistance in HT-29S is maintained by inclusion of 30 nM SN-38 in the media of stock cultures.

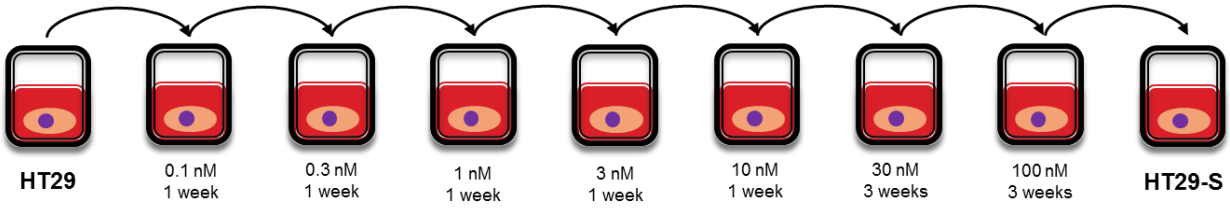

Figure 3.1: Generation of the HT-29S cell line.

Strategy for the development of the SN-38-resistant HT29-S cell line from parental HT-29 cells.

3.1.2 Routine Passaging

The CRC cell line HT29 and its SN-38-resistant derivative HT-29S were routinely grown in Nunc T25 cell culture flasks with filter caps (Thermo Scientific). Cells were cultured at 37°C in a humidified atmosphere of 5% CO_2, in Hyclone Dulbeco's Modified Eagle Medium (DMEM, Thermo Scientific) containing 4 mM L-glutamine and 4500 mg/L L-glucose, 1 mM sodium pyruvate, and 10% fetal bovine serum (FBS).To maintain drug resistance, HT29-S cell medium included 30 nM SN-38 (Sigma Aldrich). Cultures approaching confluence were passaged after being released by incubation for several minutes at 37°C with 1 mL TrypLE Express (Life Technologies). 10-15% of the resulting suspension was seeded into fresh media in a new culture vessel.

3.2 Western Blot

3.2.1 Protein Collection

Western blots were performed on whole cell protein lysates collected from HT29 or HT29-S cells using radioimmunoprecipitation assay (RIPA) buffer [table A.1]. CRC cells were seeded into the desired culture vessel and grown to approximately 80% confluence. Cells were cultured normally (see section 2.1) unless specific treatment (e.g. with PI3K inhibitors) was required. In those cases, inhibitor-treated cells were cultured in parallel with vehicle-control cultures. Upon reaching the desired confluence, medium was aspirated and the cultures were rinsed twice with an equal volume of sterile ice-cold phosphate-buffered saline (PBS) [table A.2] to remove dead cells. RIPA buffer with added HALT protease/phosphatase inhibitor cocktail (Thermo Fisher Scientific) was applied to the cultures (1 mL for a T75 flask or 240 µL per well for a 6-well plate). Cells were incubated with RIPA buffer for 30 minutes at 4°C with gentle agitation on a Rocker II model 260350 (Boekel Scientific). The resulting lysate was collected into a chilled 1.5 mL microcentrifuge tube. Complete lysis was ensured by passing the lysate through a 27 gauge needle with a 1 mL syringe several times. The lysate was subjected to one freeze-thaw cycle (-80°C to 4°C). Cell membranes were pelleted by centrifugation at 14 000 x g for 20 minutes at 4°C in a 5424R microcentrifuge (Eppendorf). The supernatant was collected and transferred to a fresh microcentrifuge tube. Protein content was determined by the Bradford assay (section 2.2.2).

For some experiments, protein lysates enriched for the cytosolic fraction were used instead of whole cell lysates. Protein samples from the nuclear and cytosolic compartments of CRC cells were collected using a nuclear extraction kit (Millipore, 2900), according to the manufacturer's directions. Cells were seeded and cultured in a T75 flask (Nunc) as described

previously, again to approximately 80% confluence. The media was then aspirated and the monolayer was rinsed with sterile ice-cold PBS. Cells were released by incubation with TrypLE for several minutes at 37°C. The resulting suspension was then passed through a 70 μm pore filter into a 50 mL Falcon tube (Corning). The culture vessel was rinsed twice with PBS, with each rinse being added to the 50 mL tube. Cells were pelleted by centrifuging the suspension at 400 x g for 5 minutes at 4°C in an Allegra X-22R centrifuge (Beckman Coulter). The supernatant was discarded, and the resulting cell pellet was rinsed twice by re-suspending in 40 mL cold PBS. Centrifugation at 400 x g for 5 minutes at 4°C was repeated. After the final wash, the cell pellet was re-suspended in 500 μL cold cytoplasmic lysis buffer by gentle inversion. The cell suspension was incubated on ice for 15 minutes. Cells were again pelleted by centrifugation at 400 x g for 5 minutes at 4°C. The supernatant was discarded, and the cells were re-suspended in 1 mL of fresh cold cytoplasmic lysis buffer. Lysis of the cytoplasmic membrane was achieved by passing the cells through a 27 gauge needle five times with a 1 mL syringe. The final ejection was into a clean 1.5 mL microcentrifuge tube. The lysed cell suspension was centrifuged at 8000 x g for 20 minutes at 4°C. The resulting supernatant, representing the cytosolic protein fraction, was collected into a new microcentrifuge tube and stored on ice. The resulting pellet contained the still-intact nuclei, which were gently re-suspended in 200 μL cold nuclear lysis buffer. Nuclear lysis was achieved by briefly pulsing the nuclear suspension five times with a probe sonicator. The lysed suspension was then incubated at 4°C with gentle agitation for 60 minutes, before centrifugation at 16 000 x g for 5 minutes at 4°C. The resulting supernatant contained the nuclear protein fraction, which was then transferred to a new 1.5 mL microcentrifuge tube and stored on ice. The protein concentrations of the collected nuclear and cytosolic fractions were

measured by the Bradford assay (section 2.2.2) before dispensing into appropriately-sized aliquots for long-term storage at -80°C.

3.2.2 Bradford Assay

The protein content of the collected protein samples was measured by the Bradford assay. A 96-well plate was loaded in triplicate with bovine serum albumin (BSA; Sigma Aldrich) standards in 20% RIPA buffer at concentrations of 0, 50, 125, 250, 375, 500, 750, and 1000 μg/mL. Protein samples were diluted 5-10 fold in MilliQ H_2O and 2-8 μL of samples were loaded in triplicate into adjacent wells on the same plate. At least two different volumes of each diluted sample was used, to improve the accuracy of the estimate. Two hundred microlitres of Bradford reagent (Coomassie Brilliant Blue G-250; Biorad) were added to each well and mixed by pipetting. Absorbance was measured at 595 nm on a M5 Spectramax spectrophotometer (Molecular devices). Protein concentrations were calculated from the standard curve generated by the known BSA standards.

3.2.3 SDS-PAGE

Proteins were separated based on molecular weight by sodium dodecyl sulphate (SDS) polyacrylamide gel electrophoresis (PAGE). Samples were prepared for SDS-PAGE by diluting all samples to an equal protein concentration in MilliQ H_2O, NuPAGE LDS sample buffer [Life Technologies, table A.3] and 50 mM (final) dithiothreitol (DTT). Diluted proteins were denatured by heating to 70°C for 10 minutes prior to loading into a 4% stacking/8% resolving polyacrylamide gel [tables 6.5 and 6.6]. Electrophoresis was performed in running buffer [table A.4] at 110V to separate the proteins by molecular weight. Separation was monitored by the migration of the phenol red and SERVA blue G250 dyes from the NuPAGE LDS sample buffer.

3.2.4 Electroblotting

The separated proteins were then transferred to a 0.2 μM polyvinylfluoridine (PVDF) membrane (Biorad) using a Trans-Blot SD Semi-dry Transfer Cell (Biorad). In preparation for transfer, the polyacrylamide gels containing the separated proteins were equilibrated and desalted in transfer buffer [table A.7] for 15 minutes prior to transferring. Extra thick blot papers (Biorad) and PVDF membranes were pre-wetted prior to transfer with transfer buffer and methanol respectively. Transfer was performed for 45 minutes at 25 volts. PVDF membranes were subsequently subjected to immunolabelling to determine the abundance of specific proteins in each sample.

3.2.4 Immunolabelling

To block non-specific binding of antibodies, PVDF membranes were blocked in tris-buffered saline with tween-20 (TBS-T) [table A.8] and 5% skim milk for one hour at room temperature, with gentle agitation. At the end of the hour, the blocking solution was poured off and the membranes were rinsed once with TBS-T before applying 10 mL of primary antibody diluted 1:500 to 1:2000 in TBS-T 1% BSA. PVDF membranes were incubated with primary antibodies at 4°C overnight with gentle agitation. For very weakly expressed proteins (e.g. phosphorylated forms of kinases) incubation was extended to approximately 40 hours. At the end of the incubation period, the primary antibody solution were removed and stored at -20°C for re-use (up to 4 times). Unbound primary antibodies were removed by washing the PVDF membranes 5 times for 5 minutes with TBS-T at room temperature with gentle agitation. Ten millilitres of species-specific horseradish peroxidase (HRP) conjugated secondary antibodies diluted 1:1000 to 1:5000 in TBS-T 1% BSA were then applied for one hour at room temperature, or overnight at 4°C for weakly expressed proteins, with gentle agitation. At the end of this

period, secondary antibodies were removed and stored at -20°C for re-use, and the membranes were again washed 5 times for 5 minutes with TBS-T at room temperature with gentle agitation, to remove unbound secondary antibodies. Antibody-bound proteins were detected by chemiluminescence generated by the HRP-conjugated secondary antibodies. The substrate for this reaction was a 1:1 mixture of luminol and peroxide from a Clarity Western ECL Substrate kit (Biorad), applied to the membrane for 5 minutes at room temperature immediately prior to detection of luminescence on an Imaging Station 4000 mm Pro camera (Kodak).

Equal loading of protein samples was validated by detection of a housekeeping protein expected to be expressed at equal levels between different cell lines. For our purposes, glyceraldehyde-3 phosphate dehydrogenase (GAPDH) was used to verify equal loading. Subsequently to detection of the protein of interest, primary/secondary antibody complexes were stripped from the PVDF membrane by incubating with 7 mL of stripping buffer (Biorad) for 7 minutes at room temperature with gentle agitation. The membranes were rinsed once with TBS-T, and blocking with TBS-T 5% skim milk was repeated as described previously. HRP-conjugated anti-GAPDH diluted 1:2000 to 1:10 000 in TBS-T 1% BSA were applied to the membranes for one hour at room temperature with gentle agitation. At the end of this period, the antibody solutions were removed and stored at -20°C for re-use, and membranes were washed 5 times for 5 minutes with TBS-T at room temperature with gentle agitation. Detection of GAPDH expression was performed by chemiluminescence as described previously.

3.3 Polymerase Chain Reaction

3.3.1 RNA Extraction

RNA extraction from adherent cell lines was performed using a GenElute^{TM} Total RNA Miniprep Kit (Sigma Aldrich). Cells were cultured in Nunc T25 flasks to approximately 70%

confluence in preparation of RNA collection. Beta-mercaptoethanol (Fisher) was added to the provided lysis solution as an inhibitor of endogenous RNase enzymes, to a final concentration of 1%. Lysis was performed directly in culture flasks by aspiration of culture medium and addition of 1 mL of the prepared lysis solution. The lysate was collected and centrifuged in a GenElute^{TM} Filtration Column at 14 000 x g for 2 minutes to remove cellular debris and to shear the genomic DNA (gDNA). A volume of 70% ethanol equal to the lysate volume was then added to the supernatant to dissolve hydrophobic components, and the resulting solution was loaded into a GeneElute^{TM} Binding Column for centrifugation at 14 000 x g for 15 seconds. During this step, RNA within the supernatant was retained by the packed silica filter of the binding column. The resulting supernatant was discarded. The column was then washed with 500 µL of the provided Wash Solution 1 by centrifugation at 14 000 x g for 15 seconds. The binding column was transferred to a new collection tube and washed with 500 µL of Wash Solution 2 (provided as a concentrate and diluted in 100% ethanol) at 14 000 x g for 15 seconds. The filtrate was discarded and an additional wash with 500 µL of wash solution 2 was performed at 14 000 x g for 2 minutes. The binding column with RNA retained within the filter was then transferred to a new collection tube. RNA was dissociated from the silica by applying 50 µL of the provided elution buffer and centrifuging the collection tube at 14 000 x g for 1 minute. Following elution, the RNA-containing solution was kept on ice to minimize degradation and loss of sample. RNA concentration was determined immediately following collection by measuring the absorbance of the sample at 260 nm using a NanoDrop® device. The purity was simultaneously assessed by the ratios of absorbance at 260 nm (RNA or DNA) to the absorbance at 280 nm (proteins) and 230 nm (organic solvents). Ratios >1.8 were considered to be acceptably pure, however with this protocol ratios >2 were usually attained. RNA was stored long-term at -80°C.

3.3.2 Reverse Transcription

All PCR experiments were performed in a 2-step protocol, which necessitated the transcription of complimentary DNA (cDNA) from RNA samples prior to amplification by PCR. Reverse transcription reactions were set up in a dedicated PCR hood (AirClean 600 PCR Workstation) to minimize the risk of introducing exogenous genetic material or nuclease enzymes into the mix. For each sample, 2.5 µg of RNA was reverse transcribed in 50 µL reactions performed in triplicate. Additionally, for each sample a mock "no-RT" reaction was performed by excluding the reverse transcriptase enzyme, in order to assess the contribution of contaminating gDNA in PCR reactions. Reactions were set-up from two master mixes. The first contained equal volumes of 0.5 µg/µL oligo dT (Invitrogen) as a primer for mRNA reverse transcription and 10 nM deoxynucleotide triphosphates (dNTP; Invitrogen). Twenty microlitres of the second master mix was required per reaction, and consisted of 10 µL 5X first strand buffer (Invitrogen), 5 µL 0.1M DTT (Invitrogen), 2.5 µL recombinant ribonuclease inhibitor (RNase out; Life Technologies), and 2.5 µL Moloney murine leukemia virus (M-MLV; Life Technologies) reverse transcriptase. For the no-RT controls, a separate master mix 2 was prepared with the M-MLV reverse transcriptase replaced by diethylpyrocarbonate (DEPC; Life Technologies)-treated H_2O. A volume of each sample containing 2.5 µg RNA was added to a PCR reaction tube diluted in DEPC-treated H_2O to a final volume of 25 µL. Five microlitres of master mix 1 was then added to the tube. The reaction tubes were capped and transferred to a Techne Genius Thermocycler® to be incubated at 65°C for 5 min. The tubes were then chilled on ice for 15 seconds before adding 20 µL of master mix 2. Tubes were returned to the thermocycler and run at 37°C for 50 minutes followed by 70°C for 15 minutes. The final reaction contained cDNA at a concentration of 50 ng/µL RNA-equivalents, and was stored at -80°C.

3.3.3 Primer Design

Many of the primer pairs used to perform the polymerase chain reaction (PCR) experiments described here were newly designed. Primer design was assisted through the use of several openly-available online resources, including PrimerBLAST from the National Center for Biotechnology Information (NCBI), OligoAnalyzer from Integrated DNA Technologies (IDT), and in silico evaluations from RTPrimerDB. Primer pairs intended for use in quantitative reverse transcription PCR (qRT-PCR) formats were designed according to a very stringent set of characteristics to ensure high-efficiency amplification of target sequences, based on recommendations from commercial suppliers of qPCR reagents and equipment[134–136]. The specifications used to guide the design of primer pairs are listed in table A.16. All primers were ordered from Life Technologies.

3.3.4 Endpoint PCR

To minimize the risk of contamination with exogenous genetic material or nuclease enzymes, all PCR reactions (endpoint and real-time) were set-up in a dedicated PCR hood (AirClean 600 PCR Workstation). For both endpoint and qRT-PCR reactions, a master mix was prepared for each pair of primers in nuclease-free 1.5 mL polypropylene tubes. For endpoint PCR reactions, master mixes consisted of 9.5 μL nuclease-free H_2O, 0.5 μL 10 μM each of forward and reverse primers (final concentration of 200 nM each), and 12.5 μL GoTaq Green Master Mix (Promega, contains *Taq* DNA polymerase, dNTPs, $MgCl_2$, reaction buffers, and loading dyes) per reaction. 23 μL of master mix was loaded into PCR reaction tubes for each sample. Each reaction was then loaded with 2 μL of sample cDNA (equivalent to 100 ng of total RNA). No template control (NTC) reactions were also performed using 2 μL of nuclease-free H_2O in place of cDNA. The reaction tubes were then sealed and transferred to a Techne Genius

Thermocycler® to be run under the following cycling conditions: 94°C for 75s (initial denature) followed by 36 cycles of 94°C for 45s (denaturation), 65°C at 45s (annealing), and 72°C for 60s (extension), finishing with a 10 min hold at 72°C (final extension).

To visualize reaction products, 5 μL of each reaction was loaded into a 1% agarose gel containing 0.2 μg/mL ethidium bromide (EtBr). Electrophoresis was performed at 94 volts for 30 min, with progress monitored by the loading dyes present in the GoTaq master mix. Upon completion, gels were imaged on an AlphaImager HP gel imaging system (Alpha Innotech) for EtBr fluorescence stimulated by ultraviolet light.

3.3.5 qRT-PCR

SYBR-green based chemistry was used to quantitatively measure gene expression by qRT-PCR. However, prior to performing a qPCR reaction, all primer pairs to be used were validated for the production of a single amplicon of the correct length by endpoint PCR, as described in section 3.3.4. Similar to endpoint PCR experiments, qRT-PCR reactions were set-up in a dedicated PCR hood (AirClean 600 PCR Workstation) by preparing a master mix for each set of primers. Each master mix was composed of 12.5 μL 2X Brilliant II SYBR green master mix (Agilent; used for *BCL2*, *ITGA5*, and *ZEB2*) or 12.5 μL 2X GoTaq qPCR master mix (Promega; used for *JUP*, *SNAI1*, *SNAI2*, *TJP1*, *TWIST1*, *VIM*, and *ZEB1*), 0.5 μL each of 10 μM forward and reverse primers (final concentration of 200 nM), 0.25 μL reference dye (Rox for the Agilent master mix, CXR for the Promega master mix), and 6.25 μL nuclease-free H_2O (Promega) per qRT-PCR reaction to be performed. Reactions were performed in a 96-well semi-skirted qRT-PCR plates (Thermo Scientific) with 20 μL of master mix and 5 μL of cDNA diluted tenfold in nuclease-free H_2O (25 ng RNA-equivalents) per well. Each sample was assayed in triplicate and with no-RT mock reactions as a control against fluorescence signals

from contaminating exogenous or unsheared gDNA. Reactions were mixed by pipetting and sealed with a clear adhesive plate seals (Thermo Scientific). The sealed plate was then placed in a StepOnePlus Real-Time PCR System (Applied Biosystems) and run under the manufacturer-recommended cycling conditions: hot-start at 95°C for 2 minutes (Promega kit) or 10 minutes (Agilent kit) followed by 40 cycles of 95°C for 15 seconds (Promega kit) or 30 seconds (Agilent kit) (melting) then 60°C for 60 seconds (annealing and extension), with SYBR fluorescence read between every cycle. Immediately after all 40 cycles were completed, a melt curve was performed. StepOnePlus's associated software used the melt curve data to generate a derivative fluorescence versus temperature plot, which was used to confirm the absence of multiple amplification products or primer-dimer contributions to SYBR fluorescence.

Amplification data from the qRT-PCR reaction was exported from the StepOnePlus software into a Microsoft Excel file for further analysis. Raw, baseline-unadjusted fluorescence data was analyzed for reaction efficiency and failure to reach the plateau phase using the LinRegPCR software, validated and described elsewhere[137,138]. For each reaction, a relative initial mRNA concentration (N_0) value (in arbitrary fluorescence units; AFU) was determined by LinRegPCR using the equation in figure 3.2.

$$N_O = {}^{N_{C_q}}\!/_{Eff^{C_q}}$$

Figure 3.2: Calculation of initial mRNA abundance.

The initial abundance of a particular mRNA species was estimated from the fluorescence at the quantification cycle ($N_{C}q$), the reaction efficiency (Eff), and the quantification cycle (C_q) number. This analysis was performed with the LinRegPCR software[137,138].

A threshold fluorescence value significantly above the fluorescence baseline was determined by LinRegPCR for each amplicon group, and the cycle at which a particular reaction achieved this fluorescence threshold was the C_q for that reaction. The fluorescence at C_q was the N_{C_q}, expressed in arbitrary fluorescence units (AFU). The efficiency of each individual reaction was determined by LinRegPCR through linear regression of the log fluorescence versus cycle number during the exponential phase of the reaction. A mean efficiency (Eff) was calculated for each amplicon group and used in the determination of $N_{O.}$

3.4 Immunofluorescence

3.4.1 Monolayer Immunofluorescence

Expression and localization of proteins within CRC cells was performed by immunofluorescence on cells grown on Nunc Lab Tek II chamberslides (Thermo Scientific). Chamber slides were prepared a day in advance of seeding by applying 300 µL of 10 µg/mL poly-L-lysine (PLL; Sigma Aldrich) for 10 minutes at 37°C. PLL was then aspirated from the wells and chamber slides were left to dry overnight at 37°C. The following day, CRC cells were seeded into the wells of the chamber slide in 400 µL DMEM 10% FBS and cultured normally. Media in HT29-S cell wells additionally included 30 nM SN-38 to maintain selective pressure for the drug-resistant population. Because of the slightly different growth rates of the HT29 and HT29-S cell lines, the initial seeding density was slightly higher for HT29-S; each well was seeded with 16 000 HT29 cells or 20 000 HT29-S cells. Upon attaining ~75-85% confluency (approximately 5 days), media were aspirated and cell monolayers were washed with cold PBS containing Ca^{2+} and Mg^{2+}. The monolayers were then fixed using one of two fixation methods depending upon the primary antibody. The first method involved applying methanol (MeOH) pre-chilled to -20°C to cells and allowing fixation to occur over a 15 minute period on ice.

Alternatively, cells were fixed using 200 μL of pre-warmed (to 37°C), freshly-prepared 3.7% paraformaldehyde (PFA; Sigma Aldrich), [table A.9] for 15 minutes at 37°C. At the end of the PFA incubation period, monolayers were washed once with PBS containing Ca^{2+} and Mg^{2+} before permeabilization of the cells with 200 μL of PBS containing Ca^{2+} and Mg^{2+} [table A.10], 1% Triton X-100 (Fisher) for 5 minutes at room temperature.

After the cells were fixed, 200 μL of 5% FBS in PBS containing Ca^{2+} and Mg^{2+} was applied to each well for 1 hour at room temperature, in order to block non-specific binding of primary antibodies. The blocking solution was then removed and 200 μL of primary antibody diluted in PBS containing Ca^{2+} and Mg^{2+} was applied to each well overnight at 4°C. At the end of this incubation period, primary antibody dilutions were removed and wells were washed 3 x 5 minutes with PBS containing Ca^{2+} and Mg^{2+}. Alexafluor fluorophore-conjugated secondary antibodies (see table A.14) directed against the host species of the primary antibodies, diluted in PBS containing Ca^{2+} and Mg^{2+} (2 μg/mL), were then applied to each well for one hour at room temperature. The secondary antibody solutions were removed and each well was again washed 3 x 5 minutes with PBS containing Ca^{2+} and Mg^{2+}. The plastic chambers were then carefully removed using the wedge tool provided by manufacturer. One drop of Fluoroshield aqueous gel mountant containing 1 μg/mL 2-(4-amidinophenyl)-1H-indole-6-carboxamidine (DAPI; Abcam) was applied to each well to counterstain cell nuclei and to mount a cover slip. Mountant was allowed to dry overnight at room temperature, protected from light. Fluorescence was detected on a Leica DM2000 light microscope with an ebq100 power supply. Images were taken using the QCapture Pro 5 software and Micropublisher 5.0 RTV camera (both from QImaging).

3.4.2 Spheroid Immunofluorescence

Spheroids were grown by seeding cells in 40 μL DMEM 10% FBS (with 30 nM SN-38 for HT-29S) into each well of a 96-well hanging drop plate. The standard seeding density was 200 cells per well, however this was at times varied to yield spheroids of different sizes. Each cell line was seeded onto a separate plate to ease the collection of spheroids. Sterile MilliQ H_2O was loaded into the outer reservoir of the plates to maintain a high humidity within the plate, and the entire plate was covered in saran wrap to maintain humidity. Plates were cultured at 37°C, 5% CO_2 for 4-5 days. Each well yielded a single spheroid, and because a precise number of spheroids was not required for immunostaining, all of the spheroids from a single plate were collected simultaneously. The plates were carefully removed from the incubator, unwrapped, and the middle section of the plate (containing the spheroids) was carefully removed. The lid of the hanging-drop plate was inverted and held underneath the middle section. These sections were raised several inches above the biosafety cabinet surface and swiftly brought down to knock all of the spheroids out of the wells and onto the lid underneath. The lid was washed twice with 5 mL of cold sterile PBS, collecting both washes into a clean and sterile labeled 50 mL centrifuge tube. The tubes were allowed to chill on ice while spheroids settled to the bottom. Spheroids are large enough to be seen with the naked eye, so once it was apparent that all spheroids had settled, PBS was carefully poured off. The spheroids were gently re-suspended in cold PBS containing Ca^{2+} and Mg^{2+} (non-sterile) and transferred to a 1.5 mL microcentrifuge tube.

Immunofluorescence was performed on CRC spheroids using a modified approach from the method described in section 2.4.1. Fixation was performed with a volume of 500 μL of 3.7 PFA or cold MeOH in microcentrifuge tubes. All washes were performed with 1 mL of cold PBS containing Ca^{2+} and Mg^{2+}. Antibody dilutions and blocking solution was applied in 200 μL

volumes. To remove washes or other solutions, microcentrifuge tubes were briefly pulsed on an SD 110 benchtop microcentrifuge (BioLynx) to pellet the spheroids, and the supernatant was poured off. At the end of the staining procedure, spheroids were re-suspended in 20-25 μL of Fluoroshield aqueous gel mountant containing 1 μg/mL DAPI, applied to a glass slide, and covered with a 22 mm circular glass coverslip. Imaging was performed as described in section 2.4.1.

3.5 Adhesion Assay

Twenty-four well plates were coated with 500 μL per well of 5 μg/mL bovine plasma fibronectin (Sigma Aldrich) in PBS overnight at 4°C. At the end of this period, the fibronectin solution was aspirated from the wells and 500 μL of serum-free DMEM containing 2% BSA was applied to each well for 10 minutes at room temperature, to block non-specific interactions. HT-29 and HT-29S cells cultured in a T25 flask were solubilized by incubation with 1 mL TrypLE. These cells were collected into 5 mL DMEM 10% FBS to inactivate the TrypLE enzyme, and spun down at 400 x g for 3 minutes at 4°C on an Allegra X-22R Centrifuge (Beckman Coulter). To remove serum, cells were washed twice by resuspension in 10 mL cold PBS, spinning down at 400 x g for 3 minutes at 4°C after each wash. After the second wash, cells were re-suspended in 5mL serum-free DMEM, and 500 μL of this suspension was diluted in PBS to a final volume of 10 mL. This dilute suspension of cells was counted on a Multisizer 4 Coulter Counter (Beckman Coulter) to obtain the concentration of cells in the original suspension. Both cell lines were diluted to a concentration of 100 000 cells/mL in serum-free DMEM. This suspension was aliquoted into two clean microcentrifuge tubes for each cell line. Glycine-arginine-glycine-aspartic acid-serine-proline (GRGDSP) or glycine-arginine-alanine-aspartic acid-serine-proline (GRADSP) (Millipore) peptides at a concentration of 10 mg/mL in MilliQ H_2O were diluted into

the microcentrifuge tubes to a final concentration of 100 µg/mL. Five-hundred microliters of each suspension was added, in triplicate, to the fibronectin-coated 24-well plate. The plate was gently shaken to ensure even distribution of the cells throughout each well. The plate was then returned to the 37°C incubator for approximately 2 hours, during which time cells were allowed to adhere to the immobilized fibronectin. At the end of this period, the plate was washed twice by gently inverting into cold PBS containing Ca^{2+} and Mg^{2+} for 10 minutes to remove non-adhered cells. The cells that remained adhered after washing were fixed and stained with hematoxylin and eosin Y (H&E), following the directions of section 2.6.

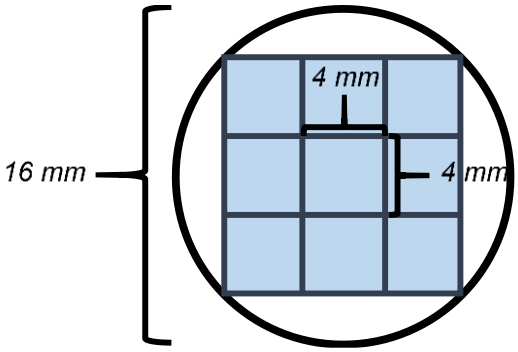

Figure 3.3: Adhesion assay well divisions.

Each well on an adhesion assay plate was divided into 9 separate fields following this layout.

Following H&E staining, each well was divided into 9 equal according to the layout shown in figure 3.3, and an image was taken from the centres of each of those sections at 100X magnification on an Eclipse TE200 inverted microscope (Nikon). This very systematic approach to image acquisition was employed to minimize bias in data collection, as dispersion of adhered cells throughout a well was often highly variable. Cells within each field were counted using ImageJ's cell counter plugin.

3.6 Hematoxylin and Eosin Y Staining

A regressive H&E staining method using Harris' Hematoxylin (Sigma Aldrich) and 1% eosin Y (Sigma Aldrich) was employed to stain adherent CRC cells. After the final wash of the adhesion assay, the remaining cells were fixed in 500 µL of 3.7% PFA overnight at room

temperature. The PFA was then aspirated and the plate was rinsed well with running tap water. 500 μL of Harris' Hematoxylin was applied each well for approximately 10 minutes at room temperature. The hematoxylin was recovered for reuse, and the plate was washed well with running tap water. Non-nuclear background staining by hematoxylin was removed by using a pipette to repeatedly apply and aspirated 500 μL of acid/alcohol [table A.11] to each well in turn for 5-10 seconds. Scot's Tap Water [table A.12] was then applied to every well at a volume at 500 μL until the cells were fully blue (approximately 5 minutes). Counterstaining was then performed by applying 500 μL of eosin Y to each well for approximately 10 minutes. Eosin Y was recovered for reuse, and each well was rinsed well with running tap water. Cells were then dehydrated through progressive rinses with 70%, 95%, and 2 x 100% ethanol. To obtain high-quality images of adhered cell morphology, wells were rinsed several times with soft tap water to remove dust before 500 μL of soft tap water was applied to rehydrate the fixed and stained cells.

3.7 Cellular Proliferation (MTT) Assay

The size of the viable cell population after challenge with chemical or environmental stressors was measured by the conversion of 3-(4,5-dimethylthiazol-2-yl)-2,5-diphenyltetrazolium bromide (MTT) by mitochondrial reductase enzymes to the 5-(4,5-dimethylthiazol-2-yl)-1,3-diphenylformazan (formazan). Cells were seeded in DMEM 10% FBS at the desired density in 96-well plates and incubated at 37°C, 5% CO_2 overnight. After allowing adhesion to the tissue culture plate, cells were challenged as desired (e.g. with drugs or serum deprivation) and cultured for at 37°C, 5% CO_2 for an assay-specific incubation period. At the end of this period, medium was aspirated and 100 μL of 0.5 mg/mL MTT in PBS containing Ca^{2+} and Mg^{2+} was applied. Cellular morphology was checked at this time. The plate was incubated with the MTT reagent at 37°C for 2-4 hours, during which time MTT was reduced to

formazan. The MTT reagent was then aspirated and the formazan crystals were dissolved in 100 μL of dimethyl sulfoxide (DMSO) for 15 minutes at 37°C. At the end of the dissolution period, the samples were mixed by gentle pipetting and the absorbance was measured at 540 nm on a SpectraMax M5 Plate Reader. Background absorbance from blank control wells were performed alongside experimental wells to account for the background absorbance.

3.9 Statistical Analysis

Analysis of the collected data was performed using GraphPad Prism 5 software. Comparisons for statistically significant differences between the HT-29 and HT-29S cell lines used the Mann-Whitney test, with $p < 0.05$ chosen as a threshold for statistically significant differences. An unpaired t-test was used instead of the Mann-Whitney test for analyzing the CRC cell nuclei diameter because of the large sample sizes in this assay. Adhesion assay data was analyzed by two-way analysis of variation (ANOVA), where peptide treatment and cell line were the variables. Statistically significant differences were determined by a Bonferroni post-test, with a threshold of $p < 0.05$ deemed to be significant. Non-linear regression and an extra sum of squares F test was performed on dose-response data to test for differences in IC50 values between treatment groups. A threshold of $p < 0.05$ was again chosen for statistical significance. Experiments were performed with a minimum of three independent biological replicates.

Chapter 4: Results

4.1 Morphology of an SN-38-Resistant HT-29 Derivative

Several distinct changes in cellular morphology and behaviour were apparent in HT-29S cells. First of all, the typical flat, cobblestone morphology of HT-29 cells grown in 2D culture conditions is disrupted in HT-29S cells Even at low confluency, HT-29S cells will begin growing over top of each other, suggesting a loss of contact inhibition. With prolonged culture periods, these areas continue to grow upwards away from the plastic culture surface, forming long, firmly attached stalks of HT-29S cells called “nodules” [fig. 4.1 A)]. Immunofluorescence experiments revealed another interesting difference between these cell lines; the nuclei of HT-29S cells are significantly larger and more heterogeneous in diameter than those of HT-29 [fig. 4.1 B) and C), table 4.1].

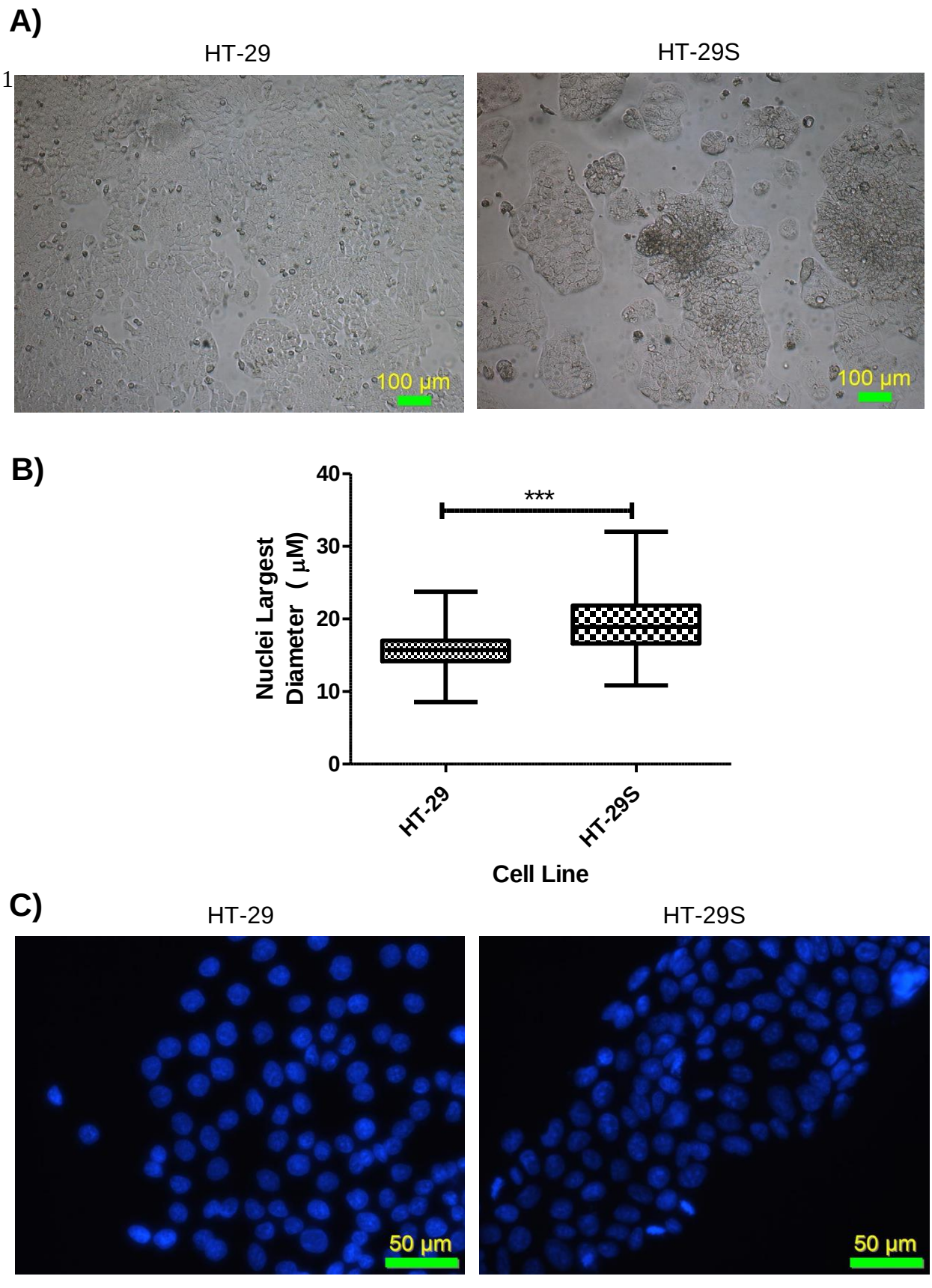
A)
HT-29
HT-29S
100 µm
100 µm
B)
Nuclei Largest Diameter (µM)
40
30
20
10
0
***
HT-29
HT-29S
Cell Line
C)
HT-29
HT-29S
50 µm
50 µm

Figure 4.1: Morphological differences between HT-29 and HT29S.

A) HT-29 and HT-29S cells were cultured in 2D culture conditions in T25 flasks (Nunc). Images were taken on a Motic AE21 inverted microscope.

B) HT-29 and HT-29S were seeded, cultured, and fixed on Nunc chamber slides prior to staining DAPI and mounting. Nuclei were measured at their widest diameter by two blinded observers using the Q-Capture Pro7 software (QImaging). The presented results represent nuclei from six independent experiments.
*** $p < 0.0001$ by the unpaired t-test.

C) Sample images of nuclei from HT-29 and HT-29S used for the measurements taken in B). Nuclei are have been stained with DAPI. Images were taken on a Leica DM2000 fluorescent microscope using the Q-Capture Pro 7 software (QImaging) at 400X magnification.

Table 4.1: Cell nuclei measurement data

	HT-29	**HT-29S**
n	451	386
Mean Diameter (µm)	15.50	19.28
Median Diameter (µm)	15.71	18.93
Standard Deviation (µm)	2.189	3.831
Minimum (µm)	8.560	10.86
Maximum (µm)	23.76	32.02

4.2 HT-29S spheroids have an increased ability to form fibronectin matrices

We wished to determine the contribution of the tumour microenvironment ECM to the phenotypic changes that occur in HT-29S cells in culture upon acquisition of SN-38 resistance. We therefore performed immunofluorescence experiments against various ECM proteins on HT-29 and HT-29S cells. In a pilot experiment using 2D cultures of our CRC cell lines, we noticed that HT-29S nodules showed stronger fibronectin staining within their nodules as opposed to the surrounding monolayer (data not shown). We reasoned that the ECM may form a scaffold for the formation of the nodules, and therefore that the ECM may be more important in 3D conditions. Further immunofluorescence experiments were therefore performed on 3D CRC spheroids generated using the hanging drop culture method. Immunofluorescence experiments of these spheroids revealed HT-29 spheroids to be nearly absent of fibronectin staining [fig. 4.2 A)] HT-29S spheroids on the other hand showed a stronger, granular staining pattern for the ECM protein [fig. 4.2 A)]. In the middle of very large HT-29S spheroids, this granular staining pattern gave way to intense, fibrous staining for fibronectin [fig. 4.2 B)]. As can be seen in figure 4.2 B) using brightfield illumination, the area of the HT-29S spheroids from which the intense fibrous staining is produced is absent of any foreign material or apparent defect of the spheroid that could potentially cause artefactual fluorescence. Thus, it appears that these areas represent genuine fibronectin matrix formation.

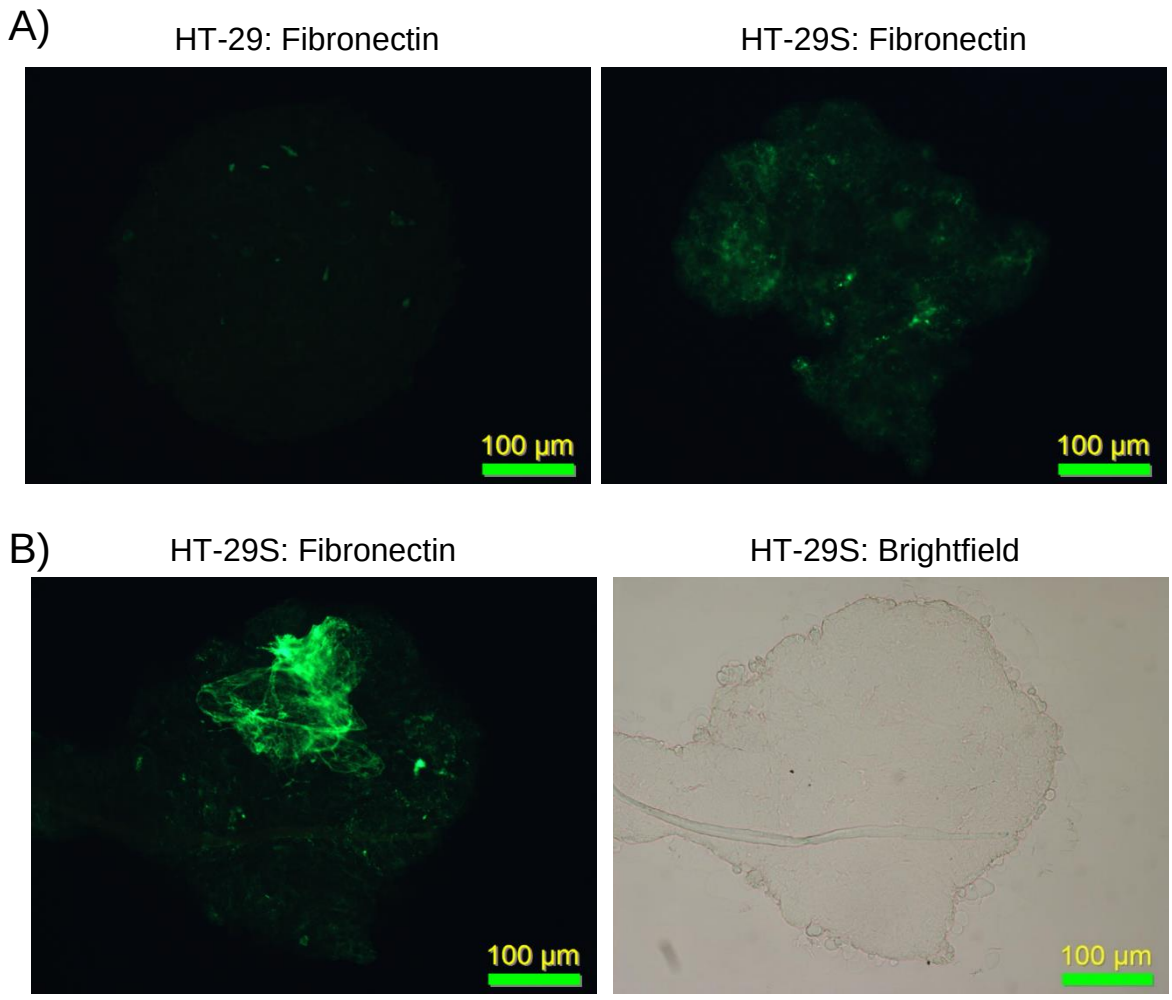

Figure 4.2: Fibronectin matrix formation in CRC spheroids.

HT-29 and HT-29S spheroids were grown by seeding CRC cells in hanging drop plates and culturing for several days at 37°C, 5% CO_2. Spheroids were collected and immunostained for fibronectin expression.

A) Fibronectin expression and matrix formation in comparably sized HT-29 and HT-29S spheroids.
B) Large HT-29S spheroid showing a fibrous staining pattern for fibronectin (left) and the corresponding brightfield image.

All images were taken on a Leica DM2000 microscope and QImaging Micropublisher 5.0 RTV camera using the QCapture Pro 7 Software (QImaging). Images are representative of four independent immunofluorescence experiments.

4.3 HT-29S cells have a strongly increased capacity for adhesion to immobilized fibronectin.

We wished to determine if the change in fibronectin deposition was related to a change in the ability of HT-29S to interact with the ECM glycoprotein. Adhesion assays were therefore performed to characterize the interaction between our CRC cells and immobilized fibronectin. CRC cells suspended in serum-free DMEM were allowed to adhere to fibronectin coated to a six-well plate over a 2-h period. Serum-free media was used in these experiments because fibronectin is abundant as a soluble dimer in serum and therefore could have interfered with the assay. A soluble GRGDSP peptide treatment group was included in the assay to test the RGD-dependence of any interaction between the CRC cells and fibronectin. The inactive peptide GRADSP was used as a control. At the end of the adhesion period, non-adhered or loosely-adhered cells were washed away and the remaining tightly-bound cells were fixed, stained, and counted. HT-29 cells showed almost no degree of adhesion in any of the conditions tested [fig. 3.4 A)]. In comparison, HT-29S cells showed a variable but higher degree of adhesion in the control and GRADSP-treated groups [fig. 4.3 A)]. Two-way ANOVA indicated that both the cell line ($p < 0.01$) and peptide treatments ($p < 0.05$) significantly influenced the number of adhered cells. Importantly, the inclusion of GRGDSP with HT-29S was sufficient to completely abolish adhesion to immobilized fibronectin, suggesting the interaction is RGD-dependent [fig. 4.3 A)]. The difference in adhesion between HT-29S cells treated with the GRGDSP and GRADSP peptides was statistically significant, as was the difference between HT-29 and HT-29S cells treated with the negative control peptide ($p < 0.01$).

There was also a significant difference in the morphology of adhered cells between HT-29 and HT-29S in this assay. The very small number of HT-29 cells that were retained at the end

of the adhesion period appeared small and spherical [fig. 4.3 B)], greatly resembling a cell that has been detached from its substratum. This suggests that these rare cells represent low affinity interactions with the plastic of fibronectin that were insufficient to trigger spreading HT-29S cells on the other hand appeared to have flattened out and produced long cellular extensions in the control and GRADSP-treated groups [fig. 4.3 B)]. This spreading morphology was lost upon treatment with the GRGDSP peptide; the few adhered HT-29S cells under these conditions appeared “rounded-up” and greatly resembled their HT-29 counterparts [fig. 4.3 B)].

A)

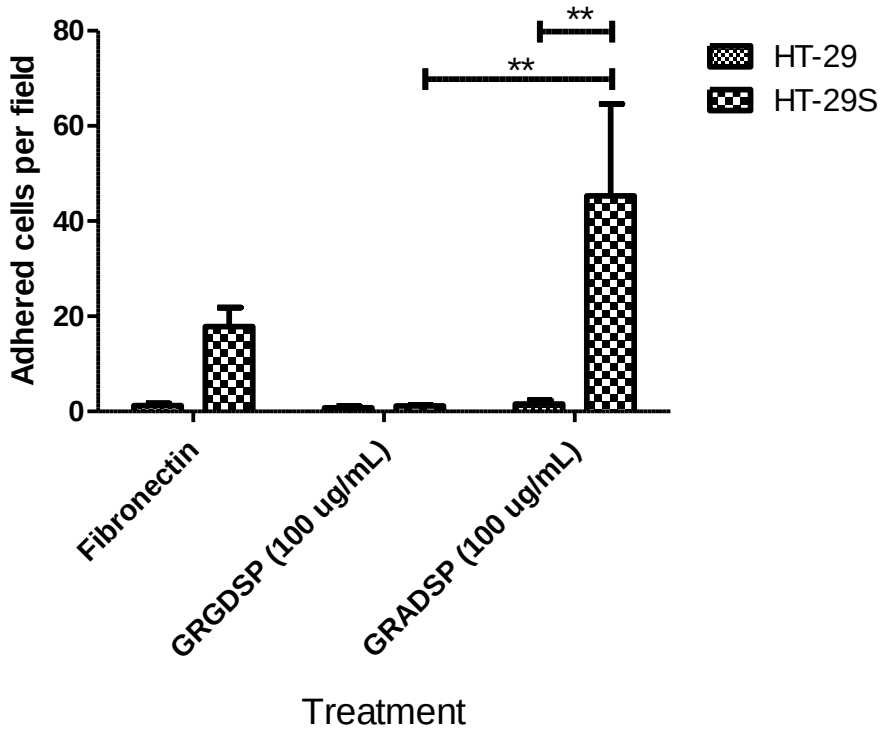
**
**
80
60
40
20
0
Adhered cells per field
HT-29
HT-29S
Fibronectin
GRGDSP (100 ug/mL)
GRADSP (100 ug/mL)
Treatment

B)

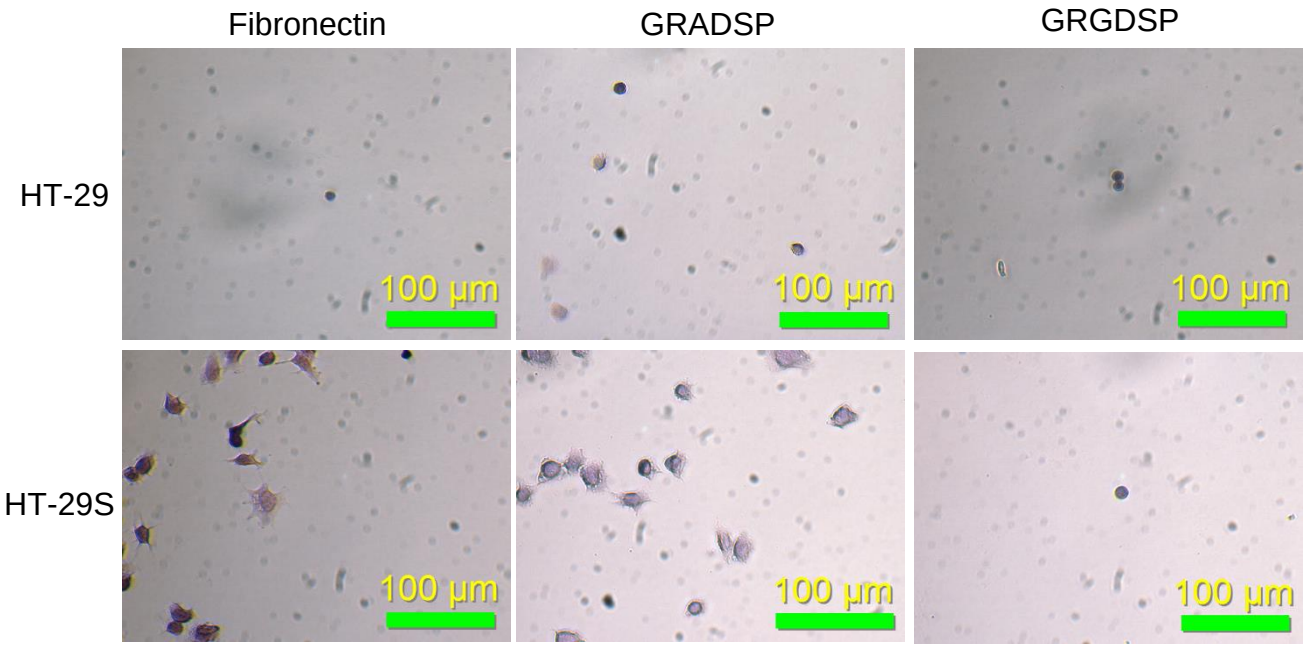
Fibronectin
GRADSP
GRGDSP
HT-29
HT-29S
100 µm

Figure 4.3: RGD-dependent adhesion of HT-29 and HT-29S cells to immobilized fibronectin.

A) HT-29 and HT-29S cells suspended in serum-free DMEM were allowed to adhere to fibronectin coated onto a six-well plate over a period of two hours. Non-adhered cells were washed away and the remaining adhered cells were fixed with 3.7% PFA and stained with H&E. Nine images were taken per well at 100X magnification and the number of adhered cells per field was counted using ImageJ. The results presented here represent four independent experiments. Differences in adhesion between HT-29 and HT-29S were assessed by two-way ANOVA (Bonferroni post-test). ** $p < 0.01$.

B) Representative images showing the morphology of adhered and stained HT29 and HT-29S cells, taken at 200X.

All images were taken on a Nikon Eclipse TE200 inverted microscope and a QImaging Micropublisher 5.0 RTV camera using the QCapture Pro 7 Software (QImaging).

4.4 Expression of the integrin α5 subunit is strongly increased in SN-38-resistant HT-29 cells.

The observation of increased fibronectin matrix assembly in HT-29S spheroids as well as the ability of the ability of the resistant cells to adhere to immobilized fibronectin in an RGD-dependent manner led us to explore the expression of various integrin subunits in the HT-29 and HT-29S cell lines. We focused on integrins which are known to dimerize to form fibronectin receptors, and were especially interested in those that do so in an-RGD dependent manner, such as integrin α5β1 and αVβ3. Integrin subunit expression was investigated at the protein level by SDS-PAGE and immunoblotting. The expression of integrin subunits α9, αV, β1, β3, and β5 were all strongly reduced in HT-29S compared to HT-29 protein lysates [fig. 4.4 A)]. The reduction in β1 expression is striking, as this is a common and major subunit that forms heterodimers with many different α integrins. Extensive exposure of integrin β1 immunoblots reveals a faint signal in HT-29S [fig. 4.4 B)]. It therefore appears that integrin β1 expression is strongly reduced but not entirely absent in the drug-resistant cell line, and that dimers containing β1 may nevertheless exist. Integrin α6 also appeared mildly reduced, but more interestingly shifted to a slightly lower molecular weight in HT-29S [fig. 4.4 A)]. In contrast to the trend of integrin downregulation in HT-29S, the expression of integrin subunit α5 was dramatically increased [fig. 4.4 A)].

To determine whether the change in integrin α5 expression was a result of increased expression of its gene *ITGA5* expression or reduced degradation of the protein, qRT-PCR was performed. The sequences and other relevant characteristics of the primer pairs used in these experiments are presented in table 6.15. Figure 4.4 C) presents the estimated initial abundance (N_0) of *ITGA5* cDNA after normalization for reaction efficiency and loading using ribosomal

protein L27 (*RPL27)* as a reference gene. *ITGA5* mRNA was over 1500 times more abundant in HT-29S than HT-29, suggesting a very strong increase in transcription from the *ITGA5* gene, or possibly a dramatic increase in the half-life of the mRNA [fig. 4.4 C)].

A)

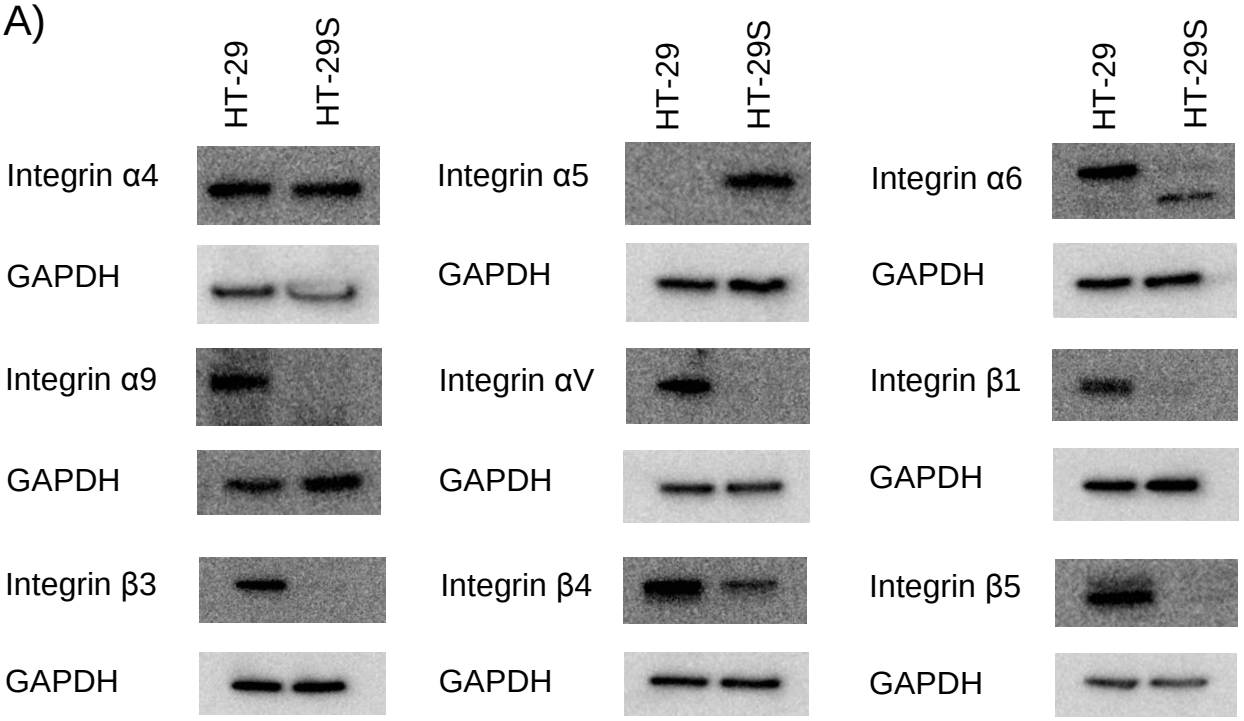
HT-29
HT-29S
Integrin α4
GAPDH
Integrin α5
GAPDH
Integrin α6
GAPDH
Integrin α9
GAPDH
Integrin αV
GAPDH
Integrin β1
GAPDH
Integrin β3
GAPDH
Integrin β4
GAPDH
Integrin β5
GAPDH

B)

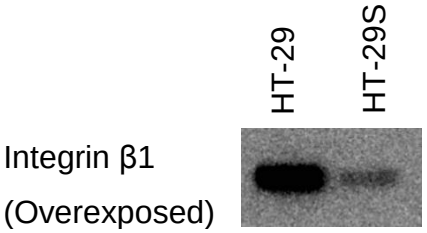
HT-29
HT-29S
Integrin β1
(Overexposed)

C)

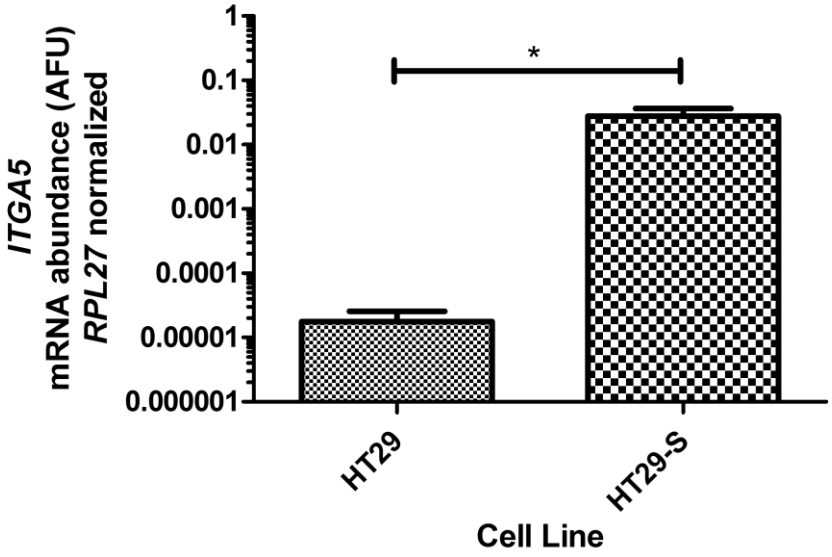
ITGA5
mRNA abundance (AFU)
RPL27 normalized
1
0.1
0.01
0.001
0.0001
0.00001
0.000001
*
HT29
HT29-S
Cell Line

Figure 4.4: Integrin subunit protein and gene-level expression by immunoblotting and real-time PCR.

A) HT-29 and HT-29S cytosolic protein fractions were immunoblotted for expression of individual integrin subunits. The primary and secondary antibodies used are recorded in tables 6.13 and 6.14. GAPDH was used as a loading control. Results shown are representative of three independent samples.

B) Integrin β1 immunoblot from A), exposed past the point of saturation.

C) The expression of the *ITGA5* gene was measured using SYBR green based qRT-PCR. Reactions were performed in triplicate on 25 ng (RNA equivalent) of reverse transcribed cDNA on a StepOnePlus Real-Time PCR system (Applied Biosystems). The primers used for these experiments are listed in table 6.15. Samples were normalized for loading differences against the housekeeping gene *RPL27*. Data is presented as the mean + SEM from four independent samples. Statistically significant differences in expression were determined by the Mann-Whitney test. * $p < 0.05$

The localization of an integrin heterodimer within the cell can reveal a great deal about the receptor; they may be clustered into points of contact with the ECM called focal adhesions, or internalized into intracellular vesicles (reviewed in [139]). We therefore performed immunofluorescence experiments to determine the localization of integrin α5 within HT-29 and HT-29S cells, and to confirm the change in expression observed by western blot and qRT-PCR. Rabbit isotype antibodies were used to establish exposure limits as a control against auto-fluorescence and background staining. Similar to the western blot results, integrin α5 appeared to be more highly expressed in the SN-38-resistant cell line. [fig. 4.5 A)].

The subcellular localization of positive integrin α5 staining was also significantly altered in HT-29 versus HT-29S cells. The parental cells had a consistent low level of fluorescence throughout the cytoplasm, not co-localizing with any apparent structures and showing no variation between cells within a colony [fig. 4.5 A)]. This suggests that a small amount of integrin α5 may be expressed in HT-29 but is not functionally active or associated with the ECM. The HT-29S cells stained for integrin α5 did not have such a uniform staining; colonies appeared to be surrounded by a thin but intense margin of integrin α5 [fig. 4.5 A)]. At high magnification, many of these margins have the appearance of thin fibrous strands [fig. 4.5 B)], which may reflect integrin α5β1 engagement with an ECM matrix, analogous to the fibrous strands of fibronectin observed in HT-29S spheroids [fig. 4.2 B)].

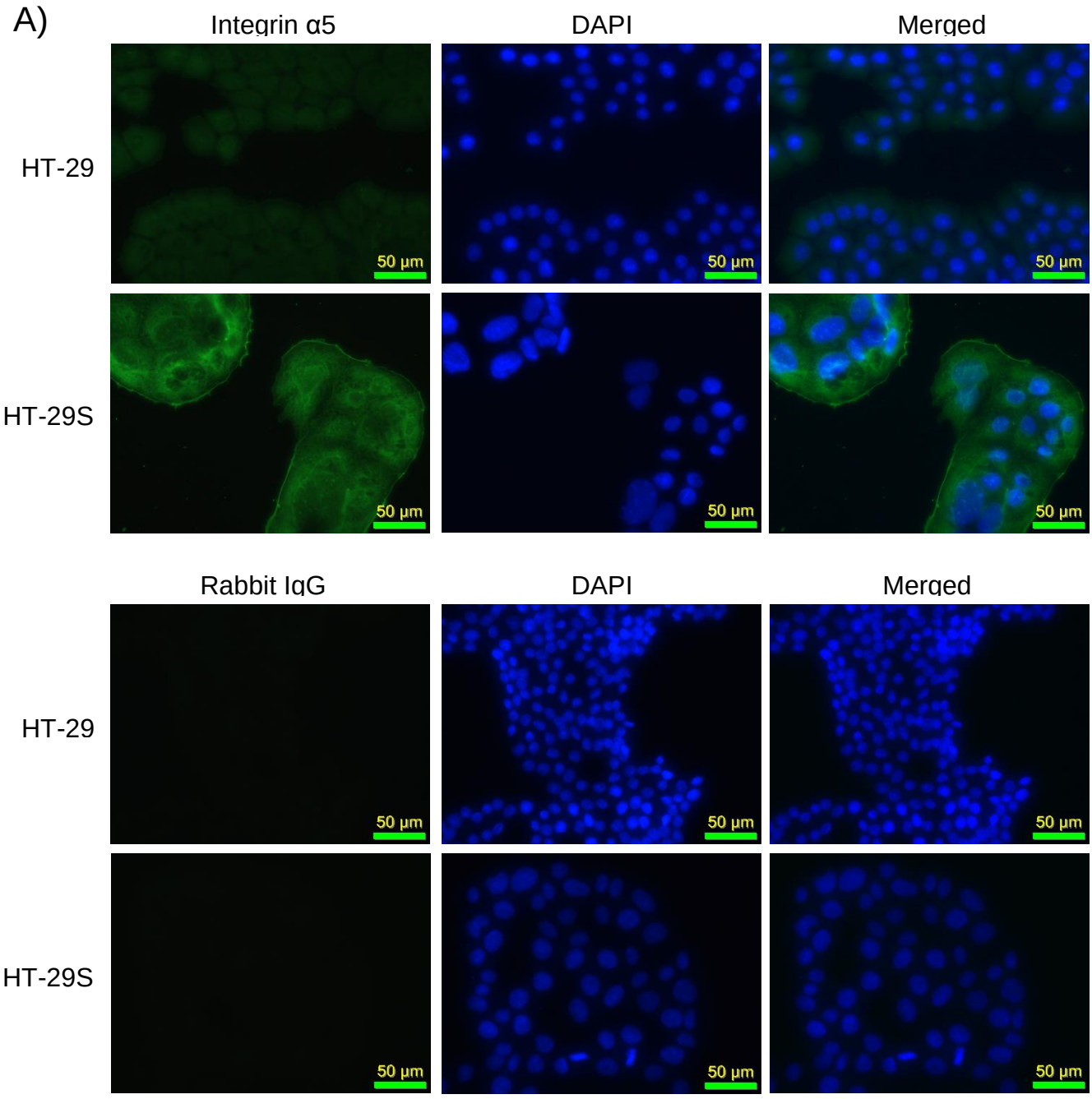
A)
Integrin α5
DAPI
Merged
HT-29
HT-29S
Rabbit IgG
DAPI
Merged
HT-29
HT-29S
50 µm

B)

HT-29S: Integrin α5

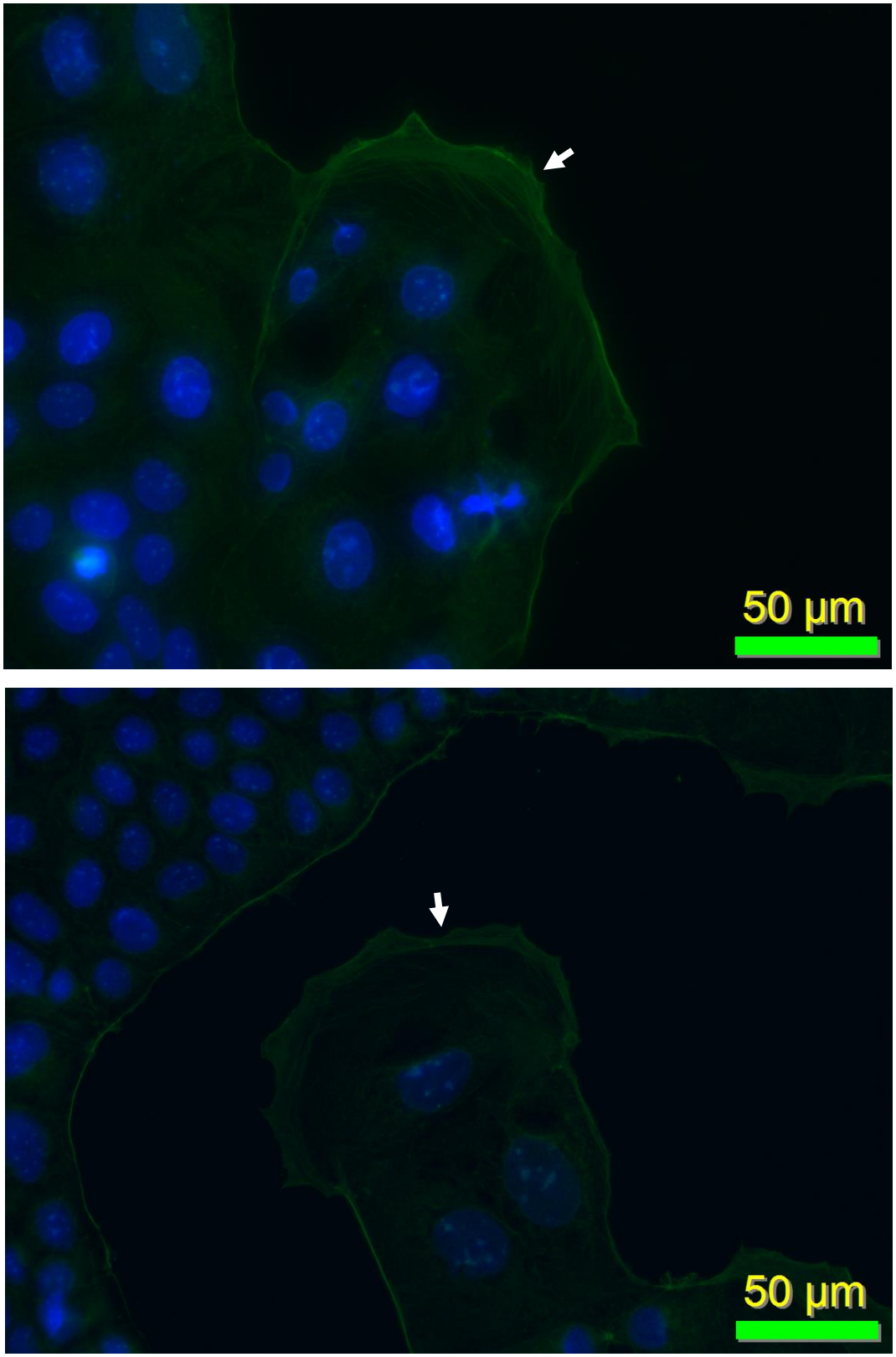

Figure 4.5: Intracellular expression and localization of integrin α5 in HT-29 and HT-29S cells.

A) HT-29 and HT-29S cells were seeded and cultured on 8-well chamber slides (Nunc), fixed with cold methanol, and immunostained for integrin α5 or integrin β1 expression and intracellular localization. Nuclei were counterstained with DAPI. Control stains with anti-rabbit IgG were performed in parallel as a negative control against nonspecific binding and cellular auto-fluorescence.

B) Fibrous staining pattern of integrin α5 at the surface of HT-29S cells, indicated by the white arrows. Nuclei were counterstained with DAPI.

All images were taken on a Leica DM2000 microscope and QImaging Micropublisher 5.0 RTV camera using the QCapture Pro 7 Software (QImaging). Images are representative of three independent immunofluorescence experiments.

4.5 HT-29S cells are resistant to extended serum deprivation

Integrin α5 is known to form only a single heterodimer, which is the α5β1 receptor[140]. As integrins only function as heterodimers and not as solitary subunits, and because the expression of integrin β1 is strongly reduced in HT-29S, the upregulation of the integrin α5 subunit is insufficient evidence to prove an increased expression of the functional α5β1 fibronectin receptor. Furthermore, the inside-out regulation of integrin activity discussed in section 1.5.3 suggests that even if the expression of the fibronectin receptor at the cell surface is increased, it may not be functionally more active. We therefore sought to test the level of functional activity of integrin α5β1 in HT-29S cells. Previous work by the labs of Erkki Ruoslahtti and Rudolph Juliano have demonstrated that ectopic expression of integrin α5 can render cells resistant to conditions of serum starvation, including in the HT-29 CRC cell line[124,125]. We therefore chose to use this trait as a marker for active integrin α5β1 signaling by depriving HT-29 and HT-29S of serum for 72 hours. At the end of this period, we performed the MTT assay to measure cellular viability. HT-29 and HT-29S cells cultured in serum-containing medium were used as a positive control, and were defined as "100% viable". As expected, HT-29 cells are highly sensitive to serum withdrawal; by the end of the 72 hour period, serum starved HT-29 cell viability was reduced to approximately 20% of control [fig. 4.6 A)]. In contrast, serum-starved HT-29S cells showed a very moderate reduction in viability, at approximately 70% of control. This difference in serum-deprivation resistance was statistically significant ($p < 0.05$). HT-29S is enhanced in its ability to survive and proliferate under serum-free conditions, consistent with activation of a fibronectin-integrin α5β1 pro-survival pathway.

We were also able to observe a significant difference in the morphology of HT-29 and HT-29S cells in response to serum deprivation. When cultured in media containing serum, both

HT-29 and HT-29S cells in short term culture have a “cobblestone” morphology characteristic of epithelial cell monolayers, as can be observed in figure 4.6 B). HT-29S retains this appearance under serum-free conditions; there was no obvious differences in cellular morphology at the end of the treatment period between the serum-starved and control HT-29S cells. The only notable feature was a mild reduction in confluency in the serum-starved HT-29S wells, which fits with the observed decrease in viability measured by MTT. There was however a significant change in the morphology of HT-29 cells that had been subjected to serum deprivation. Not only were there far fewer cells within these wells, but most of the cells that were present had lost the cobblestone appearance of healthy epithelial cells and instead appeared more spherical.

A)

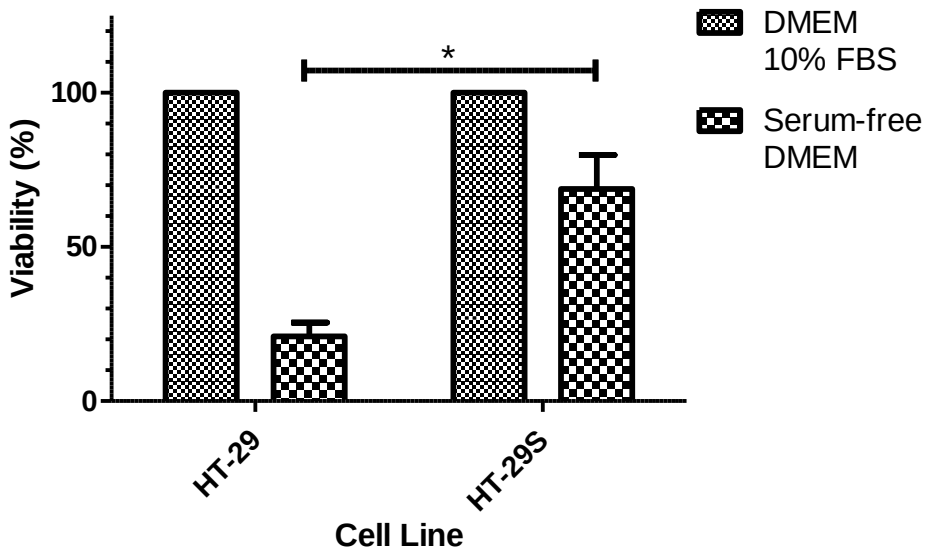
*
100
50
0
Viability (%)
HT-29
HT-29S
Cell Line
DMEM
10% FBS
Serum-free
DMEM

B)

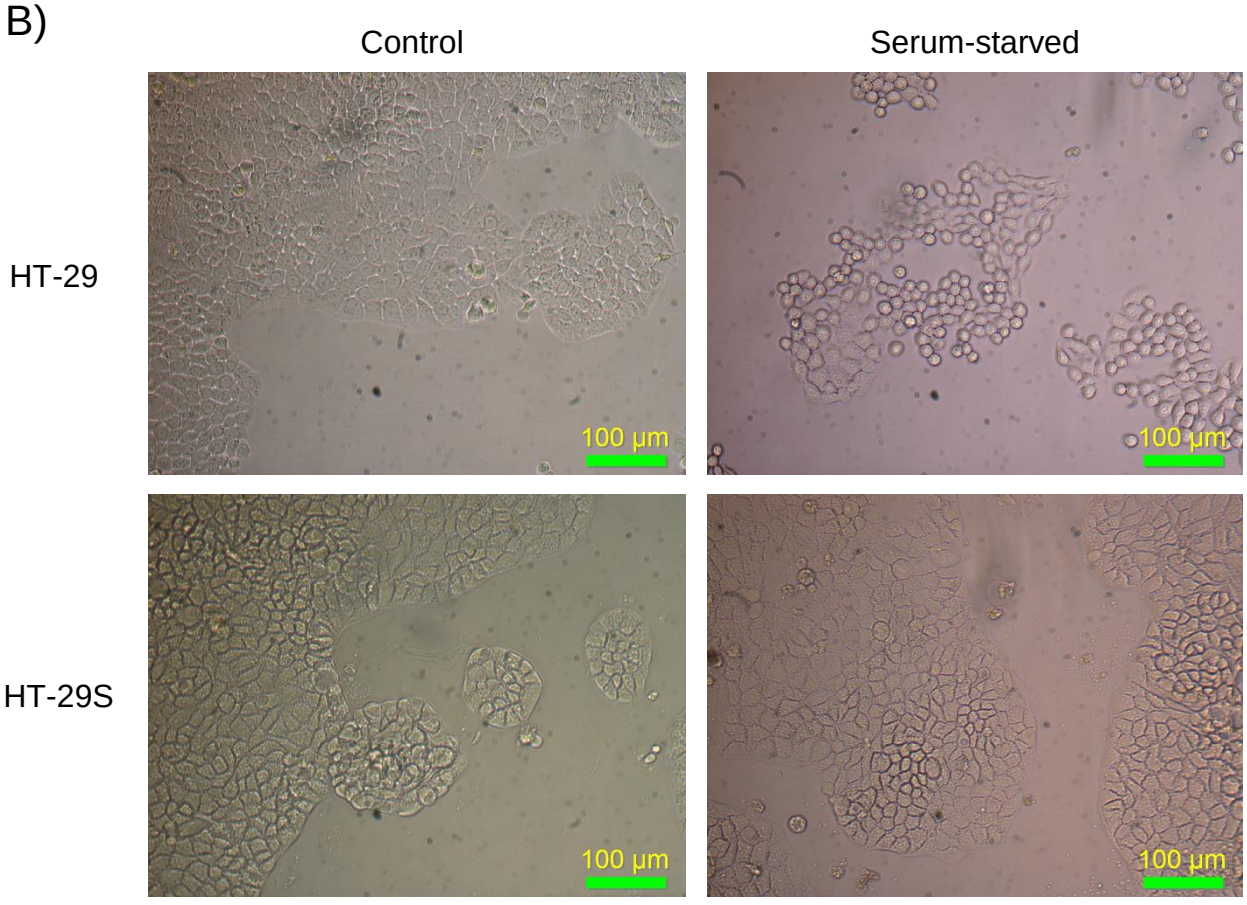
Control
Serum-starved
HT-29
HT-29S
100 µm
100 µm
100 µm
100 µm

Figure 4.6: Effect of serum deprivation on HT-29 and HT-29S cells.

A) HT-29 and HT-29S cells were seeded into the wells of a 96-well plate in triplicate for each treatment group. Cells were cultured in DMEM 10% FBS at 37°C, 5% CO_2 for 72 hours. Media was then switched to fresh DMEM 10% FBS or serum-free DMEM and the cells were cultured for a further 72 hours. At the end of this period, an MTT assay was performed to assess cellular viability. Cells cultured with serum were considered 100% viable. The results shown represent four independent experiments. The relative viabilities of serum-starved HT-29 versus HT-29S cells were compared by a Mann-Whitney test. * $p < 0.05$.

B) Representative images of control and serum-starved HT-29 and HT-29S cells at the end of the 72-hour serum deprivation period. All images were taken on a Nikon Eclipse TE200 inverted microscope and QImaging Micropublisher 5.0 RTV camera using the QCapture Pro 7 Software (QImaging).

4.6 Akt is constitutively activated in HT-29S cells

The pro-survival pathway activated by integrin α5β1 binding to fibronectin involves activation of a PI3K/Akt signalling pathway, as outlined in figure 1.4. We therefore assessed the degree of activation of Akt by western blot analysis for phosphorylation of Akt at two amino acid residues critical for its activity; serine 473 and threonine 308. Interestingly and unexpectedly, a decrease in the total Akt expression was also consistently observed in HT-29S compared to the parental cells, as can be seen in figure 4.7. Despite this reduced expression however, there was a clear increase in the phosphorylation of Akt at both the serine 473 and threonine 308 residues [fig. 4.7]. Adding weight to the results of the serum deprivation assays, this suggests that a fibronectin-integrin α5β1 signaling program is active in HT-29S but not HT-29 cells.

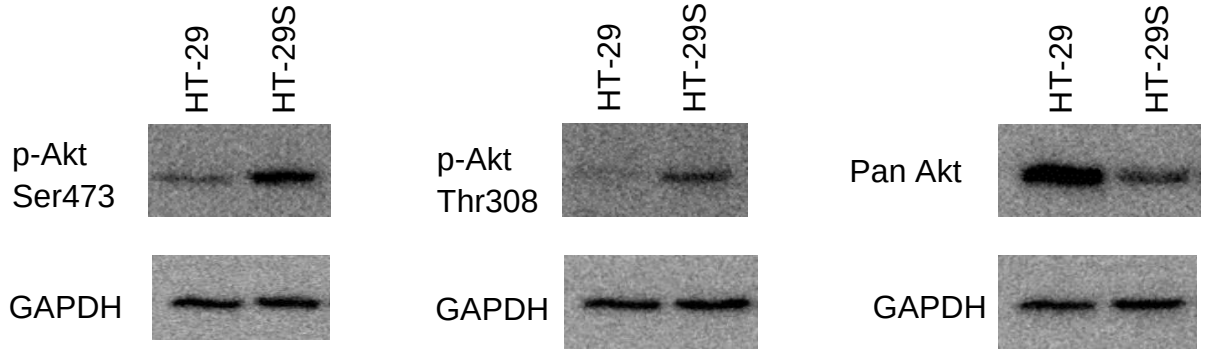

Figure 4.7: Akt activation in CRC cells.

Akt phosphorylation at Ser473 and Thr308 was assessed in HT-29 and HT-29S cell lysates by western blot. The primary and secondary antibodies used in these experiments are recorded in tables 6.13 and 6.14. GAPDH expression was used as a loading control, and is shown below each blot. The results shown are representative of three independent samples.

4.7 Expression of the *BCL2* gene is increased in HT-29S cells

Downstream of integrin α5β1/PI3K/Akt is induction of *BCL2* transcription, which mediates the pro-survival effect of this pathway[fig. 1.4][125,131,132]. We wished to determine if the upregulation of integrin α5 and activation of Akt was promoting *BCL2* expression in HT-29S, allowing these cells to resist serum deprivation. This question was addressed by assaying for the expression of *BCL2* mRNA by qRT-PCR. We consistently observed a higher level of expression of *BCL2* in HT-29S versus HT-29 [fig. 4.8], which was determined to be statistically significant ($p < 0.05$). The transcription or stability of the *BCL2* mRNA is significantly increased in HT-29S cells, consistent with the proposed mechanism.

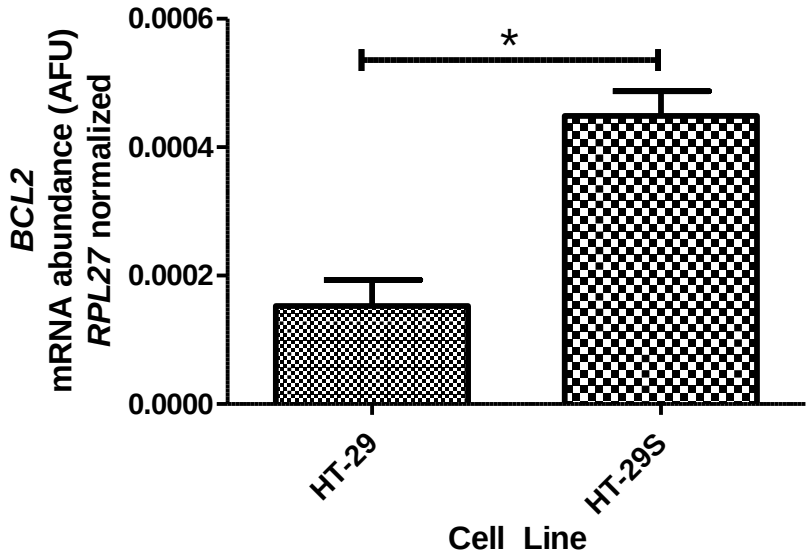

Figure 4.9: *BCL2* expression in HT-29 and HT-29S cells.

The expression of the *BCL2* gene was measured using SYBR green based qRT-PCR. Reactions were performed in triplicate on 25 ng (RNA equivalent) of reverse transcribed cDNA on a StepOnePlus Real-Time PCR system (Applied Biosystems). The primers used for these experiments are listed in table 6.15. Data is presented as the mean + SEM from four independent samples. Statistically significant differences in expression were determined by the Mann-Whitney test. * $p < 0.05$

4.8 Inhibition of PI3K sensitizes HT-29S to SN-38

To investigate if the increase in integrin α5β1-fibronectin signaling through to PI3K might contribute to a CAM-DR effect in the HT-29S cell line, we measured the sensitivity of HT-29 and HT-29S cells to SN-38 following disruption of this pathway with the PI3K inhibitor LY294002. We began by determining the sensitivity of HT-29 and HT-29S to LY294002 by measuring cellular viability at a range of LY249002 doses with the MTT assay. In agreement with previous studies[141], treatment with LY294002 reduced the proliferation and viability of HT-29 cells at higher concentrations [fig. 4.9]. HT-29S cells were somewhat (~3-fold) less sensitive to LY294002 than HT-29 cells, which may reflect the higher basal activity of PI3K/Akt in these cells [fig. 4.9]. The IC50 values of LY294002 were estimated by non-linear regression to be 5.971 μM for HT-29 and 17.44 μM for HT-29S [table 4.2]. Based on this result and a desire to treat the cell lines under comparable conditions, we chose both 5 μM and 10 μM as working concentrations for PI3K inhibition experiments, as there was a noticeable effect in both cell lines at these doses without extreme toxicity.

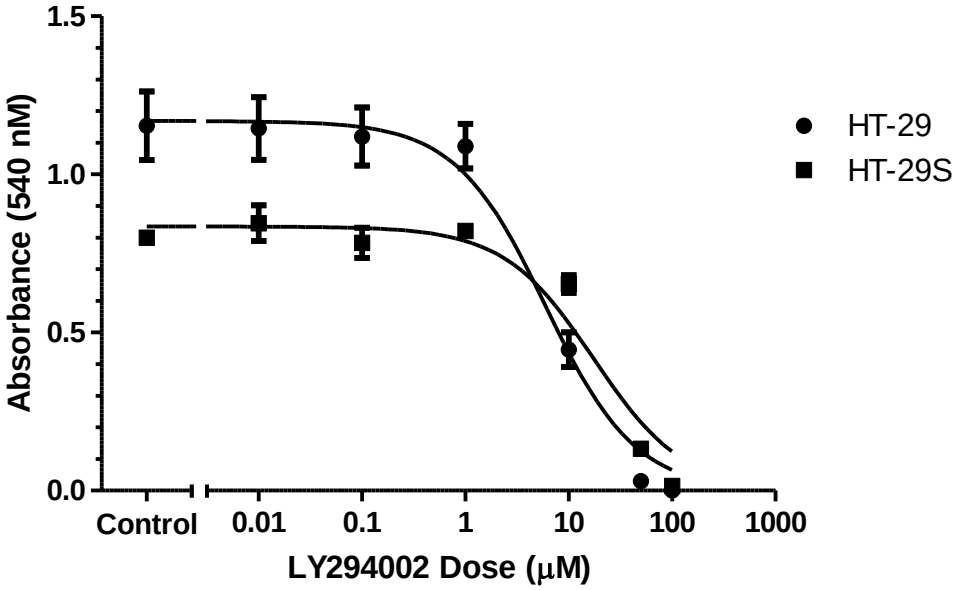

Figure 4.9. – Effect of LY294002 on HT-29 and HT-29S proliferation.

96-well plates were seeded with 2000 HT-29 and 2500 HT-29S cells, and incubated at 37°C, 5% CO_2 overnight. Cells were dosed with LY294002 or vehicle-control and incubated for a further 96 hours. At the end of this period, an MTT assay was performed. The data presented is the mean + SEM of three independent experiments.

Table 4.2: IC50 value of the PI3K inhibitor LY294002 in HT-29 and HT29-S

	LY294002 IC50 (μM)
HT-29	5.971
HT-29S	17.44

To test the effect of PI3K inhibition on the response to SN-38 treatment, HT-29 and HT-29S cells were pre-treated for 1 hour with 5 μM or 10 μM LY294002 (or vehicle-control) and subsequently dosed with SN-38. Cells were incubated with SN-38 and LY294002 for a further 96 hours, and at the end of the exposure period cellular viability was measured by the MTT assay Despite the reduction in viability observed for HT-29 cells treated with LY294002, addition of the PI3K inhibitor did not seem to have any effect on the response of these cells to SN-38 [fig. 4.10 A)]. In contrast, PI3K inhibition in HT-29S with LY294002 significantly shifted the SN-38 dose-response curve [fig. 4.10 B)]. The SN-38 IC50 values were determined by non-linear regression of the dose-response data [table 4.3] and compared by an extra sum of squares F-test. The IC50 value of SN-38 on HT-29 cells was virtually unaffected by PI3k inhibition [table 4.3], and the F-test indicated no statistically significant difference in the SN-38 IC50 values between the treatment groups. In contrast, the estimated SN-38 IC50 values for HT-29S decreased from 358.1 nM in the control group to 39.20 nM with 5 μM LY294002 and 25.46 nM with 10 μM LY294002 treatment [table 4.3]. This difference was confirmed to be statistically significant ($p = 0.0004$) by the F-test. The LY294002-treated HT-29S cells were therefore more sensitive to SN-38 than the control group, despite the modest effect of LY294002 treatment on HT-29S in the absence of SN-38. Together, these results suggest that PI3K/Akt activation contributes to the resistant status of the HT-29S cell line.

A)

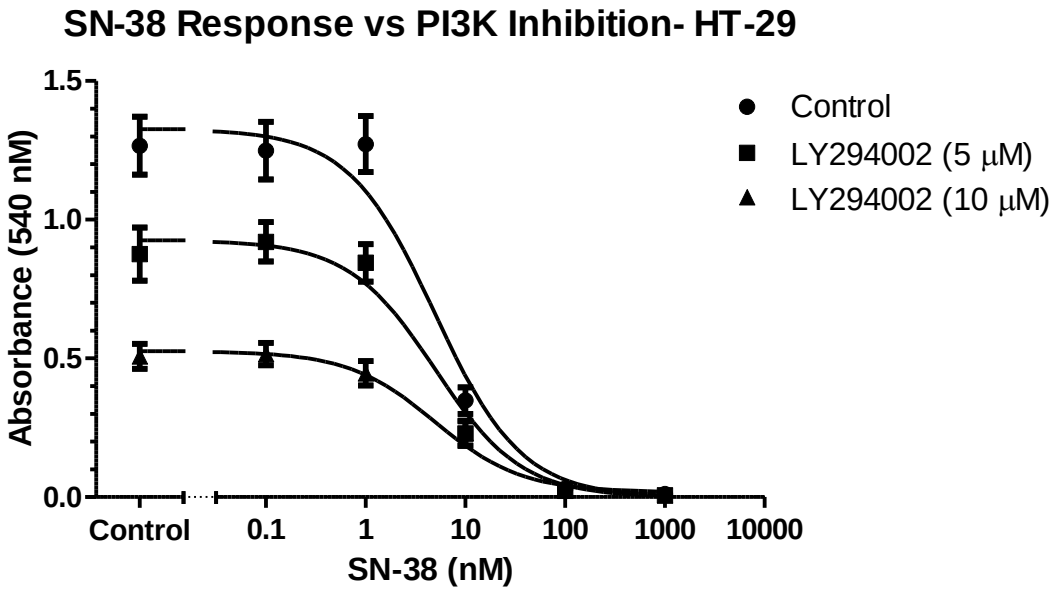
SN-38 Response vs PI3K Inhibition- HT-29
Absorbance (540 nM)
1.5
1.0
0.5
0.0
Control
0.1
1
10
100
1000
10000
SN-38 (nM)
Control
LY294002 (5 μM)
LY294002 (10 μM)

B)

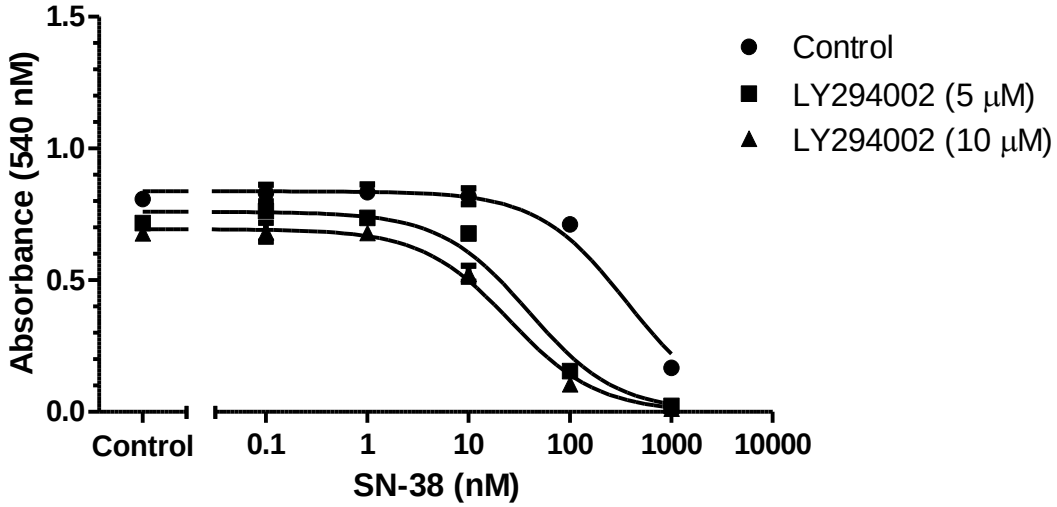
SN-38 Response vs PI3K Inhibition- HT-29S
Absorbance (540 nM)
1.5
1.0
0.5
0.0
Control
0.1
1
10
100
1000
10000
SN-38 (nM)
Control
LY294002 (5 μM)
LY294002 (10 μM)

Figure 4.10: HT-29 and HT-29S SN-38 dose-response in the presence or absence of PI3K/Akt pathway inhibition with LY294002.

A) 96-well plates were seeded with 2000 HT-29 cells, and incubated at 37°C, 5% CO_2 overnight. Cells were dosed with LY294002 or vehicle-control and incubated for one hour. At the end of the LY294002 pre-treatment period, cells were dosed with SN-38 or vehicle-control, and incubated for a final 96-hours. At the end of this period, an MTT assay was performed. The data presented is the mean + SEM of five independent experiments. The IC50 values of the different groups were compared by an extra sum of squares F test.

B) Same as A), but seeded with 2500 HT-29S instead of HT-29 cells. The IC50 values of the different groups were compared by an extra sum of squares F test.

Table 4.3: Effect of PI3K inhibition on SN-38 response in HT-29 and HT-29S

	Control	LY294002 (5 μM)	LY294002 (10 μM)
HT-29	5.005	4.412	7.796
HT-29S	358.1	39.20	25.46

4.9 HT-29S has undergone an epithelial to mesenchymal transition

The epithelial to mesenchymal transition (EMT) process has been associated with wound healing and cancer progression, and is known to involve a number of proteins and transcription factors[101,142,143]. For example, the EMT-related transcription factors zinc finger E-box binding homobox 2 (*ZEB2*) and twist-related protein 1 (*TWIST1*) have been demonstrated to promote transcription from the *ITGA5* gene during EMT in human cancer cell lines[144,145]. Because of this apparent link we wished to determine if there was a change in expression of these and other EMT-related genes between our parental and drug resistant cells. We addressed this question by performing qRT-PCR on HT-29 and HT-29S cDNA using a panel of primers directed against a panel of EMT-related genes. We found that a number of interesting changes in EMT gene expression have occurred during the acquisition of drug resistance. A small (approximately 2.7 fold) but statistically significant ($p < 0.05$) increase in expression of the *ZEB2* transcript was observed in HT-29S versus HT-29 cDNA samples. The very minimal expression of the Snail family zinc finger 2 gene (*SNAI2*) in HT-29 was dramatically increased in HT-29S cells ($p < 0.05$) [fig 4.11]. Similarly, we were consistently unable to detect any *TWIST1* in HT-29 but detected a strong expression in HT-29S [fig. 4.11]. Expression of the junction plakoglobin (*JUP*) and vimentin (*VIM*) genes also appeared to be trending towards increased expression in HT-29S, but these differences were not statistically significant [fig. 4.11]. *JUP* however was almost significant, with $p = 0.0571$. Similarly, the zinc-finger E-box binding homobox 1 (*ZEB1*) gene expression appeared to be substantially decreased in HT-29S, but this was not statistically significant [fig. 4.11]. The expression of two other EMT genes, Snail family zinc finger 1 (*SNAI1*) and the tight junction protein 1 (*TJP1*), were not substantially altered between HT-29 and HT-29S cells [fig. 4.11].

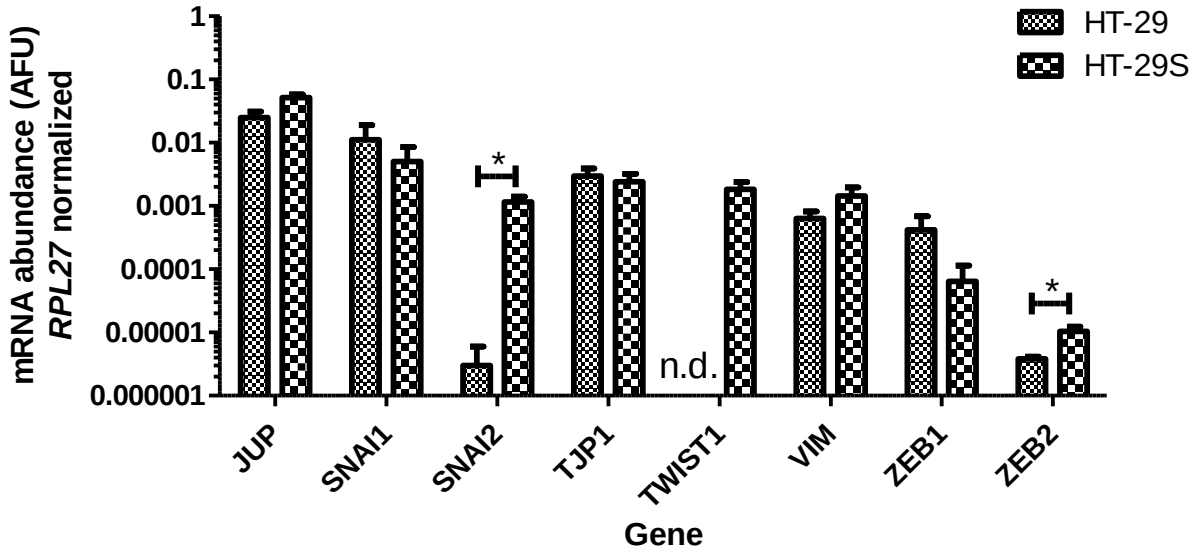

Figure 4.12: EMT gene expression in HT29 and HT29-S.

The expression of various genes was measured using SYBR green based qRT-PCR. Reactions were performed in triplicate on 25 ng (RNA equivalent) of reverse transcribed cDNA on a StepOnePlus Real-Time PCR system (Applied Biosystems). The primers used for these experiments are listed in table 6.15. Samples were normalized for loading differences against the housekeeping gene *RPL27*. Data is presented as the mean + SEM from four independent samples. Statistically significant differences in expression were determined by the Mann-Whitney test. * $p < 0.05$. n.d. – None detected.

Chapter 5: Discussion

5.1 Summary

The data presented here demonstrate that dramatic alterations in CRC cell-ECM interactions occur upon acquisition of SN-38 resistance. This change is mediated by a substantial upregulation of the integrin α5 subunit leading to an increased formation of functional integrin α5β1 receptor. It is likely that this receptor then promotes the formation of a complex fibronectin network within resistant cell colonies, and the subsequent adhesion of α5β1 to the fibronectin matrix activates an intracellular PI3K/Akt signalling pathway that opposes chemotherapy-mediated apoptosis induction through increased *BCL2* expression.

5.2 Morphology of SN-38-resistant cells

The cellular morphology of HT-29 cells is dramatically altered by acquisition of SN-38 resistance, with HT-29S cells adopting features characteristically associated with more advanced, aggressive cancers. For example, the HT-29 line grows as flat monolayers that are typical of epithelial cells or a well-differentiated tumour, but HT-29S does not. Instead these cells form the vertical outgrowths that we have named "nodules" [fig. 4.1 A)]. Since HT-29S no longer appears restricted to monolayer growth, it suggests that they may have lost contact inhibition. Loss of contact inhibition has also been associated with EMT[146], suggesting that an EMT may have occurred in HT-29S. This possibility is further discussed in section 5.9.

A second distinct change is an increase in the nuclear diameter [fig. 4.1B)] and dysmorphia [fig. 4.1 C)] of HT-29S compared to HT-29. Enlarged and irregularly-shaped nuclei are a well-described feature of progression in many types of cancer (reviewed in [147]), further suggesting that our drug-resistant CRC cell line represents a more advanced, aggressive disease

than the parental cells. There are many possible causes for alterations in nuclear size and shape during cancer progression including mutation or deletion of genes encoding the nuclear lamina, or altered chromatin organization[147], however one of particular interest in our cell lines is the effect of ECM contacts. It has been previously reported that integrin-mediated adhesion and spreading over ECM substrates such as fibronectin can cause alteration in nuclear shape and promote the release of calcium from the endoplasmic reticulum (ER) into the cytoplasm and nucleus[133]. Deformation of nuclei is likely mediated by actin bundles connecting integrin-ECM contacts to the nucleus[148]. Calcium release can activate various kinases including CaMK IV, which participates in the pro-survival fibronectin-integrin α5β1 signalling pathway [fig. 1.4]. Therefore while there are many potential explanations for the altered nuclear morphology of HT-29S, one possibility that is consistent with our data is that integrin α5β1 adhesion to fibronectin exerts mechanical stress that alters nuclei shape and encourages calcium release from the ER, which in turn activates CAMK IV and subsequently promotes *BCL2* expression through activation of CREB and NFκB.

5.3 Interactions between HT-29S and fibronectin

We have demonstrated that HT-29 cell interactions with a particular component of the ECM, fibronectin, are significantly altered along with resistance to SN-38. We observed an increased accumulation of fibronectin in HT-29S spheroids [fig. 4.2 A)] which in some cases took the appearance of a fibrous, matrix-like structure [fig. 4.2 B)]. This increased fibronectin matrix formation in HT-29S may contribute to the altered morphology of these cells by providing a scaffold for nodule formation. The increased accumulation of fibronectin in HT-29S coincided with an increased adhesive capacity of these cells for that ECM glycoprotein [fig. 4.3 A)]. HT2-29S cells that adhered to fibronectin adopted a stretched or spreading morphology that

was absent in adherent HT-29 cells, which remained spherical [fig. 4.3 B)]. Both the increased adhesion and the spreading morphology of HT-29S were reversible by a soluble GRGDSP peptide but not a control GRADSP peptide at the same concentration [fig. 4.3 A) and B)]. The interaction between HT-29S and fibronectin is therefore RGD-dependent and likely involves an αIIb, α5, α8, or αV integrin, but not an α4 or α9[149]. The spreading morphology of HT-29S suggests that the resistant cells were migrating over the fibronectin coating, and may also suggest that the resistant cells are able to exert the necessary force on fibronectin to unfold the soluble dimer form of the glycoprotein; a necessary step in the construction of a fibronectin matrix and one that can be mediated by integrin α5β1[103].

5.4 Expression of integrin subunits in HT-29 and HT-29S

Numerous changes were observed in the expression of integrin family members between HT-29 and HT-29S cell lines. The significance of those changes are discussed in sections 5.4.1 to 5.4.6, and are summarized in figure 5.1.

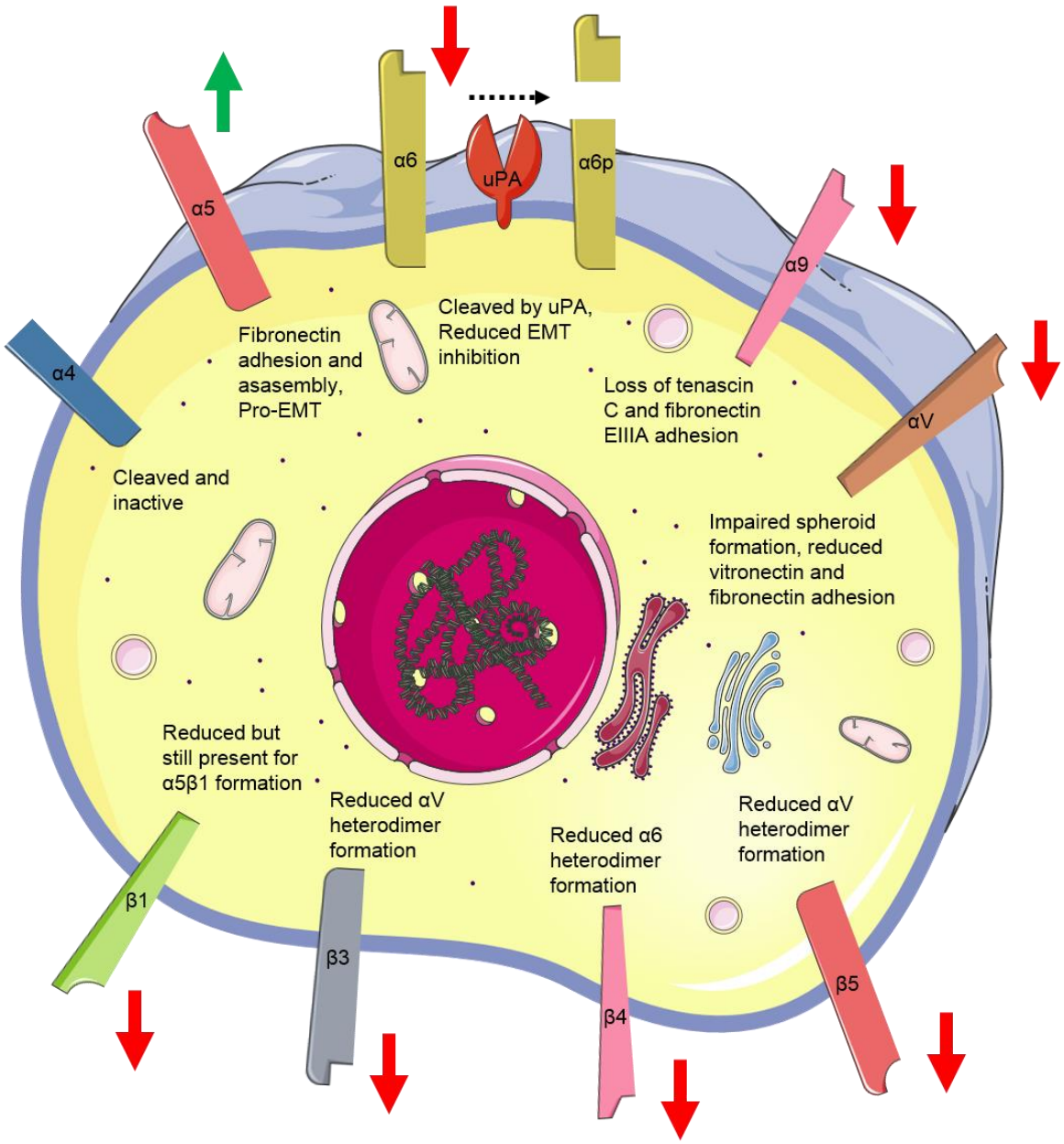

Figure 5.1: Functional significance of integrin expression changes on HT-29S cells.

The expression changes of individual integrin subunits in HT-29S relative to HT-29. Green arrows indicate an increased expression of the integrin in HT-29S, while red arrows indicate a reduced expression. Possible functional implications of these expression changes are presented below each subunit.

5.4.1 Integrin α4

Integrin α4β1is able to bind fibronectin at a distinct site from the RGD-dependent integrins, and in doing can suppress signalling pathways activated by integrin α5β1 ligation to fibronectin[86,87], meaning the effect of integrin α5 upregulation in HT-29S may depend on the activity of this subunit. Integrin α4 was detected in both HT-29 and HT-29S [fig. 4.4 A)] but its expression did not appear to be substantially altered. Somewhat surprisingly however, the only band detected for this protein corresponded to a molecular weight of approximately 55 kDa; much lower than the expected molecular size of approximately 150 kDa. It has been previously demonstrated that integrin α4 can be cleaved to a number fragments, including a 55 kDa fragment, which is not capable of forming a functional heterodimer with integrin β1[150]. Therefore, it appears that integrin α4 expression does not change between HT-29 and HT-29S, and indeed it likely does not form a functional receptor to have any impact on cellular behaviour in either cell line.

5.4.2 Integrin α5

The most notable result of the analysis of integrin expression in HT-29 and HT-29S cells by western blot was the change in integrin α5 expression [fig. 4.4 A)]. It has been well documented that this subunit is not normally expressed in HT-29 and that ectopic expression of integrin α5 on HT-29 can have profound effects on the behaviour of these cells[108,109,116,124,125]. Consistent with these results, we were could not detect any expression of integrin α5 in the parental HT-29 cell line. It appears that the upregulation of integrin α5 in HT-29S is due to an increased abundance of *ITGA5* mRNA [fig. 4.4 C)], which could reflect an increase in transcription from the *ITGA5* gene or an increase in the stability of the mRNA. We favour the

former due to an observed upregulation of transcription factors that may drive *ITGA5* expression, which will be discussed further in section 5.9.

Immunofluorescence studies on HT-29 and HT-29S monolayers confirmed the upregulation of integrin α5 in the resistant cells [fig. 4.4 A)]. These experiments also revealed a fibrous staining pattern for integrin α5 at the edges of cells [fig. 4.5 A) and B)], which may represent integrins binding along ECM fibrils. Similar patterns were observed in early immunofluorescent studies of integrins, co-localizing with fibronectin and actin bundles[62]. Fibronectin is the most likely ECM protein to form the postulated fibrils, because (i) it is the only known ECM ligand of integrin α5[149], (ii) our data show that fibrils of this glycoprotein accumulates in HT-29S spheroids, and (iii) HT-29S cells gain an adhesive capacity for fibronectin. These observations therefore suggest that integrin α5 on HT-29S cells, as part of the integrin α5β1 heterodimer, binds fibronectin, which would in turn initiate downstream signalling pathways. To the best of our knowledge, this is the first description of spontaneous expression of integrin α5 in CRC cells as a result of chemotherapy resistance. The implications of integrin α5 expression in HT-29S behaviour and response to SN-38 will be discussed further throughout this chapter.

5.4.3 Integrins α6 and β4

Another very interesting change in integrin expression between HT-29 and HT-29S involved the α6 subunit. There appeared to be a modest decrease in the expression of this subunit the resistant cell line [fig. 4.4 A)]. More interestingly however, there was also a shift in migration of the integrin α6 band, implying a reduced molecular weight of the protein in HT-29S. Such a reduced-molecular-weight-variant of integrin α6 (called α6p) has been described in a number of cancer cell lines, and appears to be a result of proteolytic cleavage of a β-barrel ligand-binding

extracellular domain[151–153]. This cleavage event is mediated by urokinase-type plasminogen activator (uPA) but seemingly not by matrix metalloproteinases (MMPs) at arginines 594 and 595[152,153]. Generation of integrin α6p is associated with increased invasion into and migration over laminin, a major constituent of the basement membrane, and thus appears to be a pro-cancer event[153]. Furthermore, while the full-length form of integrin α6 can be found in both normal and malignant prostate tissue, α6p appears to be largely cancer-specific[152]. The cleavage of integrin α6 to α6p in HT-29S would suggest that our SN-38 resistant cell line may be more aggressive and invasive than the parental cells, however this remains to be determined. This increase in aggressive behaviour may result from a loss of EMT-suppression by a laminin-integrin α6 interaction[154]. The possibility that HT-29S has undergone an EMT is discussed further in section 5.9. We cannot definitively conclude from these western blot results alone that this cleavage event is actually occurring. In order to prove that integrin α6p is formed by our resistant cell population, we could attempt to block the cleavage event by treating HT-29S with a uPA inhibitor such as amiloride hydrochloride or UK122. We would expect to see an increase in the molecular weight of the integrin α6 band in HT-29S following treatment with the uPA inhibitor. Alternatively, we could isolate and sequence the integrin α6 protein from HT-29 and HT-29S cells to determine if cleavage has occurred in HT-29S.

Further suggesting a reduced activity of integrin α6 is the reduced expression of integrins β1 and β4, both of which form heterodimers with α6 (reviewed in [149]). In fact, integrin α6 appears to be the only binding partner for integrin β6. Between the reduced expression of integrin β1 and β4, and the possible cleavage of integrin α6, it is very likely that integrin α6 activity is significantly reduced in HT-29S.

5.4.4 Integrin α9

The expression of integrin α9 was substantially reduced in HT-29S compared to parental HT-29 cells [fig. 4.4 A)]. It has previously been reported that integrin α9 is not expressed in HT-29[155]. The source of the discrepancy between these findings and our own is not clear; our results consistently and unambiguously (n = 3) showed a strong expression of integrin α9 in the HT-29 line. Integrin α9 binds to the ECM protein tenascin-C in an RGD-independent manner[156,157]. It may also bind to a splice variant of fibronectin via the EIIIA domain to promote lymphatic valve formation during development[79] and in adult lymphatic valves may promote the egress of lymphocytes from the lymph nodes[81].

5.4.5 Integrins αV, β3, and β5

Integrin αV's expression pattern was the opposite of that of integrin α5; it was highly expressed in HT-29 samples (in agreement with previous studies[109]) but absent in HT-29S [fig. 4.4 A)]. Furthermore, the expression of three β subunits which form heterodimers with integrin αV, integrins β1, β3, and β5, was substantially reduced in HT-29S.

The αVβ1 and αVβ3 heterodimers are both able to mediate adhesion to vitronectin and fibronectin[149]. Integrin αVβ6 can also bind to fibronectin and may be the main fibronectin receptor in parental HT-29 cells[158]. Integrin αVβ5 binds solely to vitronectin[149]. Despite this difference in ligand specificities, all of the αV integrins exhibit RGD-dependent binding[149] Unlike integrin α5β1, αVβ1 and αVβ3 are unable to construct a fibronectin matrix[99,159]. Integrins αVβ1 and αVβ6 are also unable to promote spreading over a fibronectin substrate[158,159]. The αV integrins have however been implicated in promoting spheroid formation in ovarian cancer cell lines through an interaction with vitronectin[160], thus the malformed spheroids of HT-29S may possibly be attributed in part to the loss of αV integrins. Cancer aggression has also been linked

to αV integrins through angiogenesis and secretion of MMPs 2 and 9[161,162]. The loss of integrin αV expression may therefore reduce some behaviours associated with cancer aggression in HT-29S but may also free up integrin β1 to form the fibronectin receptor with integrin α5.

5.4.6 Integrin β1

Integrin β1 expression was dramatically reduced in HT-29S [fig. 4.4 A)]. This was somewhat unexpected as integrin β1 is a very important member of the family and interacts with many of the α subunits to form a large number of receptors[149]. It is also the sole binding partner for integrin α5, and therefore the upregulation of integrin α5 is meaningless if no integrin β1 is available to form the full fibronectin receptor[149]. However, it was not entirely absent in these cells [fig. 4.4 B)] and as HT-29S exhibits behaviours suggestive of active integrin α5β1, including fibronectin adhesion and matrix formation, Akt activation, and resistance to serum deprivation, it seems that sufficient integrin β1 is retained in HT-29S to form the α5β1 receptor. The reduced expression of integrins α9 and αV may also help promote the formation of the α5β1 heterodimer by reducing competition for integrin β1, as these are also binding partners for this subunit[149].

5.5 Serum starvation

The results of the serum deprivation assays presented in figure 4.6 show the effect of serum withdrawal on cell viability. HT-29 cell viability was reduced to approximately 20% of control cells, indicating a high dependence on serum [fig. 4.6 A)]. In contrast, HT-29S cell viability was only reduced to approximately 70% of control cells [fig. 4.6 A)]. Integrin α5β1 has previously been demonstrated to protect against apoptosis induced by serum deprivation[124,125,132], suggesting that the upregulated integrin α5 in the HT-29S cell line may form functional α5β1 receptors.

The morphology of HT-29 and HT-29S cells following serum deprivation further supports a loss of serum dependence in the HT-29S cell line. HT-29 cells that have been deprived of serum are sparse and have largely lost their usual cobblestone appearance; many of these cells have instead adopted a "rounded-up" morphology [fig. 4.6 B)]. A similar effect occurs during apoptotic but not necrotic cell death, suggesting that, consistent with previous studies, HT-29 cells may be dying by apoptosis during serum deprivation[124,125]. In contrast, serum-starved HT-29S cells are slightly less confluent than their control counterparts but otherwise appear equally healthy [fig. 4.6 B)]. The small reduction in HT-29S cell viability upon serum withdrawal may therefore be a result of a slight reduction of proliferation due to loss of serum-derived growth factors, rather than an increase in cell death.

5.7 Akt activation and upregulation of *BCL2*

The PI3K/Akt pathway forms one branch of the downstream signalling from integrin α5β1 activation by fibronectin ligation [fig. 1.4]. We therefore assessed Akt activity in the HT-29 and HT-29S cell lines, and found that Akt phosphorylation at two amino acid residues (Ser473 and Thr308) critical for its activity were significantly increased in HT-29S [fig. 4.7]. This result is consistent with an increased activity of integrin α5β1 due to the upregulation of integrin α5 and increased fibronectin matrix formation in HT-29S, however the PI3K/Akt pathway contributes to a great number of intracellular signalling pathways. We cannot be certain that the increased Akt activity observed in HT-29S is due to integrin α5β1, although the evidence we have collected strongly suggests that it is. To support integrin α5β1 activity in HT-29S, we looked at the expression of a target gene of this pathway, *BCL2*, which also requires FAK and CAMK IV signalling dependent upon integrin α5β1 [fig. 1.4].

As can be seen in figure 4.8, *BCL2* is upregulated in HT-29S compared to HT-29. However, the upregulation of *BCL2* mRNA is quite modest- only approximately three-fold greater than HT-29. It may seem that this is too modest an increase to mediate the substantial SN-38 resistance of HT-29S, but there are a number of factors that should be considered. To begin, the change in *BCL2* expression was measured at the gene level. The small increase in *BCL2* mRNA may be greatly amplified during translation to a much greater increase in Bcl-2 protein. It should also be noted that another study which observed the pro-survival effect of Bcl-2 during serum deprivation also saw only a very minor increase in Bcl-2 expression, even at the protein level[125]. This as well as our own results is likely reflective of the nature of the Bcl-2 family; many pro- and anti-apoptotic proteins maintaining a delicate balance between cell survival and death. A small increase in an anti-apoptotic family member such as Bcl-2 may be sufficient to sway the balance towards survival, even in the face of significant cell stress.

The concept of Bcl-2 family balance raises another issue- the mere upregulation of *BCL2* expression does not necessarily prove a net anti-apoptotic effect. It is quite possible that there is a concomitant rise in the expression of one of the pro-apoptotic family members, cancelling out the upregulation of *BCL2* and leaving HT-29S no more protected against apoptosis than HT-29. To address this issue we could look further downstream in the apoptotic pathway by western blotting for markers of apoptosis induction, such as caspase 3 cleavage.

5.8 Sensitization to SN-38 by PI3K inhibition

If fibronectin and integrin α5β1 are supporting HT-29S survival during chemotherapy with SN-38, then interfering with this signalling pathway should restore HT-29S sensitivity to the drug. Previous studies have successfully interfered with the fibronectin receptor's pro-survival functions by shutting down the downstream PI3K/Akt pathway[126], presumably at least

in part by inhibiting the expression of *BCL2*. By treating HT-29 and HT-29S with the small molecule PI3K inhibitor LY294002, we found that the response to SN-38 was enhanced in the resistant population but unchanged in the parental cells [fig. 4.10 and table 4.3], supporting our hypothesis that resistance in HT-29S is mediated by activation of the fibronectin-integrin α5β1 signalling pathway outlined in fig. 1.4. The SN-38 IC50 value for HT-29S changed from approximately 358 nM in the vehicle control group to 39.2 nM with 5 μM LY294002 and 25.4 nM with 10 μM LY294002 [table 4.3], indicating a dose-dependence to the sensitization. HT-29S cells treated with 10 μM LY294002 were still more resistant to the drug than the parental cells, which had an IC50 value of 5.01 nM in the control group. This may simply indicate that some PI3K/Akt activity remained after LY294002 treatment, and that a higher dose of the inhibitor may completely restore SN-38 sensitivity. We cannot exclude the possibility though that HT-29S cells are have additional pro-survival mechanisms in place that act in concert with the fibronectin-integrin α5β1-PI3K/Akt pathway to resist the effects of SN-38. The doses of LY294002 were limited to 10 μM because higher dose would be excessively toxic to the parental HT-29 cell line [fig. 4.09 and table 4.2].

5.9 Epithelial to mesenchymal transition in HT-29S

The conversion of an epithelial cell to a mesenchymal phenotype through an EMT occurs in a number of normal conditions including during embryonic development and wound healing (reviewed in [163]). Unfortunately, this process is also frequently co-opted by cancer cells and is associated with cancer aggression, invasiveness, and chemotherapy resistance[164–166]. The expression of the EMT-promoting genes *SNAI2*, *TWIST1*, and *ZEB2* are upregulated in the HT-29S cell line, suggesting that an EMT has occurred in these cells [fig. 4.11]. Furthermore, the upregulation of integrin α5 in HT-29S is likely EMT-related, as the expression of two EMT

transcription factors that promote *ITGA5* transcription, *TWIST1* and *ZEB2*, are increased in our drug-resistant cell line[144,145]. Interestingly, many of the pro-cancer effects of a Twist1-driven EMT, such as increased invasive and migratory abilities, have been demonstrated to be mediated through integrin α5-dependent activation of FAK and c-Jun N-terminal kinase (JNK)[145]. It has also been reported that integrin α5β1 will construct pericellular fibronectin matrices as part of an EMT program[143], much like the fibronectin matrices we observe in HT-29S spheroids.

Upregulation of *SNAI2* in HT-29S was the other significant change in EMT gene expression that we observed in this set of experiments. *SNAI2* encodes the transcription factor Slug which can also promote invasion and migration. Expression of *SNAI2* can been demonstrated to be driven by both fibronectin[167] and the PI3K/Akt pathway[168], which suggests that the fibronectin-integrin α5β1 signalling axis described in HT-29S may also be responsible for driving *SNAI2* expression. This would not be entirely novel, as integrin α5β1 has been previously been implicated to driving EMTs in other systems[154,169] as have other integrins[167,170]. To the best of our knowledge however, integrin α5β1 has not previously been directly implicated in regulating *SNAI2* expression.

If an EMT has occurred in HT-29S, it likely has additional effects on their behaviour beyond promoting *ITGA5* transcription. EMTs are often considered an invasion and metastasis-enabling step in cancer progression[163], and so we may expect that our HT-29S cell line may be more aggressive than HT-29. In recent years however it has been demonstrated that multiple types of EMT are possible[163,171] and that some of these may not coincide with increased migration[172]. Therefore, we expect that the presumed EMT in HT-29S likely has increased the aggression and metastatic potential of this cell line, in part due to an upregulation of integrin α5, but this remains to be investigated. A combination of *in vitro* cell-based assays and animal

models should be performed to answer these questions. The changes in integrin expression in HT-29S and potential involvement of integrin α5β1 in the EMT experienced by these cells suggest that any changes in migratory and invasive potential of these cells will be highly dependent on the ligands with which they are presented. Invasion and migration assays should therefore be performed with a variety of ECM substrates. Given the upregulation of integrin α5β1 in HT-29S, it is reasonable to expect that fibronectin may uniquely promote invasion and migration of these cells.

It appears that an EMT program has occurred in HT-29S, and that through upregulation of *TWIST1* and *ZEB2*, it may have induced *ITGA5* expression. The α5β1 receptor then mediates the construction and ligation to a fibronectin matrix, activating a pro-survival program that upregulates *BCL2* and possibly also *SNAI2* through PI3K/Akt activation. A residual question in this model is then what event initiated the EMT and induction of *TWIST1* and *ZEB2*. Transcription of the *TWIST1* mRNA has been found to be driven by a number of factors, including steroid receptor coactivator 1 (SRC-1)[173], signal transducer and activator of transcription 3 (STAT3)[174], hypoxia-inducible factor 1 α (HIF-1α)[175], or canonical wingless-type (Wnt) signalling[176]. With so many transcriptional regulators involved, it is difficult to speculate on how the EMT process was initiated in HT-29S cells. Resolving the mechanisms of EMT induction in these cells will be an important goal in continuing the study of the SN-38 resistant phenotype. The proposed effects of the EMT in HT-29S cells are outlined in figure 5.2.

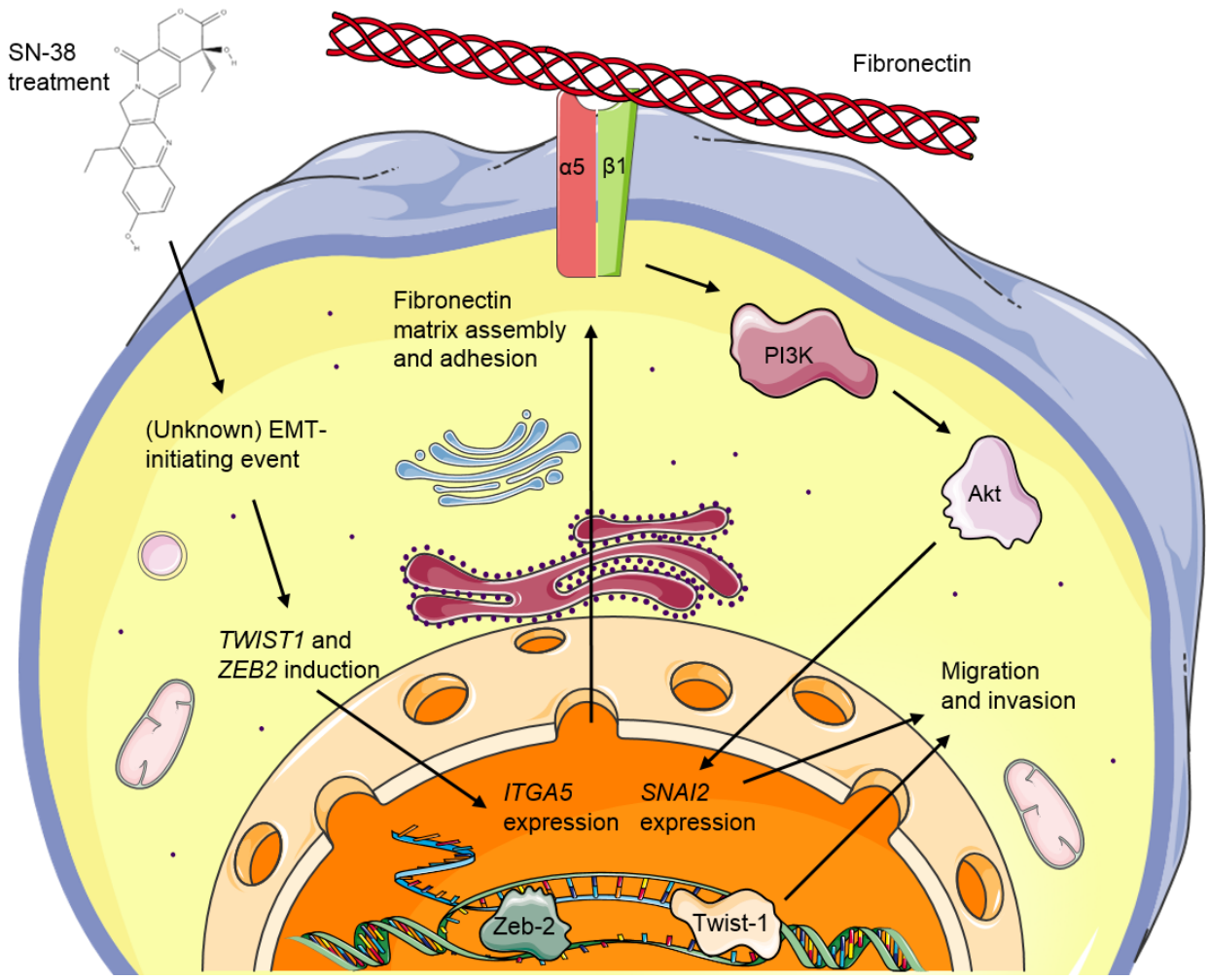

Figure 5.2: Proposed functions of EMT in HT-29S cells.

A possible role for the upregulation of the EMT genes *TWIST1*, *ZEB2*, and *SNAI2* induced by SN-38 in HT-29S, and their crossover with integrin α5β1 activity.

These images are adapted from Servier Medical Art by Servier, licensed under CC BY 3.0.

5.10 Limitations

A major limitation of the work described within this document is that it has been performed entirely *in vitro*. We cannot at this time be certain that the HT-29S cell line would retain its SN-38 resistance *in vivo*, and it should therefore be a priority going forward to study this cell line in mouse models. Doing so would also allow us to ask questions about how the

acquisition of drug resistance and in particular the EMT that HT-29S appears to have undergone have affected the aggression and metastatic capacity of this cell line.

We have compiled strong evidence but as of yet have not conclusively proven the role of integrin α5 in HT-29S resistance against SN-38. To do so we would need to either ectopically force the expression of the integrin in HT-29, or disrupt its expression in HT-29S. We have made several attempts at generating HT-29 transfectants either stably or transiently expressing a GFP-tagged integrin α5, however HT-29 is a notoriously difficult-to-transfect cell line and we have to date been unsuccessful. Our attempts at transfection have thus far been with the chemical agent X-tremeGENE HP DNA Transfection Reagent (Roche), however it may be necessary to attempt other means of transfection, such as lentiviral-mediated.

This resistance program was only studied in a single CRC cell line. Another SN-38 resistant cell line was created in parallel with HT-29S; HCT116-S derived from the CRC cell line HCT116. Despite also being highly resistant to SN-38, this cell line did not appear to share HT-29S's mechanism of resistance. HCT116-S instead appeared to resist the drug through an upregulation of the BCRP efflux pump. Although it would be interesting to see this same resistance mechanism replicated in other CRC cell lines, it is altogether not surprising there is variability in the mechanism of resistance. Cancers are a highly heterogeneous set of diseases, and even patients with the same primary tumour type may differ substantially at the cellular or genomic level. HT-29 and HCT116 differ in their cellular morphology, ploidy, p53 status, and many other traits. Some of the major differences between these cell lines are shown in table 5.1, with data from the American Type Culture Collection (ATCC) and a 2013 study on genetic features of CRC cell lines[177].

Table 5.1: HT-29 and HCT116 characteristics.

	HT-29	HCT-116
Origin	Primary CRC adenocarcinoma	Primary CRC carcinoma
Patient	44 year old male	48 year old female
Microsatellite status	Stable	Unstable
Modal Chromosome Number	71	45
BRAF	V600E	Wild-type
KRAS	Wild-type	G13D
PIK3CA	P449T	H1047R
TP53	R273H	Wild-type

5.11 Significance of the work

The contribution of integrin α5 to cancer progression has historically been controversial, with either pro- and anti-cancer functions being ascribed to the α5β1 receptor. Even recent studies that are specifically on CRC report conflicting data, with integrin α5 expression both increasing and decreasing during cancer progression[110,112]. Our demonstration of integrin α5 contributing to acquired SN-38 resistance through a CAM-DR mechanism provides support to the pro-CRC role for this protein, and does so in the context of a disease progression model that is relevant to human patients undergoing therapy. Interestingly, we also observed the reduced proliferation rate observed in other studies as a presumed anti-cancer effect of integrin α5β1[106,108]. We argue that this reduced proliferation rate should be considered, at most, a small cost in overall cell population vigour for the acquisition of drug resistance. In fact, a transient reduced proliferation rate during chemotherapy treatment may have a pro-tumour effect, as the majority of our traditional chemotherapy agents target the unregulated proliferation of cancer

cells. When the selective pressure of the chemotherapy is removed, the cancer might downregulate integrin α5 expression and resume its rapid growth. This fits well with patients who experience cancer recurrence several months or even years after chemotherapy.

Although several integrin α5β1 inhibitors are currently being developed and clinically tested, they are uniformly being proposed as anti-angiogenic agents. The role of integrin α5β1 in angiogenesis is well established and angiogenesis is a well-validated target in CRC, however our results suggest that integrin α5β1's role in cancer is not limited to angiogenesis. Ongoing preclinical and clinical studies with integrin α5β1 inhibitors should focus on determining if there is any additional benefit, beyond the anti-angiogenic effect, of integrin α5β1 inhibition in advanced CRC patients who have already failed chemotherapy with irinotecan. Such studies should combine integrin α5β1 inhibitors with irinotecan or other chemotherapy agents, as our results indicate that inhibition of the fibronectin-integrin α5β1 pathway without additional chemotherapy will be ineffective in reducing viability of CRC cells that have upregulated integrin α5 [fig. 4.10 and table 4.3].

References

1. Canadian Cancer Society's Advisory Committee on Cancer Statistics. Canadian Cancer Statistics 2015. Toronto, ON; 2015.

2. IMPACT. Efficacy of adjuvant fluorouracil and folinic acid in colon cancer. The Lancet. 1995;345(8955):939–944.

3. Bismuth H, Adam R, Lévi F, Farabos C, Waechter F, Castaing D, Majno P, Engerran L. Resection of nonresectable liver metastases from colorectal cancer after neoadjuvant chemotherapy. Annals of surgery. 1996;224(4):509–20; discussion 520–2.

4. Mitry E, Fields AL a, Bleiberg H, Labianca R, Portier G, Tu D, Nitti D, Torri V, Elias D, O'Callaghan C, et al. Adjuvant chemotherapy after potentially curative resection of metastases from colorectal cancer: A pooled analysis of two randomized trials. Journal of Clinical Oncology. 2008;26(30):4906–4911.

5. Gray R, Barnwell J, McConkey C, Hills RK, Williams NS, Kerr DJ. Adjuvant chemotherapy versus observation in patients with colorectal cancer: a randomised study. Lancet. 2007;370(9604):2020–2029.

6. D.J. J, K. S, J. M. Adjuvant systemic chemotherapy for stage II and III colon cancer following complete resection. Clinical Oncology. 2011;23(5):314–322.

7. National Comprehensive Cancer Network. Clinical Practice Guidelines in Oncology: Colon Cancer. 2015. 85 p.

8. Longley DB, Harkin DP, Johnston PG. 5-Fluorouracil: Mechanisms of Action and Clinical Strategies. Nature reviews. Cancer. 2003;3(5):330–338.

9. Graham J, Muhsin M, Kirkpatrick P. Fresh from the pipeline: Oxaliplatin. Nature Reviews Drug Discovery. 2004;3(1):11–12.

10. Andre T, Boni C, Navarro M, Tabernero J, Hickish T, Topham C, Bonetti A, Clingan P, Bridgewater J, Rivera F, et al. Improved Overall Survival With Oxaliplatin, Fluorouracil, and Leucovorin As Adjuvant Treatment in Stage II or III Colon Cancer in the MOSAIC Trial. Journal of Clinical Oncology. 2009;27(19):3109–3116.

11. Kuebler JP, Wieand HS, O'Connell MJ, Smith RE, Colangelo LH, Yothers G, Petrelli NJ, Findlay MP, Seay TE, Atkins JN, et al. Oxaliplatin Combined With Weekly Bolus Fluorouracil and Leucovorin As Surgical Adjuvant Chemotherapy for Stage II and III Colon Cancer: Results From NSABP C-07. Journal of Clinical Oncology. 2007;25(16):2198–2204.

12. Rougier P, Van Cutsem E, Bajetta E, Niederle N, Possinger K, Labianca R, Navarro M, Morant R, Bleiberg H, Wils J, et al. Randomised trial of irinotecan versus fluorouracil by continuous infusion after fluorouracil failure in patients with metastatic colorectal cancer. Lancet. 1998;352(9138):1407–1412.

13. Cunningham D, Pyrhönen S, James RD, Punt CJ, Hickish TF, Heikkila R, Johannesen TB, Starkhammar H, Topham C a, Awad L, et al. Randomised trial of irinotecan plus supportive care versus supportive care alone after fluorouracil failure for patients with metastatic colorectal cancer. Lancet. 1998;352(9138):1413–1418.

14. Douillard JY, Cunningham D, Roth a D, Navarro M, James RD, Karasek P, Jandik P, Iveson T, Carmichael J, Alakl M, et al. Irinotecan combined with fluorouracil compared with fluorouracil alone as first-line treatment for metastatic colorectal cancer: a multicentre randomised trial. Lancet. 2000;355(9209):1041–1047.

15. Saskatchewan Cancer Agency. Provincial Colorectal Cancer Treatment Guidelines . Provincial Colorectal Cancer Meeting. 2011:1–15.

16. Asmis T, Berry S, Cosby R, Chan K, Coburn N, Rother M. Strategies of sequential therapies in unresectable , metastatic colorectal cancer treated with palliative intent. Toronto, ON; 2014. 1-39 p.

17. M.E.Wall, Wani, C.E. Cook, K.H. Palmer, A.T. McPhail G a. S. Plant anitumor agents I. The isolation and structure of camptothecin, a novel alkaloidal leukemia and tumor inhibitor from camptotheca acuminata. J.Am.Chem.Soc. 88. 1966;(2):3888–3890.

18. Hsiang YH, Hertzberg R, Hecht S, Liu LF. Camptothecin induced protein-linked DNA breaks via mammalian DNA topoisomerase. 1985;260:14873–14878.

19. Stivers JT, Harris TK, Mildvan AS. Vaccinia DNA topoisomerase I: Evidence supporting a free rotation mechanism for DNA supercoil relaxation. Biochemistry. 1997;36(17):5212–5222.

20. Hsiang YH, Lihou MG, Liu LF. Arrest of replication forks by drug-stabilized topoisomerase I-DNA cleavable complexes as a mechanism of cell killing by camptothecin. Cancer Research. 1989;49(18):5077–5082.

21. Avemann K, Knippers R, Koller T, Sogo JM. Camptothecin, a specific inhibitor of type I DNA topoisomerase, induces DNA breakage at replication forks. Molecular and cellular biology. 1988;8(8):3026–3034.

22. Ryan a J, Squires S, Strutt HL, Johnson RT. Camptothecin cytotoxicity in mammalian cells is associated with the induction of persistent double strand breaks in replicating DNA. Nucleic acids research. 1991;19(12):3295–3300.

23. D'Arpa P, Beardmore C, Liu LF. Involvement of nucleic acid synthesis in cell killing mechanisms of topoisomerase poisons. Cancer research. 1990;50(21):6919–24.

24. Holm C, Covey JM, Kerrigan D, Pommier Y. Differential Requirement of DNA Replication for the Cytotoxicity of DNA Topoisomerase I and II Inhibitors in Chinese Hamster Differential Requirement of DNA Replication for the Cytotoxicity of DNA Topoisomerase I and II Inhibitors in Chinese Hamster DC3F . 1989;(8):6365–6368.

25. Morris EJ. Topoisomerase-I : Evidence for Cell Cycle-independent Toxicity. Cell. 1996;134(3):757–770.

26. Ljungman M, Hanawalt PC. The anti-cancer drug camptothecin inhibits elongation but stimulates initiation of RNA polymerase II transcription. Carcinogenesis. 1996;17(1):31–35.

27. Wu J, Liu LF. Processing of topoisomerase I cleavable complexes into DNA damage by transcription. Nucleic Acids Research. 1997;25(21):4181–4186.

28. Pommier Y. Topoisomerase I inhibitors: camptothecins and beyond. Nature reviews. Cancer. 2006;6(10):789–802.

29. Kunimoto T, Nitta K, Tanaka T, Uehara N, Baba H, Takeuchi M, Yokokura T, Sawada S, Miyasaka T, Mutai M. Antitumor activity of 7-ethyl-10-[4-(1-piperidino)-1-piperidino]carbonyloxy-camptothecin, a novel water-soluble derivative of camptothecin, against murine tumors. Cancer research. 1987;47(22):5944–7.

30. Kaneda N, Nagata H, Furuta T, Yokokura T. Metabolism and pharmacokinetics of the camptothecin analogue CPT-11 in the mouse. Cancer Research. 1990;50(6):1715–1720.

31. Shingyoji M, Takiguchi Y, Watanabe-Uruma R, Asaka-Amano Y, Matsubara H, Kurosu K, Kasahara Y, Tanabe N, Tatsumi K, Kuriyama T. In vitro conversion of irinotecan to SN-38 in human plasma. Cancer Science. 2004 [accessed 2015 Sep 15];95(6):537–540. http://doi.wiley.com/10.1111/j.1349-7006.2004.tb03245.x

32. Rivory LP, Bowles MR, Robert J, Pond SM. Conversion of irinotecan (CPT-11) to its active metabolite, 7-ethyl-10-hydroxycamptothecin (SN-38) by human liver carboxylesterase. Biochemical Pharmacology. 1996;52(7):1103–1111.

33. Khanna R, Morton CL, Danks MK, Potter PM. Proficient metabolism of irinotecan by a human intestinal carboxylesterase. Cancer Research. 2000;60(17):4725–4728.

34. Ohtsuka K, Inoue S, Kameyama M, Kanetoshi A, Fujimoto T, Takaoka K, Araya Y, Shida A. Intracellular conversion of irinotecan to its active form, SN-38, by native carboxylesterase in human non-small cell lung cancer. Lung Cancer. 2003;41(2):187–198.

35. Mathijssen RH, van Alphen RJ, Verweij J, Loos WJ, Nooter K, Stoter G, Sparreboom a. Clinical pharmacokinetics and metabolism of irinotecan (CPT-11). Clinical cancer research : an official journal of the American Association for Cancer Research. 2001;7(8):2182–2194.

36. Atsumi R, Suzuki W, Hakusui H. Identification of the metabolites of irinotecan, a new derivative of camptothecin, in rat bile and its biliary excretion. Xenobiotica; the fate of foreign compounds in biological systems. 1991 [accessed 2015 Sep 16];21(9):1159–1169. http://www.ncbi.nlm.nih.gov/pubmed/1788984

37. Rivory LP, Robert J. Identification and kinetics of a beta-glucuronide metabolite of SN-38 in human plasma after administration of the camptothecin derivative irinotecan. Cancer chemotherapy and pharmacology. 1995 [accessed 2015 Sep 16];36(2):176–9. http://www.ncbi.nlm.nih.gov/pubmed/7767955

38. Haaz MC, Rivory L, Jantet S, Ratanasavanh D, Robert J. Glucuronidation of SN-38, the active metabolite of irinotecan, by human hepatic microsomes. Pharmacology & toxicology. 1997;80(2):91–96.

39. Gupta E, Lestingi TM, Mick R, Ramirez J, Vokes EE, Ratain MJ. Metabolic fate of irinotecan in humans: Correlation of glucuronidation with diarrhea. Cancer Research. 1994;54(14):3723–3725.

40. Takasuna K, Hagiwara T, Hirohashi M, Kato M, Nomura M, Nagai E, Yokoi T, Kamataki T. Involvement of beta-glucuronidase in intestinal microflora in the intestinal toxicity of the antitumor camptothecin derivative irinotecan hydrochloride (CPT-11) in rats. Cancer Research. 1996;56(16):3752–3757.

41. Slatter JG, Schaaf LJ, Sams JP, Feenstra KL, Johnson MG, Bombardt P a, Cathcart KSUE,

Verburg MT, Pearson LK, Compton LD, et al. Pharmacokinetics , Metabolism , and Excretion of Irinotecan (Cpt-11) Following I . V . Infusion of [14 C] Cpt-11 in Cancer Patients Abstract : 2000;28(4).

42. Benoist S. Complete Response of Colorectal Liver Metastases After Chemotherapy: Does It Mean Cure? Journal of Clinical Oncology. 2006;24(24):3939–3945.

43. Li S, Kennedy M, Payne S, Kennedy K, Seewaldt VL, Pizzo S V., Bachelder RE. Model of Tumor Dormancy/Recurrence after Short-Term Chemotherapy. PLoS ONE. 2014;9(5):e98021.

44. O'Connell MJ, Campbell ME, Goldberg RM, Grothey A, Seitz J-F, Benedetti JK, Andre T, Haller DG, Sargent DJ. Survival Following Recurrence in Stage II and III Colon Cancer: Findings From the ACCENT Data Set. Journal of Clinical Oncology. 2008;26(14):2336–2341.

45. Ueda K, Cardarelli C, Gottesman MM, Pastan I. Expression of a full-length cDNA for the human "MDR1" gene confers resistance to colchicine, doxorubicin, and vinblastine. Proceedings of the National Academy of Sciences of the United States of America. 1987;84(9):3004–3008.

46. Yamagishi T, Sahni S, Sharp DM, Arvind A, Jansson PJ, Richardson DR. P-glycoprotein mediates drug resistance via a novel mechanism involving lysosomal sequestration. Journal of Biological Chemistry. 2013;288(44):31761–31771.

47. van den Heuvel-Eibrink MM, Wiemer EA, Prins A, Meijerink JP, Vossebeld PJ, van der Holt B, Pieters R, Sonneveld P. Increased expression of the breast cancer resistance protein (BCRP) in relapsed or refractory acute myeloid leukemia (AML). Leukemia : official journal of the Leukemia Society of America, Leukemia Research Fund, U.K. 2002;16(5):833–839.

48. Yu M, Ocana A, Tannock IF. Reversal of ATP-binding cassette drug transporter activity to modulate chemoresistance: Why has it failed to provide clinical benefit? Cancer and Metastasis Reviews. 2013;32(1-2):211–227.

49. Frantz C, Stewart KM, Weaver VM. The extracellular matrix at a glance. Journal of cell science. 2010;123:4195–4200.

50. Hynes RO, Zhao Q. The evolution of cell adhesion. The Journal of cell biology. 2000;150(2):F89–96.

51. Exposito JY, Larroux C, Cluzel C, Valcourt U, Lethias C, Degnan BM. Demosponge and sea anemone fibrillar collagen diversity reveals the early emergence of A/C clades and the maintenance of the modular structure of type V/XI collagens from sponge to human. Journal of Biological Chemistry. 2008;283(42):28226–28235.

52. Ioachim E, Charchanti a., Briasoulis E, Karavasilis V, Tsanou H, Arvanitis DL, Agnantis NJ, Pavlidis N. Immunohistochemical expression of extracellular matrix components tenascin, fibronectin, collagen type IV and laminin in breast cancer: Their prognostic value and role in tumour invasion and progression. European Journal of Cancer. 2002;38(18):2362–2370.

53. Fernandez-Garcia B, Eiró N, Marín L, González-Reyes S, González LO, Lamelas ML, Vizoso FJ. Expression and prognostic significance of fibronectin and matrix metalloproteases in breast cancer metastasis. Histopathology. 2014;64(4):512–522.

54. Saito N, Nishimura H, Kameoka S. Clinical significance of fibronectin expression in colorectal cancer. Molecular medicine reports. 2008;1:77–81.

55. Ruoslahti E, Vaheri A, Kuusela P, Linder E. Fibroblast surface antigen: a new serum protein. Biochimica et biophysica acta. 1973;322(2):352–358.

56. Hynes RO. Alteration of cell-surface proteins by viral transformation and by proteolysis. Proceedings of the National Academy of Sciences of the United States of America. 1973;70(11):3170–3174.

57. Hynes RO. The emergence of integrins: A personal and historical perspective. Matrix Biology. 2004;23(6):333–340.

58. Hynes RO. Cell surface proteins and malignant transformation. Biochimica et biophysica acta. 1976;458(1):73–107.

59. Chen LB, Murray a, Segal R a, Bushnell a, Walsh ML. Studies on intercellular LETS glycoprotein matrices. Cell. 1978;14(2):377–391.

60. Wartiovaara J, Linder E, Ruoslahti E, Vaheri A. Distribution of fibroblast surface antigen: association with fibrillar structures of normal cells and loss upon viral transformation. The Journal of experimental medicine. 1974;140(6):1522–1533.

61. Singer II. The fibronexus: a transmembrane association of fibronectin-containing fibers and bundles of 5 nm microfilaments in hamster and human fibroblasts. Cell. 1979;16(3):675–685.

62. Chen WT, Hasegawa E, Hasegawa T, Weinstock C, Yamada KM. Development of cell surface linkage complexes in cultured fibroblasts. Journal of Cell Biology. 1985;100(4):1103–1114.

63. Horwitz a., Duggan K, Greggs R, Decker C, Buck C. The cell substrate attachment (CSAT) antigen has properties of a receptor for laminin and fibronectin. Journal of Cell Biology. 1985;101(6):2134–2144.

64. Tamkun JW, DeSimone DW, Fonda D, Patel RS, Buck C, Horwitz a F, Hynes RO. Structure of integrin, a glycoprotein involved in the transmembrane linkage between fibronectin and actin. Cell. 1986;46(2):271–282.

65. Kishimoto TK, O'Connor K, Lee a, Roberts TM, Springer T a. Cloning of the beta subunit of the leukocyte adhesion proteins: homology to an extracellular matrix receptor defines a novel supergene family. Cell. 1987;48(4):681–690.

66. Law SK, Gagnon J, Hildreth JE, Wells CE, Willis a C, Wong a J. The primary structure of the beta-subunit of the cell surface adhesion glycoproteins LFA-1, CR3 and p150,95 and its relationship to the fibronectin receptor. The EMBO journal. 1987;6(4):915–919.

67. Brower DL, Brower SM, Hayward DC, Ball EE. Molecular evolution of integrins: genes encoding integrin beta subunits from a coral and a sponge. Proceedings of the National Academy of Sciences of the United States of America. 1997;94(17):9182–7.

68. Sebé-Pedrós A, Roger AJ, Lang FB, King N, Ruiz-Trillo I. Ancient origin of the integrin-mediated adhesion and signaling machinery. Proceedings of the National Academy of Sciences of the United States of America. 2010;107(22):10142–10147.

69. Hynes RO. Integrins: A family of cell surface receptors. Cell. 1987;48(4):549–554.

70. Wolfenson H, Lavelin I, Geiger B. Dynamic Regulation of the Structure and Functions of

Integrin Adhesions. Developmental Cell. 2013;24(5):447–458.

71. Kim C, Schmidt T, Cho E-G, Ye F, Ulmer TS, Ginsberg MH. Basic amino-acid side chains regulate transmembrane integrin signalling. Nature. 2011:1–7.

72. Tan CL, Kwok JCF, Heller JPD, Zhao R, Eva R, Fawcett JW. Full length talin stimulates integrin activation and axon regeneration. Molecular and cellular neurosciences. 2015;68:1–8.

73. Montanez E, Ussar S, Schifferer M, Bosl M, Zent R, Moser M, Fassler R. Kindlin-2 controls bidirectional signaling of integrins. Genes & development. 2008;22(10):1325–1330.

74. Kim C, Ye F, Hu X, Ginsberg MH. Talin activates integrins by altering the topology of the β transmembrane domain. The Journal of cell biology. 2012;197(5):605–11.

75. Wang J, Shiratori I, Uehori J, Ikawa M, Arase H. Neutrophil infiltration during inflammation is regulated by PILRα via modulation of integrin activation. Nature immunology. 2013;14(1):34–40.

76. Kinashi T. Intracellular signalling controlling integrin activation in lymphocytes. Nature Reviews Immunology. 2005;5(7):546–559.

77. Levi L, Toyooka T, Patarroyo M, Frisan T. Bacterial Genotoxins Promote Inside-Out Integrin β1 Activation, Formation of Focal Adhesion Complexes and Cell Spreading. PloS one. 2015;10(4):e0124119.

78. Schreiber TD, Steinl C, Essl M, Abele H, Geiger K, Müller C a, Aicher WK, Klein G. The integrin alpha9beta1 on hematopoietic stem and progenitor cells: involvement in cell adhesion, proliferation and differentiation. Haematologica. 2009;94(11):1493–1501.

79. Bazigou E, Xie S, Chen C, Weston A, Miura N, Sorokin L, Adams R, Muro AF, Sheppard D, Makinen T. Integrin-α9 Is Required for Fibronectin Matrix Assembly during Lymphatic Valve Morphogenesis. Developmental Cell. 2009;17(2):175–186.

80. Gupta SK, Vlahakis NE. Integrin alpha9beta1 mediates enhanced cell migration through nitric oxide synthase activity regulated by Src tyrosine kinase. Journal of cell science. 2009;122(Pt 12):2043–2054.

81. Ito K, Morimoto J, Kihara A, Matsui Y, Kurotaki D, Kanayama M, Simmons S, Ishii M, Sheppard D, Takaoka A, et al. Integrin α9 on lymphatic endothelial cells regulates lymphocyte egress. Proceedings of the National Academy of Sciences of the United States of America. 2014;111(8):3080–5.

82. Yoshimura K, Meckel KF, Laird LS, Chia CY, Park J-J, Olino KL, Tsunedomi R, Harada T, Iizuka N, Hazama S, et al. Integrin 2 Mediates Selective Metastasis to the Liver. Cancer Research. 2009;69(18):7320–7328.

83. Bartolomé R a, Barderas R, Torres S, Fernandez-Aceñero MJ, Mendes M, García-Foncillas J, Lopez-Lucendo M, Casal JI. Cadherin-17 interacts with α2β1 integrin to regulate cell proliferation and adhesion in colorectal cancer cells causing liver metastasis. Oncogene. 2014;33(April 2013):1658–69.

84. Pelillo C, Bergamo A, Mollica H, Bestagno M, Sava G. Colorectal Cancer Metastases Settle in the Hepatic Microenvironment Through alpha5beta1 Integrin. Journal of cellular

biochemistry. 2015;116(10):2385–2396.

85. Liu H, Radisky DC, Yang D, Xu R, Radisky ES, Bissell MJ, Bishop JM. MYC suppresses cancer metastasis by direct transcriptional silencing of αv and β3 integrin subunits. Nature cell biology. 2012;14(6):567–74.

86. Huhtala P, Humphries MJ, McCarthy JB, Tremble PM, Werb Z, Damsky CH. Cooperative signaling by alpha 5 beta 1 and alpha 4 beta 1 integrins regulates metalloproteinase gene expression in fibroblasts adhering to fibronectin. The Journal of cell biology. 1995;129(3):867–79.

87. Jia Y, Zeng Z-ZZ, Markwart SM, Rockwood KF, Ignatoski KM, Ethier SP, Livant DL. Integrin fibronectin receptors in matrix metalloproteinase-1-dependent invasion by breast cancer and mammary epithelial cells. TL - 64. Cancer research. 2004;64 VN - r(23):8674–8681.

88. Frisch SM, Francis H. Disruption of epithelial cell-matrix interactions induces apoptosis. The Journal of cell biology. 1994;124(4):619–26.

89. Sethi T, Rintoul RC, Moore SM, MacKinnon a C, Salter D, Choo C, Chilvers ER, Dransfield I, Donnelly SC, Strieter R, et al. Extracellular matrix proteins protect small cell lung cancer cells against apoptosis: a mechanism for small cell lung cancer growth and drug resistance in vivo. Nature medicine. 1999;5(6):662–668.

90. Hodkinson PS, Elliott T, Wong WS, Rintoul RC, Mackinnon a C, Haslett C, Sethi T. ECM overrides DNA damage-induced cell cycle arrest and apoptosis in small-cell lung cancer cells through beta1 integrin-dependent activation of PI3-kinase. Cell death and differentiation. 2006;13(10):1776–1788.

91. De Toni F, Racaud-Sultan C, Chicanne G, Mas VM-D, Cariven C, Mesange F, Salles J-P, Demur C, Allouche M, Payrastre B, et al. A crosstalk between the Wnt and the adhesion-dependent signaling pathways governs the chemosensitivity of acute myeloid leukemia. Oncogene. 2006;25(22):3113–3122.

92. Matsunaga T, Takemoto N, Sato T, Takimoto R, Tanaka I, Fujimi A, Akiyama T, Kuroda H, Kawano Y, Kobune M, et al. Interaction between leukemic-cell VLA-4 and stromal fibronectin is a decisive factor for minimal residual disease of acute myelogenous leukemia. Nature Medicine. 2003;9(9):1158–1165.

93. Damiano JS, Cress a E, Hazlehurst L a, Shtil a a, Dalton WS. Cell adhesion mediated drug resistance (CAM-DR): role of integrins and resistance to apoptosis in human myeloma cell lines. Blood. 1999;93(5):1658–1667.

94. Xing H, Weng D, Chen G, Tao W, Zhu T, Yang X, Meng L, Wang S, Lu Y, Ma D. Activation of fibronectin/PI-3K/Akt2 leads to chemoresistance to docetaxel by regulating survivin protein expression in ovarian and breast cancer cells. Cancer Letters. 2008;261(1):108–119.

95. Zhang L, Zou W. Inhibition of integrin β1 decreases the malignancy of ovarian cancer cells and potentiates anticancer therapy via the FAK/STAT1 signaling pathway. Molecular Medicine Reports. 2015:7869–7876.

96. Pierschbacher MD, Ruoslahti E. Cell attachment activity of fibronectin can be duplicated by

small synthetic fragments of the molecule. Nature. 1984;309(5963):30–3.

97. Pytela R, Pierschbacher MD, Ruoslahti E. Identification and isolation of a 140 kd cell surface glycoprotein with properties expected of a fibronectin receptor. Cell. 1985;40(1):191–198.

98. Ruoslahti E. RGD and other recognition sequences for integrins. Annual review of cell and developmental biology. 1996;12:697–715.

99. Huveneers S, Truong H, Fässler R, Sonnenberg A, Danen EHJ. Binding of soluble fibronectin to integrin alpha5 beta1 - link to focal adhesion redistribution and contractile shape. Journal of cell science. 2008;121(Pt 15):2452–2462.

100. Zhang Z, Morla AO, Vuori K, Bauer JS, Juliano RL, Ruoslahti E. The αvβ1 integrin functions as a fibronectin receptor but does not support fibronectin matrix assembly and cell migration on fibronectin. Journal of Cell Biology. 1993 [accessed 2015 Apr 27];122(1):235–242. http://www.pubmedcentral.nih.gov/articlerender.fcgi?artid=2119613&tool=pmcentrez&rendertype=abstract

101. Qiao L, Gao H, Zhang T, Jing L, Xiao C, Xiao Y, Luo N, Zhu H, Meng W, Xu H, et al. Snail modulates the assembly of fibronectin via α5 integrin for myocardial migration in zebrafish embryos. Scientific reports. 2014;4:4470.

102. Wu C, Keightley SY, Leung-Hagesteijn C, Radeva G, Coppolino M, Goicoechea S, McDonald JA, Dedhar S. Integrin-linked protein kinase regulates fibronectin matrix assembly, E- cadherin expression, and tumorigenicity. J Biol Chem. 1998;273(1):528–536.

103. Pankov R, Cukierman E, Katz BZ, Matsumoto K, Lin DC, Lin S, Hahn C, Yamada KM. Integrin dynamics and matrix assembly: Tensin-dependent translocation of α5β1 integrins promotes early fibronectin fibrillogenesis. Journal of Cell Biology. 2000;148(5):1075–1090.

104. Magruder HT, Quinn J a., Schwartzbauer JE, Reichner J, Huang A, Filardo EJ. The G Protein-Coupled Estrogen Receptor-1, GPER-1, Promotes Fibrillogenesis via a Shc-Dependent Pathway Resulting in Anchorage-Independent Growth. Hormones and Cancer. 2014;5:390–404.

105. Stallmach a, von Lampe B, Matthes H, Bornhöft G, Riecken EO. Diminished expression of integrin adhesion molecules on human colonic epithelial cells during the benign to malign tumour transformation. Gut. 1992;33(3):342–6.

106. Giancotti FG, Ruoslahti E. Elevated levels of the alpha 5 beta 1 fibronectin receptor suppress the transformed phenotype of Chinese hamster ovary cells. Cell. 1990;60(5):849–859.

107. Wang Y, Shenouda S, Baranwal S, Rathinam R, Jain P, Bao L, Hazari S, Dash S, Alahari SK. Integrin subunits alpha5 and alpha6 regulate cell cycle by modulating the chk1 and Rb/E2F pathways to affect breast cancer metastasis. Molecular cancer. 2011;10(1):84.

108. Varner J a, Emerson D a, Juliano RL. Integrin alpha 5 beta 1 expression negatively regulates cell growth: reversal by attachment to fibronectin. Molecular biology of the cell. 1995;6(6):725–740.

109. Schmidt R, Streit M, Kaiser R, Herzberg F, Schirner M, Schramm K, Kaufmann C, Henneken M, Schäfer-Korting M, Thiel E, et al. De novo expression of the α5β1-fibronectin receptor in HT29 colon- cancer cells reduces activity of c-src. Increase of c-src activity by attachment on fibronectin. International Journal of Cancer. 1998;76(1):91–98.

110. Yin X, Zhang Y, Guo S, Jin H, Wang W, Yang P. Large scale systematic proteomic quantification from non-metastatic to metastatic colorectal cancer. Scientific Reports. 2015;5:12120.

111. Gong J, Wang D, Sun L, Zborowska E, Willson JK, Brattain MG. Role of alpha5beta 1 integrin in determining malignant properties of colon carcinoma cells. Cell Growth & Differentiation. 1997;8(1):83–90.

112. Kim S, Kang HY, Nam EH, Choi MS, Zhao XF, Hong CS, Lee JW, Lee JH, Park YK. TMPRSS4 induces invasion and epithelial-mesenchymal transition through upregulation of integrin α5 and its signaling pathways. Carcinogenesis. 2010;31(4):597–606.

113. Boudreau NJ, Varner J a. The homeobox transcription factor Hox D3 promotes integrin alpha5beta1 expression and function during angiogenesis. The Journal of biological chemistry. 2004;279(6):4862–8.

114. Lee M-Y, Huang J-P, Chen Y-Y, Aplin JD, Wu Y-H, Chen C-Y, Chen P-C, Chen C-P. Angiogenesis in differentiated placental multipotent mesenchymal stromal cells is dependent on integrin alpha5beta1. PloS one. 2009;4(10):e6913.

115. Koivunen E. Isolation of a highly specific ligand for the alpha 5 beta 1 integrin from a phage display library. The Journal of Cell Biology. 1994;124(3):373–380.

116. Kim S, Bell K, Mousa S a, Varner J a. Regulation of angiogenesis in vivo by ligation of integrin alpha5beta1 with the central cell-binding domain of fibronectin. The American journal of pathology. 2000;156(4):1345–1362.

117. Stoeltzing O, Liu W, Reinmuth N, Fan F, Parry GC, Parikh A a., McCarty MF, Bucana CD, Mazar AP, Ellis LM. Inhibition of integrin α5β1 function with a small peptide (ATN-161) plus continuous 5-fu infusion reduces colorectal liver metastases and improves survival in mice. International Journal of Cancer. 2003;104(4):496–503.

118. Khalili P, Arakelian A, Chen G, Plunkett ML, Beck I, Parry GC, Doñate F, Shaw DE, Mazar AP, Rabbani S a. A non-RGD-based integrin binding peptide (ATN-161) blocks breast cancer growth and metastasis in vivo. Molecular cancer therapeutics. 2006;5(9):2271–2280.

119. Ramakrishnan V, Bhaskar V, Law D a, Wong MHL, DuBridge RB, Breinberg D, O'Hara C, Powers DB, Liu G, Grove J, et al. Preclinical evaluation of an anti-alpha5beta1 integrin antibody as a novel anti-angiogenic agent. Journal of experimental therapeutics & oncology. 2006;5(4):273–286.

120. Ricart AD, Tolcher AW, Liu G, Holen K, Schwartz G, Albertini M, Weiss G, Yazji S, Ng C, Wilding G. Volociximab, a chimeric monoclonal antibody that specifically binds α 5β 1 integrin: A phase l, pharmacokinetic, and biological correlative study. Clinical Cancer Research. 2008;14(23):7924–7929.

121. Besse B, Tsao LC, Chao DT, Fang Y, Soria JC, Almokadem S, Belani CP. Phase Ib safety and pharmacokinetic study of volociximab, an anti-α5β1 integrin antibody, in combination with carboplatin and paclitaxel in advanced non-small-cell lung cancer. Annals of Oncology. 2013;24(1):92–96.

122. Bell-Mcguinn KM, Matthews CM, Ho SN, Barve M, Gilbert L, Penson RT, Lengyel E,

Palaparthy R, Gilder K, Vassos A, et al. A phase II, single-arm study of the anti-α5β1 integrin antibody volociximab as monotherapy in patients with platinum-resistant advanced epithelial ovarian or primary peritoneal cancer. Gynecologic Oncology. 2011;121(2):273–279.

123. Mateo J, Berlin J, de Bono JS, Cohen RB, Keedy V, Mugundu G, Zhang L, Abbattista A, Davis C, Gallo Stampino C, et al. A first-in-human study of the anti-α5β1 integrin monoclonal antibody PF-04605412 administered intravenously to patients with advanced solid tumors. Cancer chemotherapy and pharmacology. 2014;74(5):1039–46.

124. O'Brien V, Frisch SM, Juliano RL. Expression of the integrin alpha 5 subunit in HT29 colon carcinoma cells suppresses apoptosis triggered by serum deprivation. Experimental cell research. 1996;224(1):208–213.

125. Zhang Z, Vuori K, Reed JC, Ruoslahti E. The alpha 5 beta 1 integrin supports survival of cells on fibronectin and up-regulates Bcl-2 expression. Proceedings of the National Academy of Sciences of the United States of America. 1995 [accessed 2015 Apr 28];92(13):6161–6165. C:\Users\Spencer\Downloads\pnas01489-0409.pdf

126. Lee JW, Juliano RLL. alpha5beta1 integrin protects intestinal epithelial cells from apoptosis through a phosphatidylinositol 3-kinase and protein kinase B-dependent pathway. Molecular biology of the cell. 2000 [accessed 2015 May 1];11(6):1973–1987. http://www.molbiolcell.org/content/11/6/1973.abstract

127. Spangenberg C, Lausch EU, Trost TM, Prawitt D, May A, Keppler R, Fees SA, Reutzel D, Bell C, Schmitt S, et al. ERBB2-mediated transcriptional up-regulation of the alpha5beta1 integrin fibronectin receptor promotes tumor cell survival under adverse conditions. TL - 66. Cancer research. 2006;66 VN - r(7):3715–3725.

128. Miyashita T, Reed JC. Bcl-2 oncoprotein blocks chemotherapy-induced apoptosis in a human leukemia cell line. Blood. 1993;81(1):151–157.

129. Kamesaki S, Kamesaki H, Jorgensen TJ, Tanizawa A, Pommier Y, Cossman J. bcl-2 protein inhibits etoposide-induced apoptosis through its effects on events subsequent to topoisomerase II-induced DNA strand breaks and their repair. Cancer research. 1993 [accessed 2015 Apr 28];53(18):4251–6. http://cancerres.aacrjournals.org/content/53/18/4251.abstract

130. Lock RB, Stribinskiene L. Dual modes of death induced by etoposide in human epithelial tumor cells allow Bcl-2 to inhibit apoptosis without affecting clonogenic survival. Cancer research. 1996 [accessed 2015 Apr 28];56(17):4006–12. http://cancerres.aacrjournals.org/content/56/17/4006.abstract

131. Lee B-H, Ruoslahti E. alpha5beta1 integrin stimulates Bcl-2 expression and cell survival through Akt, focal adhesion kinase, and Ca2+/calmodulin-dependent protein kinase IV. Journal of cellular biochemistry. 2005 [accessed 2015 Apr 28];95(6):1214–23. http://www.ncbi.nlm.nih.gov/pubmed/15962308

132. Matter ML, Ruoslahti E. A signaling pathway from the alpha5beta1 and alpha(v)beta3 integrins that elevates bcl-2 transcription. The Journal of biological chemistry. 2001;276(30):27757–27763.

133. Itano N, Okamoto S, Zhang D, Lipton S a, Ruoslahti E. Cell spreading controls endoplasmic and nuclear calcium: a physical gene regulation pathway from the cell surface to the

nucleus. Proceedings of the National Academy of Sciences of the United States of America. 2003;100(9):5181–5186.

134. Premier Biosoft. Primer Design Guide for PCR. 2012 [accessed 2015 May 5]:3–4. http://www.premierbiosoft.com/tech_notes/PCR_Primer_Design.html

135. Methods D, Design P, Guide A. qPCR Technical Guide. Science. 2008.

136. Biosystems A. Applied Biosystems StepOne ™ Reagent Guide. 2008:148.

137. Ramakers C, Ruijter JM, Lekanne Deprez RH, Moorman AFM. Assumption-free analysis of quantitative real-time polymerase chain reaction (PCR) data. Neuroscience Letters. 2003;339(1):62–66.

138. Ruijter JM, Ramakers C, Hoogaars WMH, Karlen Y, Bakker O, Van Den Hoff MJB, Moorman a. FM. Amplification efficiency: Linking baseline and bias in the analysis of quantitative PCR data. Nucleic Acids Research. 2009;37(6).

139. Bridgewater RE, Norman JC, Caswell PT. Integrin trafficking at a glance. Journal of Cell Science. 2012;125(16):3695–3701.

140. Takada Y, Ye X, Simon S. The integrins. Genome biology. 2007;8(5):215.

141. Mallawaaratchy DM, Mactier S, Kaufman KL, Blomfield K, Christopherson RI. The phosphoinositide 3-kinase inhibitor LY294002, decreases aminoacyl-tRNA synthetases, chaperones and glycolytic enzymes in human HT-29 colorectal cancer cells. Journal of proteomics. 2012 [accessed 2015 Sep 17];75(5):1590–9. http://www.sciencedirect.com/science/article/pii/S1874391911006622

142. Cho SH, Park YS, Kim HJ, Kim CH, Lim SW, Huh JW, Lee JH, Kim HR. CD44 enhances the epithelial-mesenchymal transition in association with colon cancer invasion. International Journal of Oncology. 2012;41(1):211–218.

143. Maschler S, Wirl G, Spring H, Bredow D V, Sordat I, Beug H, Reichmann E. Tumor cell invasiveness correlates with changes in integrin expression and localization. Oncogene. 2005;24(12):2032–41.

144. Nam E-H, Lee Y, Park Y-K, Lee JW, Kim S. ZEB2 upregulates integrin 5 expression through cooperation with Sp1 to induce invasion during epithelial-mesenchymal transition of human cancer cells TL - 33. Carcinogenesis. 2012;33 VN - r(3):563–571.

145. Nam E-H, Lee Y, Moon B, Lee JW, Kim S. Twist1 and AP-1 cooperatively upregulate integrin 5 expression to induce invasion and the epithelial-mesenchymal transition. Carcinogenesis. 2015;36(3):327–337.

146. Lee S, Lee S, Cho I, Oh M, Kang E, Kim Y, Seo D, Choi S, Nam J, Tamamori-adachi M, et al. Tetraspanin TM4SF5 mediates loss of contact inhibition through epithelial-mesenchymal transition in human hepatocarcinoma. 2008;118(4).

147. Zink D, Fische AH, Nickerson JA. Nuclear structure in cancer cells. Nature Reviews Cancer. 2004;4(9):677–687.

148. Revach O-Y, Weiner A, Rechav K, Sabanay I, Livne A, Geiger B. Mechanical interplay between invadopodia and the nucleus in cultured cancer cells. Scientific Reports. 2015;5:9466.

149. Barczyk M, Carracedo S, Gullberg D. Integrins. Cell and Tissue Research. 2010;339(1):269–280.

150. Pulido R, Campanero MR, García-Pardo a, Sánchez-Madrid F. Structure-function analysis of the human integrin VLA-4 (alpha 4/beta 1). Correlation of proteolytic alpha 4 peptides with alpha 4 epitopes and sites of ligand interaction. FEBS letters. 1991;294(1-2):121–124.

151. Davis TL, Rabinovitz I, Futscher BW, Schnölzer M, Burger F, Liu Y, Kulesz-Martin M, Cress a E. Identification of a novel structural variant of the alpha 6 integrin. The Journal of biological chemistry. 2001;276(28):26099–26106.

152. Demetriou MC, Pennington ME, Nagle RB, Cress AE. Extracellular alpha 6 integrin cleavage by urokinase-type plasminogen activator in human prostate cancer. Experimental cell research. 2004;294(2):550–8.

153. Pawar SC, Demetriou MC, Nagle RB, Bowden GT, Cress AE. Integrin alpha6 cleavage: a novel modification to modulate cell migration. Experimental cell research. 2007;313(6):1080–9.

154. Chen QK, Lee K, Radisky DC, Nelson CM. Extracellular matrix proteins regulate epithelial-mesenchymal transition in mammary epithelial cells. Differentiation. 2013;86(3):126–132.

155. Basora N, Desloges N, Chang Q, Bouatrouss Y, Gosselin J, Poisson J, Sheppard D, Beaulieu JF. Expression of the alpha9beta1 integrin in human colonic epithelial cells: resurgence of the fetal phenotype in a subset of colon cancers and adenocarcinoma cell lines. International journal of cancer. Journal international du cancer. 1998;75(5):738–43.

156. Yokosaki Y, Matsuura N, Higashiyama S, Murakami I, Obara M, Yamakido M, Shigeto N, Chen J, Sheppard D. Identification of the ligand binding site for the integrin alpha9 beta1 in the third fibronectin type III repeat of tenascin-C. The Journal of biological chemistry. 1998;273(19):11423–8.

157. Yokosaki Y, Palmer EL, Prieto a L, Crossin KL, Bourdon M a, Pytela R, Sheppard D. The integrin alpha 9 beta 1 mediates cell attachment to a non-RGD site in the third fibronectin type III repeat of tenascin. The Journal of biological chemistry. 1994;269(43):26691–6.

158. Kemperman H, Wijnands YM, Roos E. [alpha]V Integrins on HT-29 Colon Carcinoma Cells: Adhesion to Fibronectin Is Mediated Solely by Small Amounts of [alpha]V[beta]6, and [alpha]V[beta]5 Is Codistributed with Actin Fibers. Experimental Cell Research. 1997;234(1):156–164.

159. Zhang Z, Morla AO, Vuori K, Bauer JS. The alpha v beta 1 integrin functions as a fibronectin receptor but does not support fibronectin matrix assembly and cell migration on fibronectin. The Journal of cell …. 1993.

160. Kellouche S, Fernandes J, Leroy-Dudal J, Gallet O, Dutoit S, Poulain L, Carreiras F. Initial formation of IGROV1 ovarian cancer multicellular aggregates involves vitronectin. Tumor Biology. 2010;31(2):129–139.

161. Contois LW, Akalu A, Caron JM, Tweedie E, Cretu A, Henderson T, Liaw L, Friesel R, Vary C, Brooks PC. Inhibition of tumor-associated αvβ3 integrin regulates the angiogenic switch by enhancing expression of IGFBP-4 leading to reduced melanoma growth and angiogenesis in

vivo. Angiogenesis. 2015;18(1):31–46.

162. Gu X, Niu J, Dorahy DJ, Scott R, Agrez M V. Integrin alpha(v)beta6-associated ERK2 mediates MMP-9 secretion in colon cancer cells. British journal of cancer. 2002;87(3):348–351.

163. Kalluri R, Weinberg R a. The basics of epithelial-mesenchymal transition. The Journal of clinical investigation. 2009;119(6):1420–8.

164. Zuo JH, Zhu W, Li MY, Li XH, Yi H, Zeng GQ, Wan XX, He QY, Li JH, Qu JQ, et al. Activation of EGFR promotes squamous carcinoma SCC10A cell migration and invasion via inducing EMT-like phenotype change and MMP-9-mediated degradation of E-cadherin. Journal of Cellular Biochemistry. 2011;112(9):2508–2517.

165. Li T, Guo H, Song Y, Zhao X, Shi Y, Lu Y, Hu S, Nie Y, Fan D, Wu K. Loss of vinculin and membrane-bound beta-catenin promotes metastasis and predicts poor prognosis in colorectal cancer. Molecular Cancer. 2014.

166. Kim JJ, Yin B, Christudass CS, Terada N, Rajagopalan K, Fabry B, Lee DY, Shiraishi T, Getzenberg RH, Veltri RW, et al. Acquisition of paclitaxel resistance is associated with a more aggressive and invasive phenotype in prostate cancer. Journal of Cellular Biochemistry. 2013;114(6):1286–1293.

167. Knowles LM, Gurski L a, Engel C, Gnarra JR, Maranchie JK, Pilch J. Integrin αvβ3 and fibronectin upregulate Slug in cancer cells to promote clot invasion and metastasis. Cancer research. 2013;73(20):6175–84.

168. Fenouille N, Tichet M, Dufies M, Pottier A, Mogha A, Soo JK, Rocchi S, Mallavialle A, Galibert M-D, Khammari A, et al. The Epithelial-Mesenchymal Transition (EMT) Regulatory Factor SLUG (SNAI2) Is a Downstream Target of SPARC and AKT in Promoting Melanoma Cell Invasion. PLoS ONE. 2012;7(7):e40378.

169. Lee M, Chou C, Tang M. Epithelial-Mesenchymal Transition in Cervical Cancer : Correlation with Tumor Progression , Epidermal Growth Factor Receptor Overexpression , and Snail Up-Regulation Epithelial-Mesenchymal T ransition in Cervical Cancer : Correlation withT. 2008;14(15):4743–4751.

170. Gupta SK, Oommen S, Aubry M-C, Williams BP, Vlahakis NE. Integrin α9β1 promotes malignant tumor growth and metastasis by potentiating epithelial-mesenchymal transition. Oncogene. 2013;32(2):141–50.

171. Huang RY-J, Wong MK, Tan TZ, Kuay KT, Ng a HC, Chung VY, Chu Y-S, Matsumura N, Lai H-C, Lee YF, et al. An EMT spectrum defines an anoikis-resistant and spheroidogenic intermediate mesenchymal state that is sensitive to e-cadherin restoration by a src-kinase inhibitor, saracatinib (AZD0530). Cell death & disease. 2013;4(11):e915.

172. Schaeffer D, Somarelli J a, Hanna G, Palmer GM, Garcia-Blanco M a. Cellular migration and invasion uncoupled: Increased migration is not an inexorable consequence of EMT. Molecular and Cellular Biology. 2014;34(18):3486–3499.

173. Qin L, Liu Z, Chen H, Xu J. The Steroid Receptor Coactivator-1 Regulates Twist Expression and Promotes Breast Cancer Metastasis. Cancer Research. 2009;69(9):3819–3827.

174. Cheng GZ, Zhang WZ, Sun M, Wang Q, Coppola D, Mansour M, Xu LM, Costanzo C,

Cheng JQ, Wang L-H. Twist is transcriptionally induced by activation of STAT3 and mediates STAT3 oncogenic function. The Journal of biological chemistry. 2008;283(21):14665–73.

175. Yang M-H, Wu M-Z, Chiou S-H, Chen P-M, Chang S-Y, Liu C-J, Teng S-C, Wu K-J. Direct regulation of TWIST by HIF-1α promotes metastasis. Nature Cell Biology. 2008;10(3):295–305.

176. Reinhold MI, Kapadia RM, Liao Z, Naski MC. The Wnt-inducible Transcription Factor Twist1 Inhibits Chondrogenesis. Journal of Biological Chemistry. 2006;281(3):1381–1388.

177. Ahmed D, Eide PW, Eilertsen IA, Danielsen SA, Eknæs M, Hektoen M, Lind GE, Lothe RA. Epigenetic and genetic features of 24 colon cancer cell lines. Oncogenesis. 2013;2(9):e71.

Appendix

A.1 Buffers

Table A.1: RIPA buffer

NaCl	150 mM
Tris-HCl	50 mM
Triton X-100	1%
Na-deoxycholate	0.5%
SDS	0.1%
EDTA	1 mM
MilliQ H_2O	
pH 7.4	

Table A.2: PBS

NaCl	1370 mM
KCl	27 mM
Na_2HPO_4	100 mM
KH_2PO_4	18 mM
MilliQ H_2O	
pH 7.4	

Table A.3: 4X NuPAGE LDS Sample Buffer (Life Technologies)

Tris-HCl	106 mM
Tris base	141 mM
Lithium dodecyl sulfate (LDS)	2%
Glycerol	10%
EDTA	0.51 mM
SERVA Blue G250	0.22 mM
Phenol red	0.175 mM
pH 8.5	

Table A.4: Running buffer

Glycine	192 mM
Tris base	25 mM
SDS	0.1%
MilliQ H_2O	

Table A.5: Polyacrylamide resolving

Acrylamide/bisacrylamide	8%
Tris-HCl, pH 8.8	0.4 M
SDS	0.10%
Ammonium persulfate	0.05%
TEMED	0.07%
MilliQ H_2O	

Table A.6: Polyacrylamide stacking gel

Acrylamide/bisacrylamide	4%
Tris-HCl, pH 6.8	0.13 M
SDS	0.1%
Ammonium persulfate	0.05%
TEMED	0.1%
MilliQ H_2O	

Table A.7: Transfer buffer

Glycine	192 mM
Tris base	25 mM
MeOH	20%
MilliQ H_2O	

Table A.8: TBS-T

Tris base	50 mM
NaCl	150 mM
Tween-20	0.2%
MilliQ H_2O	
pH to 7.6	

Table A.9: 3.7% PFA

PFA	3.7 mg
MilliQ H_2O	9 mL
5 N NaOH	20 µL
10X PBS	1 mL
5 N HCl	20 µL

Combine PFA and MilliQ. Add NaOH to assist in solubilisation, and stir with gentle heating. Add 10X PBS. Once PFA is fully dissolved, add HCl to neutralize the NaOH.

Table A.10: PBS with Ca^{2+} and

NaCl	1370 mM
KCl	27 mM
Na_2HPO_4	100 mM
KH_2PO_4	18 mM
$CaCl_2 \cdot 2H_2O$	1 mM
$MgCl_2 \cdot 6H_2O$	0.5 mM
MilliQ H_2O	
pH 7.4	

Table A.11: Acid alcohol

Ethanol	70%
Concentrated HCl	1%
MilliQ H_2O	

Table A.12: Scot's tap water

$KHCO_3$	20 mM
Mg_2SO_4	166 mM
Distilled H_2O	

A.2 Antibody information

Table A.13: Primary Antibodies

Target	Clonality	Host Species	Application	Manufacturer
Akt	C67E7	Rabbit	Western blot	Cell Signalling
Akt p-Ser473	D9E	Rabbit	Western blot	Cell Signalling
Akt p-Thr308	D25E6	Rabbit	Western blot	Cell Signalling
Fibronectin	F1	Rabbit	Immunofluorescence	Abcam
Integrin α4	D2E1	Rabbit	Western blot	Cell Signalling
Integrin α5	Polyclonal #4705	Rabbit	Western blot, immunofluorescence	Cell Signalling
Integrin α6	Polyclonal #4750	Rabbit	Western blot	Cell Signalling
Integrin α9β1	Y9A2	Mouse	Western blot, immunofluorescence	Abcam
Integrin αV	Polyclonal #4711	Rabbit	Western blot	Cell Signalling
Integrin β1	D2E5	Rabbit	Western blot	Cell Signalling
Integrin β3	D7X3P	Rabbit	Western blot	Cell Signalling
Integrin β4	Polyclonal #4707	Rabbit	Western blot	Cell Signalling
Integrin β5	D24A5	Rabbit	Western blot	Cell Signalling

Table A.14: Loading control, secondary, and isotype antibodies

Target	Clonality	Host Species	Application	Manufacturer	Conjugate
GAPDH	1 E6 D9	Mouse	Western blot	Proteintech	HRP
None	DA1E	Rabbit	Immunofluorescence (isotype)	Cell signalling	None
Rabbit IgG	Polyclonal A-11034	Donkey	Immunofluorescence	Life Technologies	Alexa Fluor 488
Rabbit IgG	Polyclonal #7074	Goat	Western blot	Cell Signalling	HRP

A.3 Primer information

Table A.15: Primers

Gene	Orientation	Sequence (5' to 3')	Primer length (nt)	Amplicon size (nt)	Exon-Exon junction?	Reference
BCL2	Forward	ACACCAGAATCAAGTGTTCCG	21	273	No	Designed by SB
	Reverse	ACATCTCCCGCATCCCACT	19		No	
ITGA5	Forward	AAGTGTTTGGGGAGCAGAACC	21	160	Yes	Designed by SB
	Reverse	CCTGGGTGTCTGACGAGTC	19		No	
JUP	Forward	CCCCATACTCAGTAGCCA	18	245	Yes	Designed by MC
	Reverse	CTGGTACTCCAGATCACCT	19		Yes (2 nt only)	
RPL27	Forward	ATCGCCAAGAGATCAAAGATAA	22	123	No	de Jonge H, e898, 2007
	Reverse	TCTGAAGACATCCTTATTGACG	22		No	
SNAI1	Forward	ACCCCAATCGGAAGCCTAAC	20	65	No	Designed by SB
	Reverse	CTGCTGGAAGGTAAACTCTGG	21		Yes	
SNAI2	Forward	CACATACAGTGATTATTTCCCC	22	256	Yes	Designed by MC
	Reverse	TCATCACTAATGGGGCTTTC	20		No	
TJP1	Forward	CCCCGTGGAGAAGACC	16	255	No	Designed by MC
	Reverse	CTCCATTGCTGTGCTCTTG	19		Yes (4 nt only)	
TWIST1	Forward	CGGAGACCTAGATGTCATTG	20	237	Yes	Designed by MC
	Reverse	CAGAATGCAGAGGTGTGAG	19		No	
VIM	Forward	GATGGACAGGTTATCAACGA	20	220	Yes	Designed by MC
	Reverse	AAATCTTGTAGGAGTGTCGG	20		No	
ZEB1	Forward	GGGAATGCTAAGAACTGCTG	20	269	No	Designed by MC
	Reverse	GCATCTGGTGTTCCATTTTCAT	22		Yes	
ZEB2	Forward	AAGAAAATGACCTGCCACCTG	21	106	Yes	Designed by SB
	Reverse	ATGTGCTCCTTCAGTGATGTC	21		No	

Table A.16: Primer design characteristics

	Ideal Primer Characteristics
Melting Temperature	As close to 60°C as possible
Amplicon Length	50-200 base pairs
GC Content (%)	30-80. Avoid GC rich stretches
3' Terminus	No more than 2 G or C in the last 5 bps
Runs	Avoid runs of >4 identical bases (especially G)
Position	One primer in each pair must span an exon-exon junction
Splice variants	Picks up all variants with equal-sized amplicons
Single Nucleotide Polymorphism (SNP)	Avoid SNPs within primer-binding sequences
Hairpin Formation	ΔG > -2 kCal/mol
Homodimer formation	Internal: ΔG > -6 kCal/mol 3’ Terminus: ΔG > -5 kCal/mol
Heterodimer formation	Internal: ΔG > -6 kCal/mol 3’ Terminus: ΔG > -5 kCal/mol